

SIMULATION OF GLOW DISCHARGE PLASMAS BY USING PARALLEL PARTICLE
IN CELL / MONTE CARLO COLLISION METHOD: THE EFFECTS OF NUMBER OF
SUPER PARTICLES USED IN THE SIMULATIONS

A THESIS SUBMITTED TO
THE GRADUATE SCHOOL OF NATURAL AND APPLIED SCIENCES
OF
MIDDLE EAST TECHNICAL UNIVERSITY

EMRAH ERDEN

IN PARTIAL FULFILLMENT OF THE REQUIREMENTS
FOR
THE DEGREE OF MASTER OF SCIENCE
IN
MECHANICAL ENGINEERING

SEPTEMBER 2013

Approval of the thesis:

**SIMULATION OF GLOW DISCHARGE PLASMAS BY USING PARALLEL PARTICLE
IN CELL / MONTE CARLO COLLISION METHOD: THE EFFECTS OF NUMBER OF
SUPER PARTICLES USED IN THE SIMULATIONS**

submitted by **EMRAH ERDEN** in partial fulfillment of the requirements for the degree of
**Master of Science in Mechanical Engineering Department, Middle East Technical Uni-
versity** by,

Prof. Dr. Canan Özgen
Dean, Graduate School of **Natural and Applied Sciences**

Prof. Dr. Süha Oral
Head of Department, **Mechanical Engineering**

Inst. Dr. Tahsin Ali Çetinkaya
Supervisor, **Mechanical Engineering Department, METU**

Assoc. Prof. Dr. İsmail Rafatov
Co-supervisor, **Physics Department, METU**

Examining Committee Members:

Assoc. Prof. Dr. Tuba Okutucu
Mechanical Engineering Department, Bilkent University

Inst. Dr. Tahsin Ali Çetinkaya
Mechanical Engineering Department, METU

Assist. Prof. Dr. Metin Yavuz
Mechanical Engineering Department, METU

Inst. Dr. Özgür Bayer
Mechanical Engineering Department, METU

Assist. Prof. Dr. Nevsan Şengil
Astronautical Engineering Department, THK University

Date:

I hereby declare that all information in this document has been obtained and presented in accordance with academic rules and ethical conduct. I also declare that, as required by these rules and conduct, I have fully cited and referenced all material and results that are not original to this work.

Name, Last Name: EMRAH ERDEN

Signature :

ABSTRACT

SIMULATION OF GLOW DISCHARGE PLASMAS BY USING PARALLEL PARTICLE IN CELL / MONTE CARLO COLLISION METHOD: THE EFFECTS OF NUMBER OF SUPER PARTICLES USED IN THE SIMULATIONS

Erden, Emrah

M.S., Department of Mechanical Engineering

Supervisor : Inst. Dr. Tahsin Ali Çetinkaya

Co-Supervisor : Assoc. Prof. Dr. İsmail Rafatov

September 2013, 82 pages

Parallel Particle in Cell/Monte Carlo Collision (PIC/MCC) numerical codes for glow discharge plasma simulations are developed and verified. The method is based on simultaneous solution of the Lorentz equations of motion of super particles, coupled with the Poisson's equation for electric field. Collisions between the particles are modeled by the Monte Carlo method. Development and validation of the helium and argon codes for gas discharge plasmas, speed up algorithms such as sub-cycling, null-collision methods and parallelization are described. Proper choice of super particle weighting is critically important in order to perform adequate and efficient PIC simulations of plasma. Herein, effects of particle weighting on the simulations of capacitive radio-frequency (RF) argon plasma discharges are studied in details. Furthermore, a Townsend gas discharge is modeled with full three-dimensional (3D3v) MCC approach, transport parameters are calculated for a specified range of reduced electric field (E/n), and the results are validated. Finally the collisional electron spectroscopy (CES) method for impurity detection, is modeled with a modified PIC/MCC model. The effect of electric field configuration on the electron energy distribution function (EEDF) is investigated

for the helium-argon gas mixture plasmas.

Keywords: Particle in Cell, Monte Carlo, Glow Discharge, Super Particle Weighting, Collisional Electron Spectroscopy

ÖZ

İŞİLTİLİ GAZ DEŞARJ PLAZMALARININ PARALEL HÜCREDE PARÇACIK / MONTE CARLO ÇARPIŞMA YÖNTEMİ İLE MODELLENMESİ: KULLANILAN SÜPER PARÇACIK SAYISININ SİMULASYON SONUÇLARINA OLAN ETKİLERİ

Erden, Emrah

Yüksek Lisans, Makina Mühendisliği Bölümü

Tez Yöneticisi : Öğr. Gör. Tahsin Ali Çetinkaya

Ortak Tez Yöneticisi : Doç. Dr. İsmail Rafatov

Eylül 2013 , 82 sayfa

Bu çalışmada ışıltılı gaz deşarj plazmaları için paralel Hücrede Parçacık / Monte Carlo Çarpışma (PIC/MCC) yöntemi kullanılarak nümerik kodlar geliştirilmiş ve doğrulanmıştır. Yöntem, süper parçacıkların Lorentz hareket denklemlerinin Poisson denkleminde elde edilen elektrik alan değeriyle beraber çözülmesine dayanır. Parçacıklar arası çarpışmalar Monte Carlo yöntemi ile modellenmiştir. Helyum ve argon gaz deşarj plazmaları için üretilen kodların geliştirilmesi ve doğrulanması, sub-cycling, null-collision ve paralel programlama gibi hızlandırıcı yöntemlerle ilgili bilgiler verilmiştir. Süper parçacık ağırlıklarının seçimi doğru ve verimli bir şekilde PIC analizlerinin yapılabilmesi için kritik öneme sahiptir. Bu çalışmamızda parçacık ağırlıklarının kapasitif radyo-frekans (RF) argon gaz deşarj plazma analiz sonuçlarına olan etkisi detaylı bir şekilde incelenmiştir. Ayrıca, Townsend gaz deşarj örneği tamamen üç boyutlu (3D3v) bir MCC analizi ile tetkik edilmiş, transport parametreleri belirli bir indirgenmiş elektrik alan değeri (E/n) için hesaplanmış ve sonuçlar doğrulanmıştır. Son olarak da yabancı parçacıkların algılanması için kullanılan Çarpışmalı Elektron Spektroskopisi (CES)

yöntemi, modifiye edilmiş PIC/MCC ile modellenmiştir. Elektrik alan konfigürasyonunun elektron enerji dağılım fonksiyonuna (EEDF) olan etkileri helyum-argon gaz karışım plazmaları için araştırılmıştır.

Anahtar Kelimeler: Hücrede Parçacık, Monte Carlo, Gas Deşarjı, Nümerik Modelleme, Süper Parçacık Ağırlığı

Aileme. Hakkınız Ödenmez...

ACKNOWLEDGMENTS

I would like to express deepest gratitudes to my coadvisor, and the Tubitak research project coordinator Dr. İsmail Rafatov for his patience, faith and providing me with an excellent atmosphere for research in the physics department. Without your help, this study would have been impossible.

Although plasma physics is not one of the principal branches of our department, we have shown that a mechanical engineer can work and succeed in multidisciplinary subjects. Thank you Dr. Tahsin Ali Çetinkaya for your reliance and support.

Thank you, my room mate and precious friend Ender Eylenceoğlu. Hours of brain storming about the codes and ofcourse your assistance about the plasma physics is unforgettable.

Deepest thanks to Dr. Zoltan Donkó and Dr. Miles Turner for answering my questions, sharing their work and correction of my codes. It would have been impossible for me to validate the study without their amazing aid.

I cannot express enough thanks to Dr. Nevşan Şengil and his Molecular Dynamics course in the Aerospace Engineering Department. Your course improved my coding skills, and gave invaluable information about the particle simulations. I wish to see your lectures in METU again.

Thank you Dr. Anatoly Kudryavtsev, you have lighten up our path for future studies. I believe, we will be able to model the collisional electron spectroscopy method in the future.

Special thanks to METU Computer Engineering Department - High Performance Computing Center and to İlkan Keleş for his patient support.

I also want to thank Technical Research Council of Turkey (TUBITAK) for the financial support during my study.

TABLE OF CONTENTS

ABSTRACT	v
ÖZ	vii
ACKNOWLEDGMENTS	x
TABLE OF CONTENTS	xi
LIST OF TABLES	xv
LIST OF FIGURES	xvi
LIST OF ABBREVIATIONS	xxiii
CHAPTERS	
1 INTRODUCTION	1
1.1 Motivation	1
1.2 Literature Survey	1
1.3 The Present Study	3
1.4 The Outline	4
2 THE GAS DISCHARGE PLASMAS	5
2.1 Plasmas	5
2.2 Single Particle Motions, Collisions and Boundary Interactions	5
2.2.1 Motions	5
2.2.2 Collisions	6

2.2.3	Processes at the Boundaries	8
2.3	Gas Discharge Plasmas	9
2.3.1	Types of Gas Discharge Plasmas	10
2.3.2	Glow Discharge Plasmas	11
2.4	Two Examples of Industrial Applications of Gas Discharge Plasmas .	12
2.4.1	Reactive Ion Etching	12
2.4.2	Plasma Electron Spectroscopy	14
2.5	Basic Components of Industrial Plasma Sources	18
2.5.1	Vacuum System	18
2.5.2	Gas Delivery System	19
2.5.3	Cooling System	19
2.5.4	Power System	19
2.6	Langmuir Probes	20
2.7	Information About Local, Non-Local Plasmas and Maxwellian Dis-	
	tributions	20
2.7.1	Basic Numerical Modeling Techniques for Plasmas	24
2.7.1.1	Kinetic Approach	24
2.7.1.2	Fluid/Continuum Approach	24
2.7.1.3	Hybrid Approach	25
3	PARTICLE IN CELL METHOD FOR LOW PRESSURE GLOW DISCHARGES:	
	NUMERICAL METHOD, PARALLELIZATION AND SUBCYCLING	27
3.1	PIC/MCC Model	27
3.1.1	Determination of Time Step Size (Δt), and Grid Size (Δx) .	30
3.2	The Parallel Algorithm	32

3.3	Subcycling	34
4	VALIDATION OF THE PARALLEL PIC/MCC CODES	37
4.1	Helium RF Glow Discharge PIC/MCC Example	37
4.2	Argon RF Glow Discharge PIC/MCC Example	38
4.2.1	α -Type Glow Discharge Analysis Results	39
4.2.2	γ -Type Glow Discharge Analysis Results	39
4.3	Detailed RF Argon Glow Discharge PIC/MCC Test	47
4.3.1	Detailed Analysis of the Parallel Code	48
4.3.1.1	Charge Densities	48
4.3.1.2	Electric Field	48
4.3.1.3	Current Densities	49
4.3.1.4	Average Particle Energies	49
4.3.1.5	Energy Distribution Functions in the Quasi-neutral Region	49
4.3.1.6	Single Ion Path	50
4.3.1.7	Ion Energies on the Electrodes	50
5	THE EFFECT OF NUMBER OF SUPER PARTICLES USED IN THE PIC/MCC SIMULATIONS	55
6	3D3V MCC MODEL OF DC ARGON TOWNSEND DISCHARGE	59
7	DC COLLISIONAL ELECTRON SPECTROSCOPY: NUMERICAL MODEL AND INVESTIGATION OF THE RESULTS	63
7.1	Modeling of DC Collisional Electron Spectroscopy (CES) of Helium-Argon Gas Mixture Discharge by Using PIC/MCC Method	63
7.1.1	Problem and Parameters	63
7.1.2	Results of CES PIC/MCC Model	64

7.2	The Effect of Electric Field Configuration at the Center of the Discharge	66
7.2.1	Conclusions concerning the Penning Electron MCC Analysis	69
8	CONCLUSION	71
	REFERENCES	73
	APPENDICES	
A	INFORMATION ABOUT THE PARALLEL PIC/MCC FORTRAN CODES	77

LIST OF TABLES

TABLES

Table 4.1 1D RF argon glow discharge. PIC/MCC model problem parameters.	47
Table 5.1 Effect of particle weighting on the total number of super electrons, average number of super electrons per grid cell, Debye length, λ_D , and number of super electrons per Debye length, N_D , at the end of the simulations, $t \approx 7.37 \times 10^{-5}$ s. (λ_D and N_D are calculated at the midplane of the discharge.)	55
Table 6.1 Townsend swarm 3D3v MCC simulation problem parameters.	61
Table 7.1 1D DC Helium-Argon Mixture Problem Parameters.	64
Table 7.2 1D DC Helium-Argon Gas Mixture Solution Parameters.	64
Table A.1 Information about the input parameters in the parallel helium PIC/MCC initializer (PFPIC1D_Init_He_v10.f90). REAL(8) format refers to double precision (64 bit) floating point number.	79
Table A.2 Information about the solution parameters in the parallel helium PIC/MCC initializer (PFPIC1D_Init_He_v10.f90). REAL(8) format refers to double precision (64 bit) floating point number.	79

LIST OF FIGURES

FIGURES

Figure 2.1 (a) A thin gas layer of thickness Δx , the red sphere refers to the particle for which the collision probability is calculated [17] (b) Side view of M thin slabs of thickness Δx (each), where overall thickness is s [17].	8
Figure 2.2 Collision cross sections for argon gas, (a) electron-neutral, (b) ion-neutral. Cross section info taken from references [12, 13].	8
Figure 2.3 An example gas discharge configuration (discharge tube), where, K: Cathode, A: Anode [32].	10
Figure 2.4 Gas discharge reactions [1].	10
Figure 2.5 V-I plot for short electrode distance, self-sustaining gas discharge plasmas. V_B the breaking voltage [33].	11
Figure 2.6 Regions in a DC glow discharge. (a) Short distance between the electrodes (b) Long distance between the electrodes. CDS: cathode dark space, NG: negative glow, FDS: faraday dark space, PC: positive column, AZ: anode zone [1].	12
Figure 2.7 Reactive ion etcher configuration [3].	13
Figure 2.8 (a) An example process for chlorine ion etching diagram [3], (b) RIE example for single-crystall silicon electrostatic driven comb resonator [35].	14
Figure 2.9 (a) Helium metastable energy levels [36], (b) Ionization energy for some atoms and molecules [37].	14

Figure 2.10 (a) Conversion of wall type probe's current-electric potential plot to EEDF [28]; (b) EEDF (with arbitrary units) obtained from wall probe placed in DC He-Ar mixture plasma at 4 Torr [28].	17
Figure 2.11 (a) View of the ring type probe and the CES gas analyzer [29], (b) EEDF for He-Ar gas mixtures for helium pressure 26 Torr, and 0.4% argon with modulating 1V probe voltage [29].	18
Figure 2.12 Gas discharge plasma source components: (a) Pumping system [3], (b) Power system [3].	19
Figure 2.13 A Langmuir probe assembly with carbon probe tip [3].	20
Figure 2.14 LTE helium gas at 298.15 K (a) Speed distribution, (b) energy distribution in logscale.	21
Figure 2.15 DC Townsend discharge helium gas electron swarm simulation. Helium gas at 41.4 Pa, temp. 300 K, 4 cm electrode distance. $E/n=500$ Td. Number of electrons at the start is 100	22
Figure 2.16 DC Townsend discharge helium gas electron swarm simulation. Helium gas at 4.14 Pa, temp. 300 K, 4 cm electrode distance. $E/n=5000$ Td. Number of electrons at the start is 100	23
Figure 3.1 Selection of the collision type for a particle j , which can possibly do T types of collisions. Here $\sigma_t(\epsilon_j)$ is collision cross section of the particle for the specific collision type t . Energy of the particle j is denoted by ϵ_j	31
Figure 3.2 Azimuth and scatter angles in the collision frame. Note that azimuth angle is in yz plane [14].	31
Figure 3.3 Single processor PIC/MCC algorithm. I) Initialization, II) Calculation of charged particle densities on grid points, III) Solution of Poisson's equation, IV) Electric field calculation V) Interpolation of electric field values to charged particles, VI) Solution of Lorentz equations and implementation of boundary conditions, VII) Collisions.	32

Figure 3.4 The theoretical speedup of a program as a function of the parallelized fraction of the program [43].	34
Figure 3.5 Example of parallel system with 4 processors: (a) ion densities [10^{18} m^{-3}] accounted by the processor #1 (b) global sum of the ion densities computed by the master worker.	35
Figure 3.6 Parallel PIC/MCC algorithm for a system with C processors. Black arrows refer to a communication between the processors (MPI_Reduce & MPI_Bcast). Processor #0 is the master processor, responsible for density collection, electric potential and electric field calculation and delivering the results to remaining workers. I) Initialization, II) Calculation of charged particle densities on grid points, III) Solution of Poisson's equation, IV) Electric field calculation, V) Interpolation of electric field values to charged particles, VI) Solution of Lorentz equations and implementation of boundary conditions, VII) Collisions.	35
Figure 4.1 Schematic of the capacitively coupled RF gas discharge.	37
Figure 4.2 Collision cross sections used in the simulations for helium gas: (a) electron-neutral, (b) ion-neutral.	38
Figure 4.3 Comparison with the previously done PIC/MCC study [24]. The symbol \square refers to the case II in [24], and continuous lines to recent study. (a) Ion density profile, (b) ion density profile at the center of the discharge, (c) ion heating rate, (d) electron heating rate, (e) ionization source, (f) normalized electron energy distribution function $f(\varepsilon)$	40
Figure 4.4 α -type discharge. Current study results. $p = 80 \text{ Pa}$, $V = 100 \text{ V}$, $L = 1.5 \text{ cm}$, $f = 13.56 \text{ MHz}$, $T = 350 \text{ K}$, $\gamma = 0$. Spatio-temporal plots for (a) Electron heating rate [W], (b) Central region electric field detail [V/m].	41
Figure 4.5 α -type discharge. Current study results. $p = 80 \text{ Pa}$, $V = 100 \text{ V}$, $L = 1.5 \text{ cm}$, $f = 13.56 \text{ MHz}$, $T = 350 \text{ K}$, $\gamma = 0$. Spatio-temporal plots for (a) Electron density [10^{15} m^{-3}], (b) Electric field [V/m].	42

Figure 4.6 RF α type argon gas discharge. Results of reference [44]. $p = 80$ Pa, $V = 100$ V, $L = 1.5$ cm, $f = 13.56$ MHz, $T = 350$ K, $\gamma = 0$. Spatio-temporal plots for (a) Electron heating rate [10^5 W], (b) Central region electric field detail [10^3 V/m], (c) Electron density [10^{15} m $^{-3}$].	43
Figure 4.7 γ -type discharge. Current study results. $p = 80$ Pa, $V = 200$ V, $L = 1.5$ cm, $f = 13.56$ MHz, $T = 350$ K, $\gamma = 0.2$. Spatio-temporal plots for (a) Electron heating rate [10^5 W], (b) Central region electric field detail [V/m].	44
Figure 4.8 γ -type discharge. Current study results. $p = 80$ Pa, $V = 200$ V, $L = 1.5$ cm, $f = 13.56$ MHz, $T = 350$ K, $\gamma = 0.2$. Spatio-temporal plots for (a) Electron density [10^{15} m $^{-3}$], (b) Ion density [10^{15} m $^{-3}$].	45
Figure 4.9 RF γ type argon gas discharge. Results of reference [44]. $p = 80$ Pa, $V = 200$ V, $L = 1.5$ cm, $f = 13.56$ MHz, $T = 350$ K, $\gamma = 0.2$. Spatio-temporal plots for (a) Electron heating rate [10^5 W], (b) Central region electric field detail [10^3 V/m], (c) Electron density [10^{15} m $^{-3}$].	46
Figure 4.10 Comparison of the analysis results. Problem parameters are taken from [45]. $p = 10$ Pa, $V = 250$ V, $L = 2.5$ cm, $f = 13.56$ MHz, $T = 350$ K, $\gamma = 0.1$. The \square symbol indicates the results from [45] and continuous lines indicate the recent study results. (a) Mean electron density profile, (b) ion energy distribution on the electrodes.	47
Figure 4.11 Problem parameters: $p = 10$ pa, $T = 350$ K, $V = 250$ V, $f = 13.56$ MHz, $L = 2.5$ cm, $\gamma = 0.1$, $W_e = W_i = 1.5 \times 10^8$. Results are displayed at $\omega t/2\pi = 0$, $\omega t/2\pi = 0.25$, $\omega t/2\pi = 0.50$ and $\omega t/2\pi = 0.75$. (a) Ion densities, (b) electron densities.	50
Figure 4.12 Problem parameters: $p = 10$ pa, $T = 350$ K, $V = 250$ V, $f = 13.56$ MHz, $L = 2.5$ cm, $\gamma = 0.1$, $W_e = W_i = 1.5 \times 10^8$. Results are displayed at $\omega t/2\pi = 0$, $\omega t/2\pi = 0.25$, $\omega t/2\pi = 0.50$ and $\omega t/2\pi = 0.75$. (a) Electric field, (b) electric field detail at the center of the discharge.	51

Figure 4.13 Problem parameters: $p = 10$ pa, $T = 350$ K, $V = 250$ V, $f = 13.56$ MHz, $L = 2.5$ cm, $\gamma = 0.1$, $W_e = W_i = 1.5 \times 10^8$. Results are displayed at $\omega t/2\pi = 0$, $\omega t/2\pi = 0.25$, $\omega t/2\pi = 0.50$ and $\omega t/2\pi = 0.75$. (a) Ion current density, (b) electron current density, (c) displacement current density, (d) total current density. 51

Figure 4.14 Problem parameters: $p = 10$ pa, $T = 350$ K, $V = 250$ V, $f = 13.56$ MHz, $L = 2.5$ cm, $\gamma = 0.1$, $W_e = W_i = 1.5 \times 10^8$. Average electron and ion energies at (a) $\omega t/2\pi = 0$, (b) $\omega t/2\pi = 0.25$, (c) $\omega t/2\pi = 0.50$, (d) $\omega t/2\pi = 0.75$ 52

Figure 4.15 Problem parameters: $p = 10$ pa, $T = 350$ K, $V = 250$ V, $f = 13.56$ MHz, $L = 2.5$ cm, $\gamma = 0.1$, $W_e = W_i = 1.5 \times 10^8$. Average electron and ion energies at $\omega t/2\pi = 0$ 52

Figure 4.16 Problem parameters: $p = 10$ pa, $T = 350$ K, $V = 250$ V, $f = 13.56$ MHz, $L = 2.5$ cm, $\gamma = 0.1$, $W_e = W_i = 1.5 \times 10^8$. Average energy distribution functions at the center of discharge for (a) electrons, (b) ions. 53

Figure 4.17 Problem parameters: $p = 10$ pa, $T = 350$ K, $V = 250$ V, $f = 13.56$ MHz, $L = 2.5$ cm, $\gamma = 0.1$, $W_e = W_i = 1.5 \times 10^8$. (a) Grid point position and (b) speed of the ion #0 as function of time. 53

Figure 4.18 Problem parameters: $p = 10$ Pa, $T = 350$ K, $V = 250$ V, $f = 13.56$ MHz, $L = 2.5$ cm, $\gamma = 0.1$, $W_e = W_i = 1.5 \times 10^8$. Ion energy distributions at the electrodes. 54

Figure 5.1 Effect of the super particle weightings on (a) the electron density profiles, (b) the ion density profiles, (c) the mean electron density profile over one RF cycle, (d) the maximum electron density vs average number of super electrons per grid, at simulation time $t \approx 7.37 \times 10^{-5}$ s. 57

Figure 5.2 Effect of the super particle weightings on (a) Total current density profile for simulation #1, (b) Total current density profile for simulation #6 at time $\omega t/2\pi = 0.25$, $\omega t/2\pi = 0.50$, and $\omega t/2\pi = 0.75$ 57

Figure 5.3	Effect of the super particle weighting on (a) electric field profiles, (b) electric field profile details at the center of the discharge, (c) mean electron energy profiles at the center of the discharge, (d) mean ion energy profiles at the center of the discharge. Time $\omega t/2\pi = 0.25$ of the RF period.	58
Figure 5.4	Effect of the super particle weighting on (a) electron energy distribution function at the center of the discharge, (b) ion energy distribution function at the center of the discharge. Time $\omega t/2\pi = 0.25$ of the RF period.	58
Figure 6.1	$L=1$ cm, $E/n= 500$ Td. Transport parameters of an electron swarm in argon gas: (a) mean energy, (b) drift velocity. The symbol \square refers to results from Donkó et. al. [14], and continuous lines show recent study results.	60
Figure 6.2	$L=1$ cm, $E/n= 500$ Td. Transport parameters of an electron swarm in argon gas: Townsend ionization coefficient. The symbol \square refers to results from Donkó et. al. [14], and continuous lines show recent study results.	61
Figure 7.1	Results of the PIC/MCC analysis for DC CES example.	65
Figure 7.2	Example CES configuration, setup and electric potential [27].	66
Figure 7.3	Input electric field configurations for test MCC simulations. (a) Ideal case - Test 1, (b) Input electric field from the analysis in 7.1.2 - Test 2, (c) Averaged electric field profile with reduced noise from the analysis in 7.1.2 - Test 3, (d) Closer view of the electric field configurations of Test 1 - Test 2- Test 3.	67
Figure 7.4	Results of Test 1. (a) Kinetic energy and position of a random Penning electron versus time (b) Electric potential configuration.	68
Figure 7.5	Results of Test 2. (a) Kinetic energy and position of a random Penning electron versus time (b) Electric potential configuration.	68
Figure 7.6	Results of Test 3. (a) Kinetic energy and position of a random Penning electron versus time (b) Electric potential configuration.	69

Figure A.1 Section of the initializing program, PFPIC1D_Init_He_v10.f90, where input and solution parameters are entered into the program. 80

Figure A.2 Section of the main program, PFPIC1D_Main_He_v10.f90, where solution and display parameters are entered into the program. 81

Figure A.3 Illustration of the root program folder. 82

LIST OF ABBREVIATIONS

B	Magnetic field [T]
D_j	Diffusion coefficient of particle type j [$\text{m}^2 \text{s}^{-1}$]
E	Electric field [V m^{-1}]
e	Elementary charge [$1.602176565 \times 10^{-19} \text{ C}$]
E_j	Required energy for the process j [eV]
F	Force field [N]
f	Electrode frequency [Hz]
$f(v)$	Speed distribution function
$f(\varepsilon)$	Energy distribution function
J_e	Electron current density for 1D PIC/MCC simulations [$\text{m}^{-2} \text{s}^{-1} \text{ C}$]
J_d	Displacement current density for 1D PIC/MCC simulations [$\text{m}^{-2} \text{s}^{-1} \text{ C}$]
J_i	Ion current density for 1D PIC/MCC simulations [$\text{m}^{-2} \text{s}^{-1} \text{ C}$]
k_B	Boltzmann constant [$1.3806488 \times 10^{-23} \text{ m}^2 \text{ kg s}^{-2} \text{ K}^{-1}$]
L	Distance between the electrodes [m]
m	Mass of the the particle [kg]
n	Neutral gas density [m^{-3}]
n_{ion}	Ionized particle density [m^{-3}]
n_j	Density of particle type j [m^{-3}]
q	Electric charge of the particle [C]
P	Collision probability of the process
p	Gas pressure [Pa]
P_j	Heating rate of particle type j [W m^{-3}]
R	Uniform random number between 0-1
r	Reflection coefficient
R_i	Ionization source [$\text{m}^{-3} \text{s}^{-1}$]
R_{i-n}	Ratio between the ionized and neutral particles inside the gas in thermal equilibrium
T	Temperature of the gas [K]
T_j	Temperature of the particle type j [K]
t	Simulation time [s]
U_i	Ionization energy of the gas [eV]
V	Electric potential [V]

\mathbf{v}	Velocity field [m s ⁻¹]
v	Speed of the particle [m s ⁻¹]
v_{th}^m	Thermal velocity [m s ⁻¹]
v_x	x-Component velocity of the particle [m s ⁻¹]
v_y	y-Component velocity of the particle [m s ⁻¹]
v_z	z-Component velocity of the particle [m s ⁻¹]
W_j	Weighting of the super particle type of j
α	Townsend ionization coefficient [m ⁻¹]
χ	Scattering angle [rad]
δ	Rate of energy loss after the elastic electron-neutral collision
Δt	Time step size [s]
Δx	Grid distance [m]
ΔV	Volume element [m ³]
ϵ_{rel}	Maximum relative error
ϵ	Energy of the particle [eV]
ϵ_0	Permittivity of free space [8.85418782 × 10 ⁻¹² F m ⁻¹]
η	Azimuth angle [rad]
γ	Secondary electron yield coefficient
Γ_j	Flux of particle type j [m ⁻² s ⁻¹]
λ	Mean free path [m]
λ_D	Debye length [m]
μ_j	Mobility coefficient of particle type j [m ² V ⁻¹ s ⁻¹]
ν	Collision frequency [s ⁻¹]
σ	Collision cross section of the process [m ⁻²]
τ_e	Relaxation time for electrons [s]
θ, ϕ	Pre-collision spherical velocity angles [rad]

CHAPTER 1

INTRODUCTION

1.1 Motivation

Gas discharge plasmas have wide variety of uses in the industry such as high efficiency illumination, surface modification of materials, lasers, impurity gas detection. They also have a wide range of applications in the medical sector. For instance production of bio-compatible materials, ozone and hydrogen-peroxide plasma sterilization [1]. But the most important one is the microprocessor production. For an ordinary microchip, one has to put millions of transistors inside. Each element dimension is in the orders of nano meters. It is not possible to obtain such accuracy without the use of plasma technologies [2]. Another fundamental advantage of the low-temperature gas discharge plasmas is high rates of chemically reactive species generation at low temperatures without damaging or changing the main properties of the target material [3].

Using numerical simulation codes for modeling the gas discharge plasma may give information about the essential mechanisms and increase the accuracy of the industrial processes. The principal subject of our study, the Particle in Cell / Monte Carlo Collision (PIC/MCC) method, is a reliable and sound tool for understanding gas discharge plasmas at both microscopic and macroscopic level. As it will be mentioned in the following chapters, the particle model of interest is one of the few choices to correctly model the non-local discharge plasmas. The central aim of this subject is to first develop a working and validated PIC/MCC code. Although complex atomic interactions and higher dimension geometries were not included in this thesis study, the validated codes may be a good starting ground for more complicated models. The work is still underway, and the development continues.

1.2 Literature Survey

For most of the studies in literature about the gas discharge plasma simulations, fluid (continuum) approach is used. The detailed information and comparison of the hybrid and particle methods can be found in one of the studies of Donkó et. al.[4]. A more developed but computationally expensive method, and the principal focus of this study; the Particle in Cell method

(PIC), has been used since the end of the 1950s. The method was first introduced by Dawson [5]. The first implementations were directly calculating the forces acting between charged particles according to the Coulomb's law and manipulating the positions. The simulations represented somehow modification of the molecular dynamics. It is also obvious that computer technology was not as advanced as we have nowadays. Later, rather than calculating all the interactions between the particles, charge densities in the grid points were calculated (which reduced the mathematical operations significantly, N^2 vs N). In the mid 1960s again Dawson modeled Landau damping phenomena with PIC method [6]. To calculate the collisions for particles at each time step, collision probabilities of all the charged particles have to be checked within the standard algorithms. Since the method is highly time consuming, a very efficient algorithm called the null-collision method was developed [7] to check not all the particles but some portion. Later, PIC method was used to simulate the sheath regions of the direct current glow discharges in 1977 [8]. To reduce the noise levels and refine the results, filtering algorithms were introduced by Birdsall et. al. in his very valuable book "Plasma Physics via Computer Simulation" [9]. Application of the method for radio-frequency (RF) glow discharges in 1D was studied by Boswell et. al. [10] in 1988. At the beginning of the 1990s Berkeley study group incorporated a detailed Monte Carlo collision algorithm into PIC to model for the collisional plasmas. In 1991, Birdsall published his very valuable study about the PIC/MCC method [11]. The technique uses standard PIC and collisions are modeled with the Monte Carlo approach by using predefined collision cross sections [12, 13]. The method is well defined in the references [14, 15, 16, 17]. Since the ions and slow electron groups generally tend to stay as Maxwellian in the simulations these kind of charged particle groups can be modeled as fluid and fast electrons as particles. The method is called as the hybrid method and have some advantages over pure particle codes in terms of computational time [18]. In addition to these techniques, 2D RF glow discharge PIC/MCC simulations was first introduced by Porteous et. al. [19]. Secondary electrons created from electron collisions with boundaries were introduced by Gopinath et. al. [20]. Numerical heating of the particles due to noise in the simulations were studied by Hitchon [21]. Although the PIC/MCC is an accurate model for non-local plasma of interest, unlike the continuum/fluid models, it is computationally demanding. Speed up methods were introduced to increase the efficiency and to reduce the computational time. Some of these methods, parallelization, implicit solvers, ion sub-cycling are described by Kawamura et. al. [22]. Donkó and Derzsi compared all the three principal gas discharge simulation techniques (fluid, particle and hybrid) for the simulation of the DC glow discharges, and studied the effect of particle weightings for the specified discharge types [4, 23]. Finally, in 2013 Miles et. al. published a very important PIC/MCC benchmarking study [24]. From now on, the mentioned study can be accepted as base study for evaluation of the accuracy of the particle codes including the current study.

The plasma electron spectroscopy method (PLES), by which the impurity particles can be detected in plasma, is an alternative to classical gas analysing techniques. The collisional electron spectroscopy method (CES) is a variation of the PLES method, which can be applied in higher pressure ranges [25]. Bogdanov et. al. studied simulation of a pulse helium micro glow discharges for CES application [26]. Chirtsov et. al. introduced a two plane

parallel electrode CES analyser configuration for pulsed glow discharges [27]. Experimental application of the method by using wall electrodes were introduced by Demidov et. al. [28]. Kudryavtsev et. al. modified the electrode configuration to a ring shaped one at the center of the discharge, which further simplified the experimental setup [29].

1.3 The Present Study

This study initiates development of a parallel numerical code using Particle in Cell/Monte Carlo collision (PIC/MCC) method, created by using C and Fortran languages with MPI (Message Passing Interface) parallel programming. Details about the programs, logic, structure, as well as the theory were also included in this thesis study.

Validation of the parallel PIC/MCC codes was first done with the help of Dr. Zoltan Donkó (private e-mail communication) who has made a great contribution to the glow discharge simulation techniques. Codes for helium and argon gasses have also been validated with the studies in the literature. Apart from these studies, a higher dimensional (3D3v) simulation code for argon Townsend gas discharge was developed, diffusion and mobility coefficients were also calculated for a specified E/n value.

Since this is the first development of the particle method by our study group, we need to correctly understand the effect of a very important solution parameter: the number of particles used in the PIC/MCC simulations, which is often ignored. For the case of capacitive RF discharge in argon gas, we demonstrated the effect of weighting on the main characteristics of the discharge, such as the profiles of charged particle densities, electric field, current density, average energies of charged particles and energy distribution functions. Results show that the discharge characteristics are highly dependent on the number of particles used in the simulations. We have shown that the adequate number of super particle per grid cell, sufficient to have weighting independent results, is about 1200.

After validation and reinforcement of the parallel codes, an industrial gas discharge application was studied, by which the impurity atoms in helium gas can be detected. Argon-helium gas mixture collisional electron spectroscopy application was modeled with the PIC/MCC model. Our aim is to obtain similar peaks on electron distribution functions (EEDF) as done previously in experimental studies. The code resembles the hybrid codes in terms of drift-diffusion approximation used for excited helium atoms, but ions and electrons were modeled with pure particle approach. The simulation results were not as expected as in the previously done experiments [29, 28], so the reasons creating the problem were investigated in the study. For investigation, another MCC model was developed to track the energies and positions of the Penning electrons created. Consequently, it was clearly understood that electric field noise in the quasi-neutral region and excessively high average electron energy due to lack of particles are the main reasons for the unexpected result. Recommendations were made for the progression of the study.

We are now able to model glow discharge plasmas for inert gases and basic geometries. With improvements and extensions of the parallel PIC/MCC product, it will be easier to understand and model industrial gas discharge plasma applications in a better fashion.

1.4 The Outline

In the second chapter, firstly information about the plasmas and single particle motions, collisions and boundary interactions are given to provide essential information about the subject. Secondly, gas discharge plasmas and types were introduced. Two important industrial plasma applications, namely reactive ion etching and plasma electron spectroscopy were discussed. Later, fundamental components of industrial plasma sources and Langmuir probes were summarised briefly. Before the introduction of the plasma numerical modeling techniques, information about local and non-local plasmas were given.

The third chapter is about the PIC/MCC method. Algorithm of the method was introduced in detail as well as some of the key points that has to be paid attention during the development of the codes. Some of the speed-up algorithms such as parallel algorithm and subcycling were introduced in brief.

In chapter four, our PIC/MCC codes were validated through three different low pressure gas discharge problems. One of the validated test problem (Chapter 4.3) was analysed in detail.

The fifth chapter illustrates the effect of the number of particles used in the PIC/MCC simulations.

In chapter six, results of 3D3v MCC model for Townsend gas discharges for specified E/n value was introduced and validated.

Chapter seven is about development of a PIC/MCC code with metastable helium atoms modeled with continuum approach for collision electron spectroscopy technique.

The last chapter summarizes the study and suggests ideas for the future studies.

CHAPTER 2

THE GAS DISCHARGE PLASMAS

2.1 Plasmas

Plasma is a quasi-neutral gas of charged ions, electrons etc. and neutral particles, which exhibits collective behaviour. There is a general quotation which says "99% of the matter in the entire universe is plasma". Inter-galactic space, gaseous nebulas are mostly plasmas. Lightning bolts, north lights (Aurora Borealis) are the two general examples of naturally occurring plasmas, but it is not very common to encounter plasmas in daily life basis. Although most of the universe is plasma, what happens and why the plasmas observed are so rare in daily life is the central question. To be able to make an explanation, the Saha equation should be studied. It is possible to determine the ratio between the ionized and neutral particles inside a gas in thermal equilibrium (R_{i-n}) by using the Saha equation,

$$R_{i-n} = n_{ion}/n = 2.4 \times 10^{21} \frac{T^{3/2}}{n_{ion}} e^{-U_i/kT}, \quad (2.1)$$

where n_{ion} is the ionized particle density, n neutral gas density, T temperature of the gas, U_i ionization energy of the gas, k_B Boltzmann's constant. When speaking for the earth's atmosphere, the ratio is extremely small in the orders of 10^{-122} . This is because of the comparatively high pressure and low temperature values in the earth's atmosphere. Without an external energy source, it is not possible to create plasma for such high pressure mediums [30].

2.2 Single Particle Motions, Collisions and Boundary Interactions

2.2.1 Motions

Charged particles move according to the Lorentz force equation,

$$m_j \frac{d\mathbf{v}_j}{dt} = q_j(\mathbf{E}_j + \mathbf{v}_j \times \mathbf{B}_j). \quad (2.2)$$

where \mathbf{v}_j is the velocity, \mathbf{E}_j is the electric field, \mathbf{B}_j is the magnetic field acting on the particle j with mass m_j and charge q_j . In different external electric and magnetic field configurations,

particles move in a different fashion. For electrostatic plasmas of interest, where magnetic effects are neglected, electric field only alters the velocity of the particles in its direction. The direction of the velocity vector may also be altered by the collisions [30].

2.2.2 Collisions

Collisions are one of the main processes determining the plasma properties, such as spatial diffusion of the charged particles in the plasma. They are categorized into two main groups, namely elastic and inelastic. For the first one, total momentum and kinetic energy conservation rules are valid, but not for the second one. Coulomb collisions and polarization scattering of the neutral and charged particles are examples of elastic collisions. Excitation, ionization, and recombination collisions are examples of the inelastic type. Ionization collisions determine the ionization rate of the plasmas [31].

Collision cross-section of the process (σ) is the main parameter, determining the rates of the collisions. It doesn't only effect the mean free path and collision frequency of the particles. Collision cross-section can be described as an area of interaction between the particles of the collision process. Also, it is possible to derive the collision probability (P_{coll}) for each particle by using the cross section information. P_{coll} is calculated as follows,

$$P_{coll} = 1 - e^{-nv\Delta t \sigma_{total}}, \quad (2.3)$$

where n , v and Δt denote the gas density, relative velocity of the particles and time step size [14]. The formula is also used directly in the Monte Carlo algorithms of the plasma simulations to model the particle interactions (collisions). Hence it is a crucial formula for the study and will be derived in this section. In Figure 2.1(a) a thin short gas slab of thickness Δx and area A is shown. The red sphere refers to the particle which has a chance to hit the neutral gas particles inside the thin slab. For this configuration, collision probability can be written as

$$P_{coll} = \frac{A'}{A}, \quad (2.4)$$

where A' is the total area of collision inside the thin slab. A' can be further expressed as

$$A' = N\sigma. \quad (2.5)$$

Here, N is the total number of neutral particles inside. N can be described by using volume of the slab (V) and neutral particle density (n):

$$A' = nV\sigma. \quad (2.6)$$

V can be expressed by using A and Δx . Therefore,

$$P_{coll} = \frac{nV\sigma}{A}, \quad (2.7a)$$

$$= \frac{nA \Delta x \sigma}{A}, \quad (2.7b)$$

$$= n\Delta x \sigma. \quad (2.7c)$$

One can argue that plasmas can be formed by using many of the slabs above mentioned. In Figure 2.1(b) side view of the M number of slabs, with thickness s can be seen. The chance for a particle to pass the gas without colliding with any of molecules/atoms (P_{trans}) can be expressed as

$$P_{trans} = (1 - P_{coll})^M, \quad (2.8a)$$

$$= (1 - n\Delta x \sigma)^{s/\Delta x}, \quad (2.8b)$$

$$= (1 - n\Delta x \sigma)^{\frac{-ns\sigma}{-n\Delta x \sigma}}. \quad (2.8c)$$

By using the identity below,

$$\lim_{a \rightarrow 0} (1 - a)^{-\frac{1}{a}} = e, \quad (2.9)$$

equation (2.8c) can be written as

$$P_{trans} = e^{-ns\sigma}, \quad (2.10a)$$

$$P_{coll} = 1 - P_{trans} = 1 - e^{-ns\sigma}, \quad (2.10b)$$

$$= 1 - e^{-nv\Delta t \sigma}. \quad (2.10c)$$

Finally, the equation (2.3) is obtained [17].

Atoms have a radius in the orders of 10^{-8} cm, and their collision cross sections tend to be in the orders of 10^{-16} cm², but these values are also highly dependent on the energy of the particles. In Figure 2.2 electron-neutral, and ion-neutral collision cross sections for argon gas are shown. At high speeds (or high energies), electrons tend to collide less frequently. In addition, at a certain point the electron collision cross-section has the minimum value. This value is called the Ramseur minimum, which can be observed for the noble gasses.

Compared to electron-neutral collisions, ion-neutral collisions have higher collision cross sections. At the same time, ions may lose their energy more easily since they have similar mass to the neutral particles. While an ion is passing near a neutral particle, it may pull off the neutral's electron, so that the ion becomes neutral, the neutral becomes ion. The process is called charge exchange collision. [32].

Energy of a particle can be calculated as follows,

$$v = \sqrt{v_x^2 + v_y^2 + v_z^2}, \quad (2.11)$$

$$\varepsilon = \frac{1}{2} m v^2, \quad (2.12)$$

where v , v_x , v_y , v_z , ε , m are speed, x-component, y-component, z-component of velocities, energy, and mass of the selected particle respectively. If SI units are used in the calculation, one can find the energy as in the unit of [kg m² s⁻²] or Joules. To obtain energy in terms of electron volts [eV], value has to be divided by $1.602176565 \times 10^{-19}$.

If a particle has enough energy, it can break off an electron from an atom, resulting in an inelastic collision (single ionization). For example, for electron-argon gas collisions, the minimum required energy for the electron for ionization is 15.76 eV. Occasionally, electron may

move into a higher energy level, resulting in excitation. The atom may come to a metastable state. The excited atom may return to its ground state by emitting a photon at a specified energy. It may also be ionized by collision with another electron which has sufficient energy. This process is called stepwise ionization. Single ionized particle may also ionize further to become doubly ionized, but the process is very rare for low pressure plasmas of interest [3].

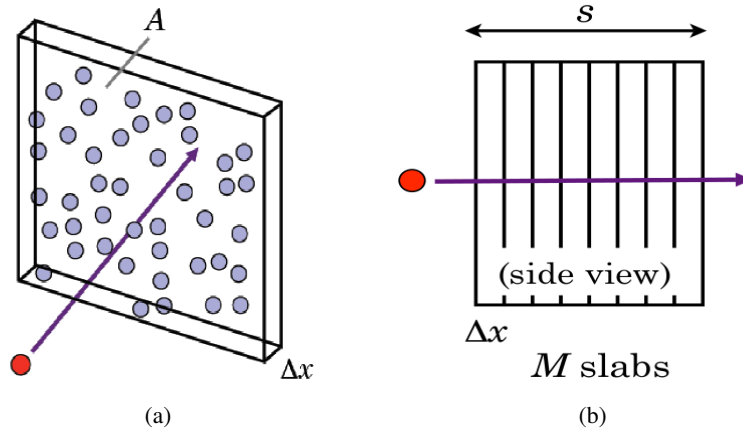


Figure 2.1: (a) A thin gas layer of thickness Δx , the red sphere refers to the particle for which the collision probability is calculated [17] (b) Side view of M thin slabs of thickness Δx (each), where overall thickness is s [17].

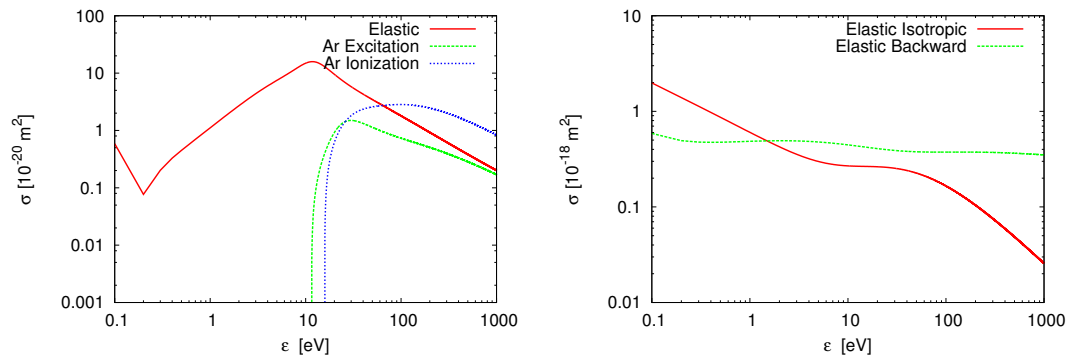


Figure 2.2: Collision cross sections for argon gas, (a) electron-neutral, (b) ion-neutral. Cross section info taken from references [12, 13].

2.2.3 Processes at the Boundaries

Interaction processes include neutralization, secondary electron yield, reflection, sputtering etc. The electrode surfaces may be very rough, and greatly influence the process in the boundaries [32]. Two of the most significant boundary processes for gas discharge plasmas are listed

below:

- **Neutralization:** Although neutralization by recombination process is very low in the gas discharge plasma volume, it is the central process occurring at the electrodes. One can say that electrodes are the so called black-holes for charged particles. Electrodes absorb nearly all of the incoming charged particles in the gas discharge plasmas. Example three body recombination process for ion A, electron and surface material S can be given as [31],



Some of the charged particles may reflect back from the boundaries rather than be neutralized. This process is called as reflection.

- **Secondary Electron Yield:** Electron emission can be created by the impact of various particles such as ions, electrons, metastables, photons, etc. to electrode material. Secondary electron yield has fundamental importance for self-sustaining gas discharge plasmas. The created electrons in the sheath regions accelerate and gain enough energy, so that they contribute to ionization to compensate the loss of electrons. The secondary electron yield is mainly resulted from positive ions. This can be explained by quantum mechanical tunneling of electrons, which is not however in the scope of this study [32].

The secondary electron yield coefficient, γ , is the parameter of the process. It is the value for the number of electrons created per particle hit. The value is highly dependent on gas type, electrode composition and microscopic topography [31, 32]. As will be discussed in section 4.2.1, the value has high impact on plasma properties and discharge state.

2.3 Gas Discharge Plasmas

Gas discharge plasmas can be created between two parallel electrodes when sufficiently large electric potential difference is applied. Of course, there are other ways to create plasma, but this study mainly focuses on capacitively coupled glow discharge plasmas. In Figure 2.3 a representative experimental set-up for a gas discharge can be seen. Gas is confined inside a glass vacuum tube, where electric potential difference is applied between the electrodes. Discharge tube size can be variable in diameter and length. Also, the gas pressure and composition are the other variables. When a small amount of (in the order of a few ten volts) electric potential is applied between the electrodes, no current is measured excepting very precise measurement devices. The current is in the orders of 10^{-15} A and not self-sustaining. If the voltage is kept increasing, at some point, the existing electrons in the discharge tube move like an avalanche and increase in number by ionization collisions. Some of the created charged particles are neutralized on boundaries or recombine with each other to form neutral particles. The cathode region (-) of the discharge is an attraction region for positive ions created from the inelastic electron-neutral gas collisions (positive ions are called as ions in

this study). When an ion hit the cathode, it may create secondary electrons and may sputter material from the electrode. The created secondary electrons are accelerated with the high electric potential gradient on the sheaths. When they reach sufficiently large energy levels, they may cause inelastic collisions with the neutral particles. Excited atoms then de-excite and emit visible radiation, which result in illumination (glow) in the discharge. In self-sustaining plasmas or glow discharges, charged particles are created and deleted at equal rates. There is continuous charge creation and depletion on the discharges. The reactions taking place in a gas discharge is well defined in Figure 2.4. The created plasma may not always be stable, may also dissipate over time [32].

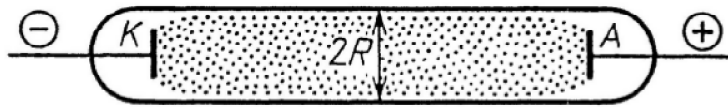


Figure 2.3: An example gas discharge configuration (discharge tube), where, K: Cathode, A: Anode [32].

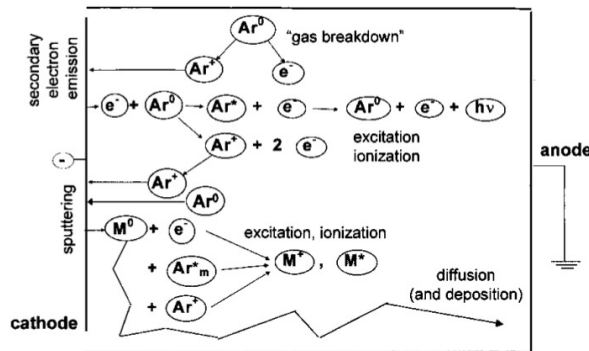


Figure 2.4: Gas discharge reactions [1].

2.3.1 Types of Gas Discharge Plasmas

As stated before, different current values between the electrons can be obtained with different configurations in the DC gas discharges. Electric potential vs current curve for self-sustaining short electrode distance gas discharges can be seen in Figure 2.5.

The break-down voltage V_B is a critical parameter and depends on plasma parameters such as temperature, pressure, gas type and electrode distance. The discharges between A-B are called as Townsend discharges. It should be noted that it is possible to modify the discharge current

by using external electric circuit set-ups. After the critical value in the current is attained, it is possible to generate plasma at low electric potential differences. The region between B-C is called as transition regime, C-D sub-normal, D-E normal glow, E-F the ab-normal, and F-G as arc transition regime. The main topic of the current study covers, C-F region which is called glow discharge regime.

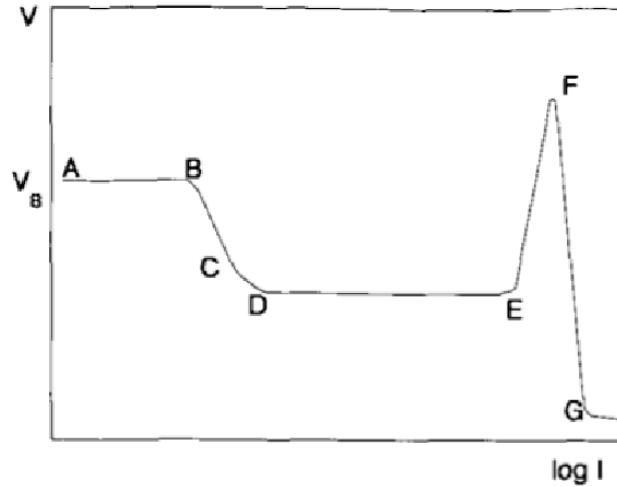


Figure 2.5: V-I plot for short electrode distance, self-sustaining gas discharge plasmas. V_B the breaking voltage [33].

2.3.2 Glow Discharge Plasmas

Electric potential applied between the electrodes in a gas discharge is not distributed equally inside. There are some distinct regions. In Figure 2.6, schematic representation of a glow discharge plasma with different regions for short and long electrode distances can be observed.

For industrial applications of the glow discharges such as surface modification the distance between the electrodes is much lower than the electrode diameter. Plasma parameters (charged particle densities, field configurations, mean energies etc.) only vary in the symmetry axis. Therefore, it is possible to model the industrial glow discharges in one-dimension (1D) [33]. Furthermore, vast majority of the plasmas in this study is analogue to configuration in Figure 2.6(b).

Normal glow discharge is a type of DC electric discharge observed in the pressure range of 1 to 10 Torrs and the voltage is about a few hundred Volts. Current is in the order of 10^{-6} to 10^{-1} amperes for tubes with a radius of 1 cm. For glow discharges, charged particle densities are about 6 to 8 orders lower than the neutral background gas density. Quasi-neutral region is where there is electrical neutrality, but in the sheath regions, positive ions are denser compared

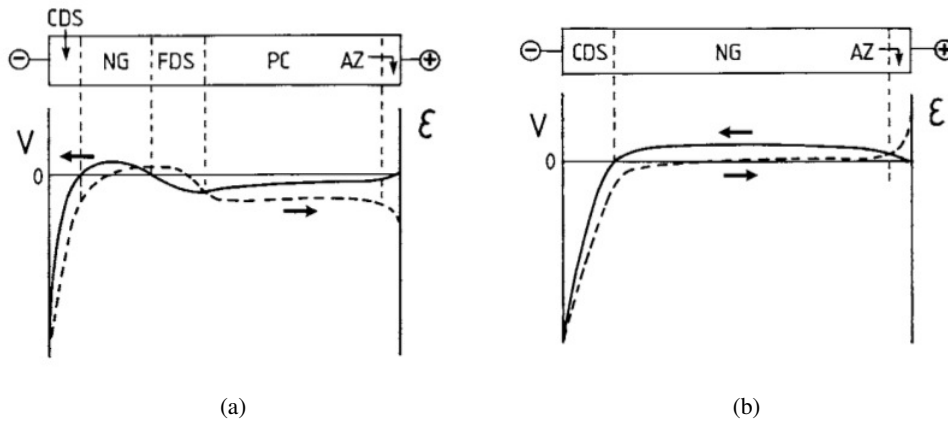


Figure 2.6: Regions in a DC glow discharge. (a) Short distance between the electrodes (b) Long distance between the electrodes. CDS: cathode dark space, NG: negative glow, FDS: faraday dark space, PC: positive column, AZ: anode zone [1].

to electrons. Electrons are at higher energies in the center of the discharge when compared to ions and background gas. For example, electron energies are at the orders of eVs and the ion energies are close to neutral gas temperature. For these types of gas discharges, electrons are in non-equilibrium and far from local thermodynamic equilibrium (LTE) [34].

2.4 Two Examples of Industrial Applications of Gas Discharge Plasmas

Low temperature and pressure gas discharge plasmas have a wide variety of usage in the industrial applications such as surface modification by coating, hardening, etching, deposition, high efficiency illumination, TV displays, lasers, production of bio compatible materials and sterilization by taking advantage of chemically rich environment without excess heat [1]. This section of the study gives information about reactive ion etching (RIE) gas discharge system and collisional electron spectroscopy methods.

2.4.1 Reactive Ion Etching

Plasmas can be used to modify the surfaces of the materials. One of the main applications of these modifications is the integrated circuit (IC) production. Trenches created by the glow discharges can be extremely accurate in the orders of nanometers. Not only for trenching but also in many other steps of the IC production, glow discharges can be used. IC production steps can be summarized briefly as follows:

- (a) Film material is coated (Can be done with glow discharges - Deposition)
- (b) Photo-resist is coated, a layer which is resistant to light penetration (Can be done with

glow discharges - Deposition)

- (c) Some portions of the photo-resist film is etched to form the desired pattern. (Can be done with glow discharges - Etching / Reactive Ion Etching)
- (d) Photo-resist film developed.
- (e) Material is etched by anisotropic ions. (Can be done by glow discharge - Etching)
- (f) Remaining photo-resist film is removed.

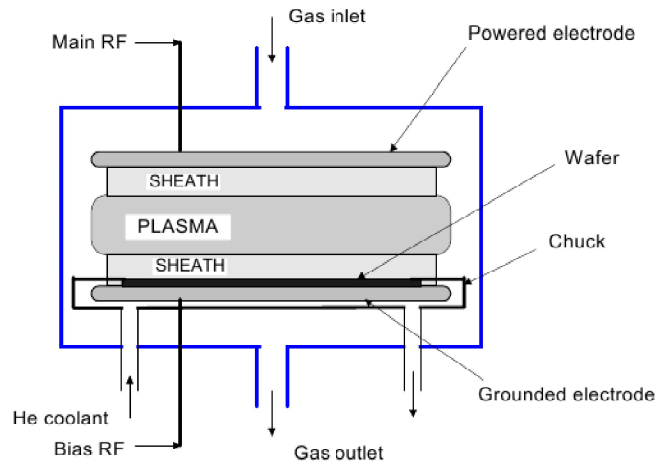


Figure 2.7: Reactive ion etcher configuration [3].

Set-up for the etching is shown in Figure 2.7. Material to be etched (wafer) is held by the component chuck. RF power applied is either single-frequency RF or dual-frequency RF. Gas is fed into the chamber and quickly ionized by the electric field. Electrons create avalanches and the created high energy ions trench the material. An example process for chlorine ion etching diagram, and detailed photo of a trench created by RIE is shown in Figure 2.8. Some of the parameters have special importance for an industrial RIE reactor. These are:

- **High etch rate:** High ion flux and energy on the boundaries is a requirement. Also, high particle densities should be provided inside the discharge.
- **Plasma Uniformity:** The plasma affecting the wafer should be uniform. Otherwise, the microchips produced at the edge of the wafers give lower performance.
- **Ion Anisotropy:** The ions should hit the wafer as vertical as possible to maximize the etching. Otherwise, trenches may not be sharp and uniform.
- **Suitable Temperature:** Plasma temperature should be kept in safe limits. Otherwise, the material can be damaged due to high heat [3, 31].

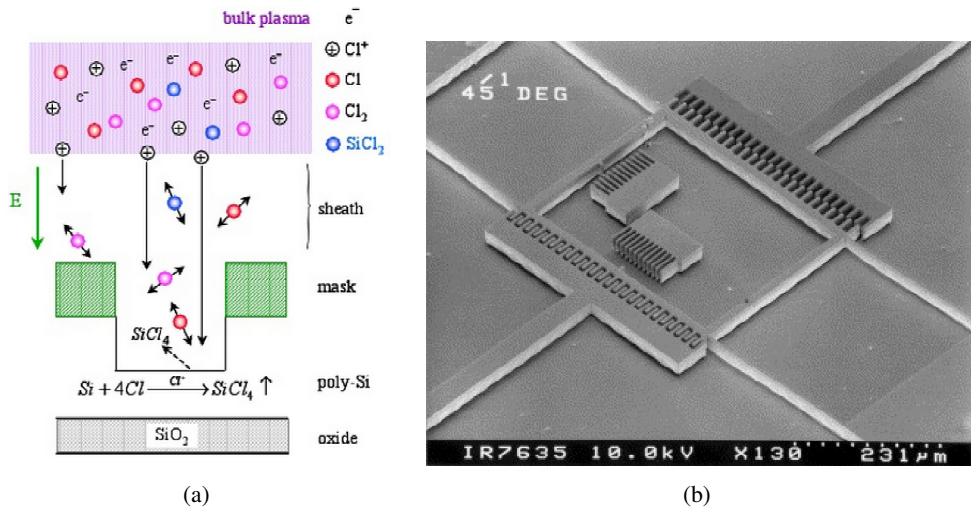


Figure 2.8: (a) An example process for chlorine ion etching diagram [3], (b) RIE example for single-crystalline silicon electrostatic driven comb resonator [35].

2.4.2 Plasma Electron Spectroscopy

Chromatography, mass spectroscopy and traditional electron spectroscopy methods are some of the methods to reveal the composition of a gas. The devices required for these methods are non-compact, relatively complex and require deep vacuums. Plasma electron spectroscopy (PLES) is another method, which is capable of determining the foreign substances in the composition by examining the electron energy distribution function (EEDF) of the created plasma [27].

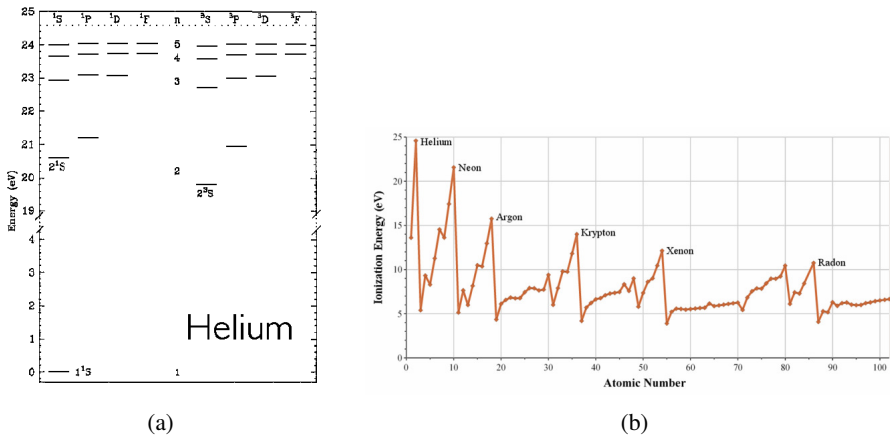


Figure 2.9: (a) Helium metastable energy levels [36], (b) Ionization energy for some atoms and molecules [37].

The excitation levels of the helium gas, and ionization energies of some atoms or molecules

are given in Figure 2.9(a) and 2.9(b) respectively. The idea of the PLES method is simple. Helium gas has the highest excitation levels known among the atoms or molecules. Furthermore, excitation energy of the helium gas is higher than ionization energies of all the atoms or molecules (except neon). If an excited helium atom collides with an impurity atom in the plasma, there is a possibility of ionization of the impurity. This ionization type is called penning ionization,



Denoting He^* excited helium atom, A impurity atom at the base energy level, and A^+ as ionized impurity atom. The electron created from the reaction, e_p , has predefined energy level dependent on the reaction type,

$$\varepsilon(e_p) = \varepsilon(He^*) - \varepsilon(A^+) \quad (2.15)$$

where ε is energy of the selected particle type in terms of eVs. The energy $\varepsilon(e_p)$ of the created electron depends only on the type of reaction, like a finger print. If the electrons created from the Penning ionization do not lose their energy, then a peak can be observed in the EEDF. It is possible to detect the Penning reactions that take place in the plasma, so do the type and concentration of the impurities inside the helium gas mixture. This part is common for both PLES and CES methods. PLES requires low pressures, to protect the electrons from any kind of collisions, so that one can detect the types from EEDF. Collisional electron spectroscopy (CES) is another variant of the PLES, where deep vacuum is not a requirement. The method can be applied to after-glow and DC glow discharge plasmas if necessary conditions are satisfied:

- High metastable creation rate or density,
- High Penning ionization rate,
- Short interelectrode distance,
- Low operation voltage,
- Relatively high pressure mediums.

Whenever an electron involves in elastic collision with the neutral gas particle, it loses some portion of its kinetic energy. This value can be deduced from conservation of total kinetic energy and momentum,

$$\delta = 2(1 - \cos(\chi)) \frac{m_e}{M}. \quad (2.16)$$

Here, χ is the scattering angle (rad), m_e mass of electron, M mass of the target atom. δ is the rate of the energy loss. For each of the electrons colliding with the helium gas, energy is lost at about $2 \times (9.109 \times 10^{-31}) / (6.67 \times 10^{-27}) \approx 1.37 \times 10^{-4}$ rate. Time required for electrons

to lose their energy, and gain Maxwellian energy distribution is called relaxation time for the electrons (τ_e),

$$\tau_e = \frac{1}{\delta\nu}, \quad (2.17)$$

where ν is the collision frequency. Electrons move λ_e distance (energy relaxation length) in the relaxation time. λ_e is the critical distance. If the dimension of the plasma is much longer than this value, there is a risk of loss of peak in the EEDF. If electrode distance (L) and plasma pressure (p) satisfy the condition

$$L \times p \approx 3 - 5 [Torr.cm], \quad (2.18)$$

then electrons may not have enough time to relax, plasma will be non-local [29].

To summarize, even at high pressures there is a possibility of conservation of the created Penning electron energies. Non-local plasma condition is one of the sufficient conditions for CES analysis. Furthermore, electric potential configuration of the plasma is another important subject. Total energy of an electron created within an electrostatic plasma ($T.E.$) can be written as,

$$T.E. = \frac{1}{2}m_e v^2 + eV_e. \quad (2.19)$$

Here e is unit charge, V_e is the electric potential value of that point. The electrons created due to Penning ionization:

1. Should not be involved in inelastic collisions (ionization or excitation),
2. Should not be involved in too many elastic collisions, otherwise electrons lose their energy and can not be tracked in the EEDF.
3. Also there should not be any potential difference between the created Penning electrons in different locations of the plasma. Stated in other words, quasi-neutral region should be as equ-potential as possible. Otherwise, electron kinetic energies may vary while the electrons are changing their positions.

In Figure 2.6, short and long cathode discharge configurations are shown. If long cathode discharge is selected for the CES analysis, it may not be possible to correctly detect the Penning electrons in the EEDF due to criteria (3) mentioned above. As stated by Kudravytsev et. al., for a short cathode glow discharge with low electron energy at the center of the discharge it is possible get information about the whole discharge by taking measurements at any point inside [29].

It is possible to obtain energy distribution functions of the electrons in experiments by taking the second derivative of the current-electric potential plot obtained by the probes in the gas discharge [28]. In Figure 2.10(a) this relation is shown.

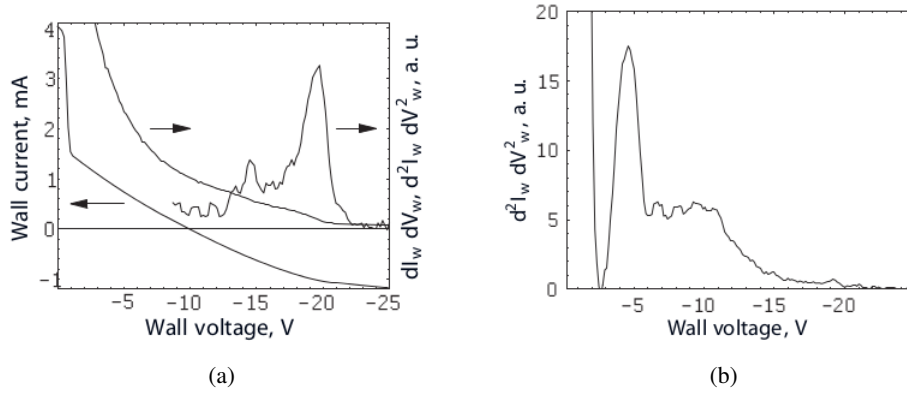
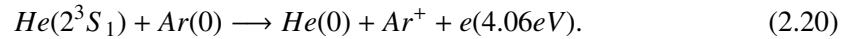


Figure 2.10: (a) Conversion of wall type probe's current-electric potential plot to EEDF [28]; (b) EEDF (with arbitrary units) obtained from wall probe placed in DC He-Ar mixture plasma at 4 Torr [28].

The EEDF results from a previously done experimental CES set-up for helium (95%) and argon (5%) gas mixture short cathode DC glow discharge at 4 Torr pressure is shown in Figure 2.10(b). The maximum near 4 eV is obvious, which is created due to reaction,



For this experiment a wall probe was used [28]. Also Kudryavtsev et. al. experimentally validated the CES theory by using a ring shaped probe at the center of the discharge as seen in Figure 2.11(a). The results of the helium-argon gas mixtures (Figure 2.11(b)) are similar to ones obtained by Demidov et. al.. More experimental results for various helium gas mixtures can be found in the reference [29].

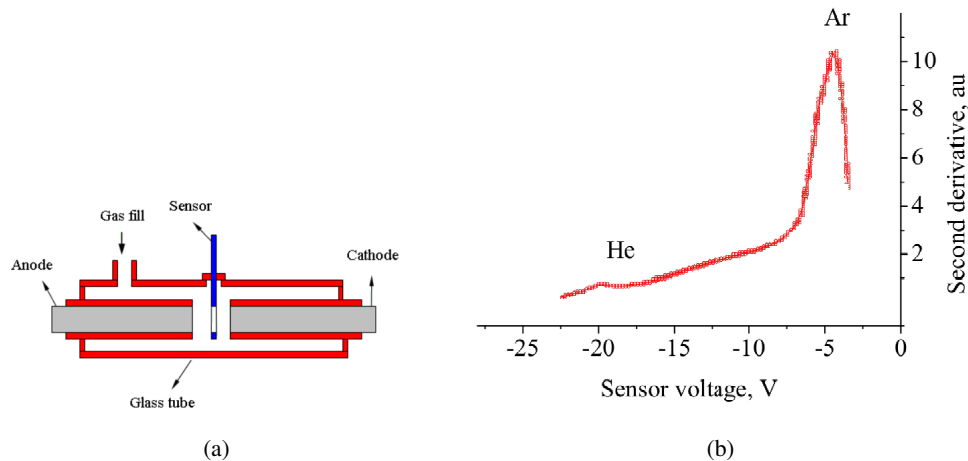


Figure 2.11: (a) View of the ring type probe and the CES gas analyzer [29], (b) EEDF for He-Ar gas mixtures for helium pressure 26 Torr, and 0.4% argon with modulating 1V probe voltage [29].

2.5 Basic Components of Industrial Plasma Sources

In Figure 2.7, the scheme of an reactive ion etcher discharge and the position of the created plasma is given. This is, of course, not the entire setup. A typical industrial plasma source consist of mainly four subsystems, namely: vacuum, gas delivery, cooling and power systems [3]. Below, information about these systems is given in brief.

2.5.1 Vacuum System

The industrial plasmas of interest requires low vacuum values (in general 1 mTorr - 100 Torr). External vacuum systems are essential to reduce the atmospheric pressure to operational pressure. But the necessary base pressure values are much lower, such as 10^{-5} to 10^{-6} Torr, since the foreign gases should be removed from the chamber before the initialization of the process. The system requires enhanced vacuum pumps (such as turbomolecular pumps), which are electronically controlled. Due to high difference between the base and atmospheric pressure, a second pump (forepump) support the turbomolecular pump. Forepump maintains the back pressure between 1-50 mTorr. There is also a third pump in the system, roughing pump, which works at the start up of the operation and which can bring the process chamber to low pressure values (≈ 50 mTorr). If corrosive gasses are used in the process, all the components are selected from chemically inert materials [3]. In Figure 2.12(a) an example of a vacuum system configuration for an industrial gas discharge process chamber is shown.

2.5.2 Gas Delivery System

Industrial gas discharges require a high amount of process gas/gas mixtures during the operation. The reason is high consumption in the plasma. Gas has to be fed uniformly and steadily, and for this reason shower heads are used for delivery. The created waste particles and gasses have to be removed out of the discharge as soon as possible, which require large and firm turbopumps.

2.5.3 Cooling System

As stated previously, one of the greatest advantages of low pressure plasmas is the operation at low temperatures. But during the process, high amounts of heat is dissipated. Some of the excess heat can be removed by cooling of the electrodes. Wafer is the most heat sensitive location in the processes, helium gas is ejected from the back of the wafer, and fairly uniform heat distribution is achieved. In Figure 2.7 helium cooling system can be seen.

2.5.4 Power System

In the industrial systems, electrical power is generally applied in radio-frequency (3 Hz - 300 MHz) or microwave-frequency (300 MHz - 300 GHz). Oscillator generates the signal, and the signal is amplified. Then, match box power is fed into the system by the antenna. An example setup in the case of inductively coupled plasma discharge can be seen in Figure 2.12(b).

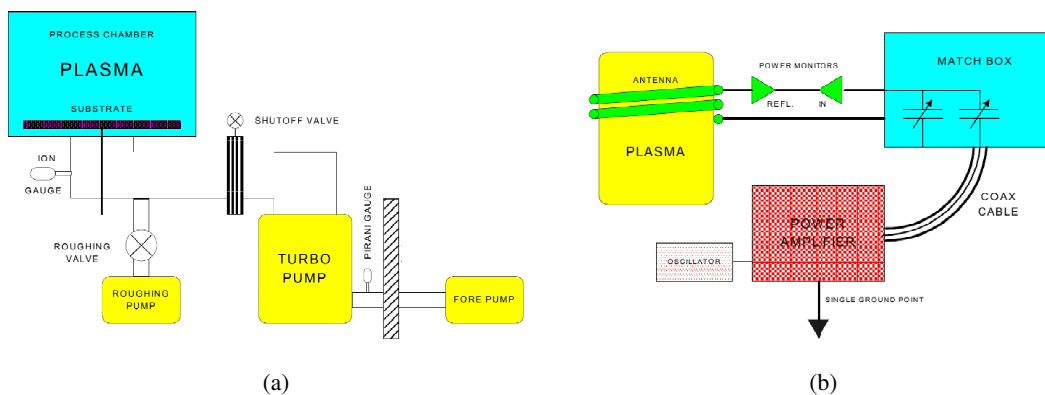


Figure 2.12: Gas discharge plasma source components: (a) Pumping system [3], (b) Power system [3].

2.6 Langmuir Probes

Langmuir probes are specially crafted sensors immersed in plasmas, which can give information about charge densities, electron temperature, and even electron energy distribution function. The probes are produced as thin as possible (generally 0.1-1 mm diameter tungsten material), in order not to effect the plasma conditions. The thin material is encapsulated by ceramic material for insulation. When working with high density plasmas special cautions are taken, although the materials are highly resistant to high temperatures. Langmuir probes may operate in a vacuum, so that the assembly has stainless or glass connectors [3]. Various plasma properties are derived from the voltage-current curve of the probes [3]. In Figure 2.13, an example of Langmuir probe configuration is displayed.

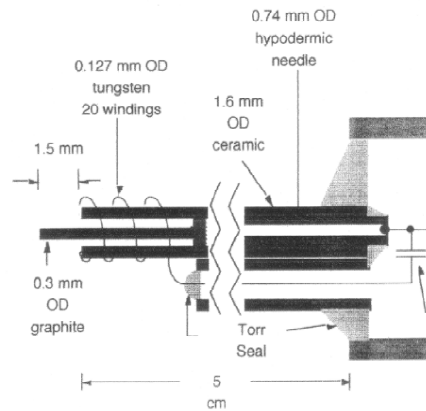


Figure 2.13: A Langmuir probe assembly with carbon probe tip [3].

2.7 Information About Local, Non-Local Plasmas and Maxwellian Distributions

For most of the fluids of interest, relaxation lengths of the particles are very small compared to the flow dimensions. The particles of the fluids have generally enough time and space to do various collisions. Hence, they are close to local thermodynamic equilibrium. Under these circumstances all the properties of a fluid can be described by using density, temperature and three velocity components. Furthermore, it is also possible to obtain the velocity distribution of the particles for an ideal gas under local thermodynamic equilibrium (LTE) [34]. Speed distribution for an ideal gas can be written as

$$f(v) = \sqrt{\left(\frac{m}{2\pi k_B T}\right)^3} 4\pi v^2 \exp\left[\frac{-mv^2}{2k_B T}\right], \quad (2.21)$$

where $f(v)$ is the speed distribution function, m mass of the particle, k_B Boltzmann constant, T temperature in terms of K, v is the speed of the particles.

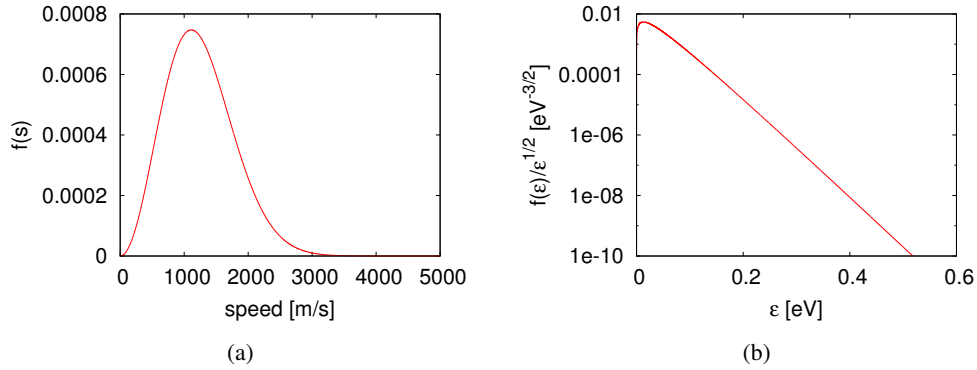


Figure 2.14: LTE helium gas at 298.15 K (a) Speed distribution, (b) energy distribution in logscale.

In Figure 2.14 speed and energy distribution functions of helium gas at 298.15 K can be observed. It should be kept in mind that if energy distribution function for any particle type is a linear line when logarithmic scale is used, then it has Maxwellian distribution (in other words it is in LTE) as in the Figure 2.14(b). However, LTE can not always be satisfied for some fluids or plasmas of interest, so it may not be possible to use moment equations to model them.

Example of both locality and non-locality are given by the help of a Townsend discharge simulation. Detailed information about the Townsend discharge simulations will be discussed in Chapter 6. In Figure 2.15, collective movement and multiplication process of electrons initiated from the cathode region of the Townsend discharge can be observed. Distance between the electrodes (L) is 4 cm, gas temperature (T) 300 K, and pressure is 41.4 Pa . In Figure 2.16, pressure is set to 4.14 Pa, at which the mean free path of the electrons is longer due to lowered pressure. Both simulations differ only in pressure, which effect E/n values. In Figure 2.15, electrons simultaneously multiply, drift, and diffuse until they are absorbed by the boundaries. But for the lower density simulation, the same phenomenon cannot be observed. Electrons run out the boundaries before generating group motion. Hence, the second discharge is a non-local one for the electrons.

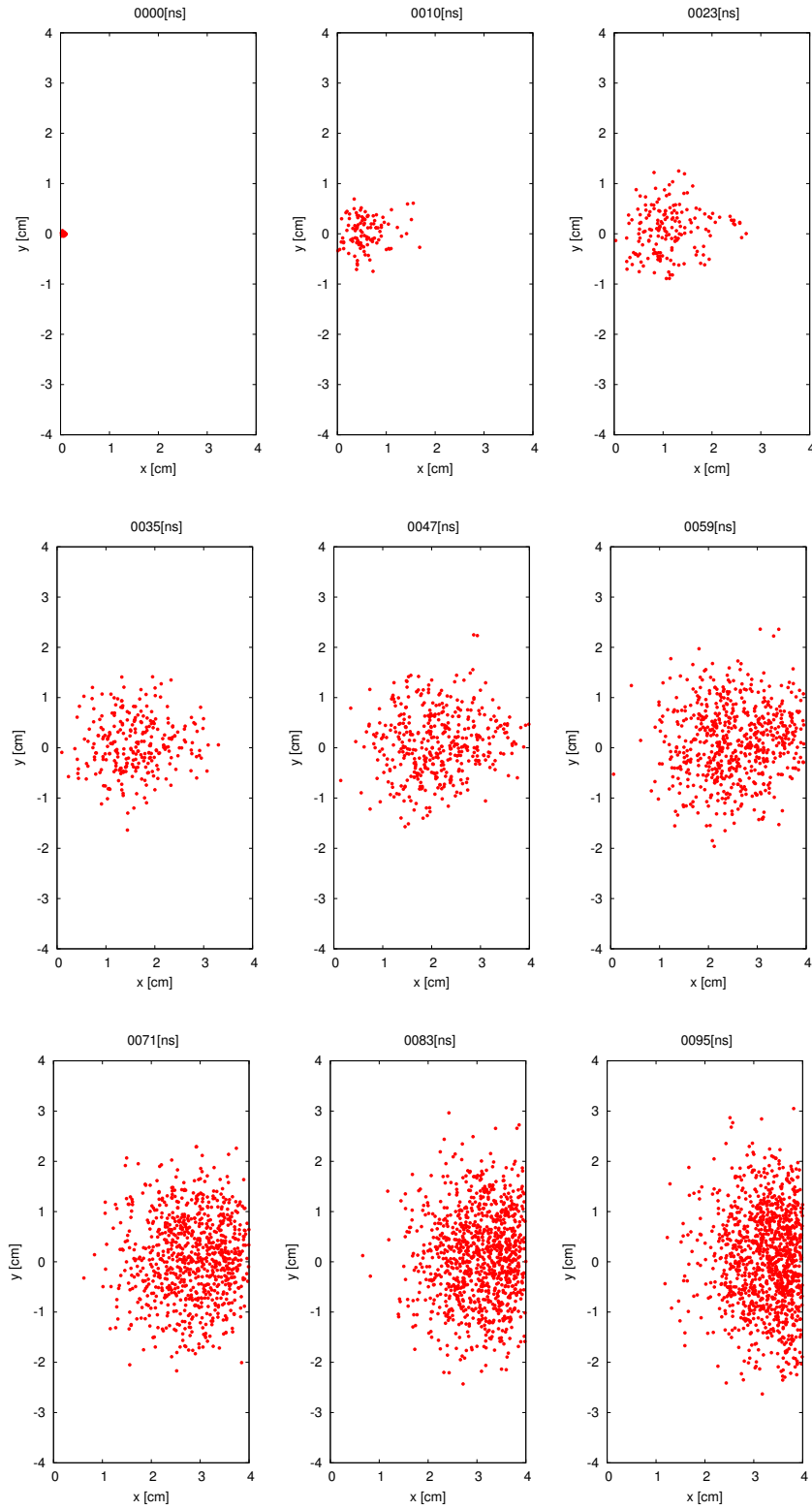


Figure 2.15: DC Townsend discharge helium gas electron swarm simulation. Helium gas at 41.4 Pa, temp. 300 K, 4 cm electrode distance. $E/n=500$ Td. Number of electrons at the start is 100

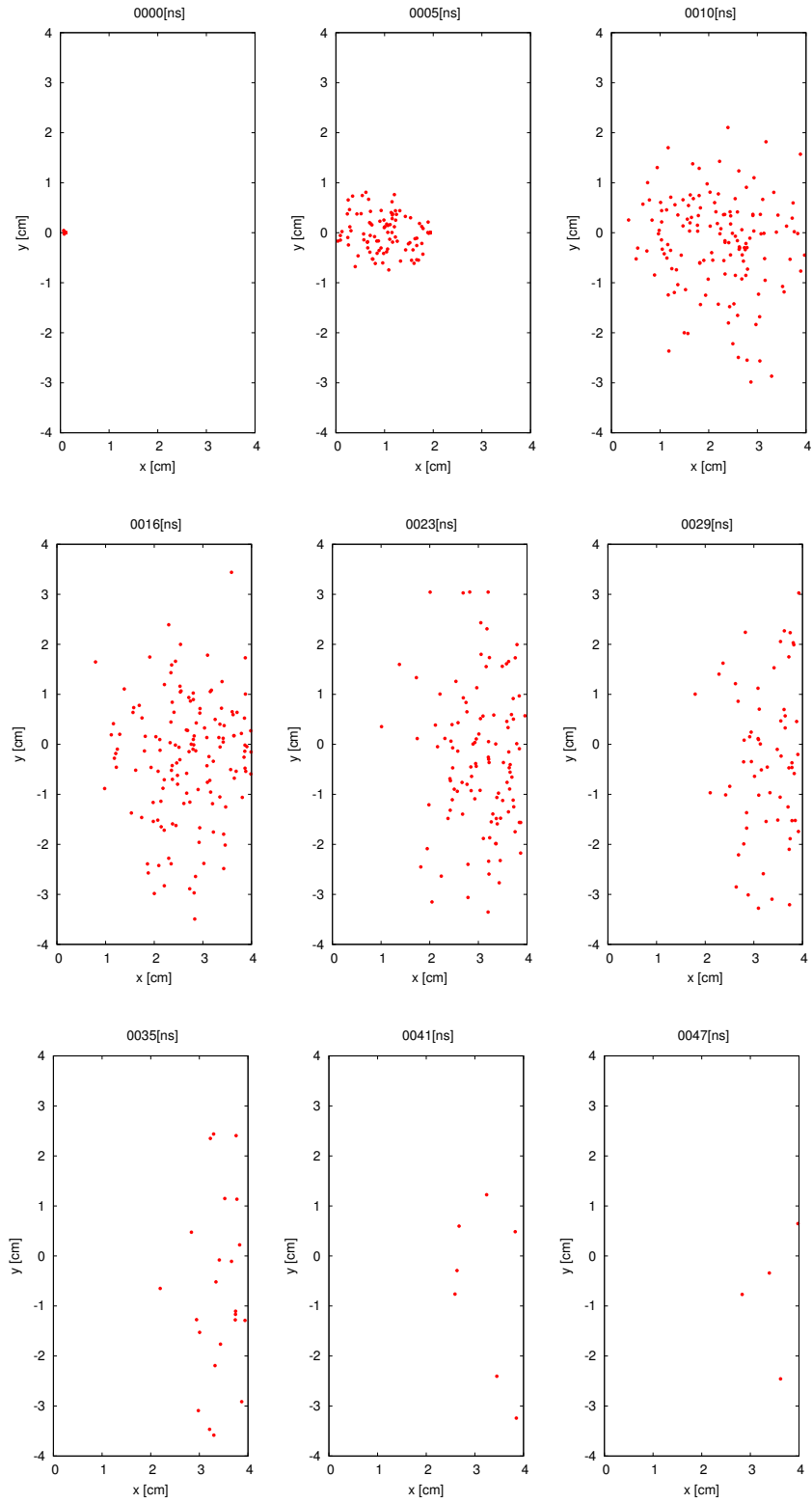


Figure 2.16: DC Townsend discharge helium gas electron swarm simulation. Helium gas at 4.14 Pa, temp. 300 K, 4 cm electrode distance. $E/n=5000$ Td. Number of electrons at the start is 100

2.7.1 Basic Numerical Modeling Techniques for Plasmas

2.7.1.1 Kinetic Approach

Boltzmann equation for each species in the plasma can be written as

$$\frac{\partial f}{\partial t} + \mathbf{v} \cdot \nabla_r f + \frac{\mathbf{F}}{m} \cdot \nabla_v f = \left. \frac{\partial f}{\partial t} \right|_{\text{collision}}, \quad (2.22)$$

$$\mathbf{F} = q(\mathbf{E} + \mathbf{v} \times \mathbf{B}), \quad (2.23)$$

where f is defined as distribution function dependent on position, velocity and time, \mathbf{F} force field, \mathbf{v} velocity field, \mathbf{E} electric field and \mathbf{B} magnetic field respectively. The equations for each of the species are coupled with the appropriate Maxwell equations, and solved using some approximations such as two-term expansion. However, it is not easy to solve this equation. Even in one dimensional simulations kinetic models have high degree of freedom [38].

2.7.1.2 Fluid/Continuum Approach

It is possible to model the plasmas by using continuum or fluid equations. Fluid equations are obtained by taking the integral moments of the Boltzmann equation in the velocity space. The zeroth moment leads to continuity. The first is conservation of momentum equations and second is conservation of energy. The simplest fluid model for the electrostatic plasmas employs the first two moments (conservation of mass and momentum) for each species in the discharge and coupled with the Poisson's equation via electric field. Equations are closed by setting the boundary conditions. Here are the equations for the two component system which consist of electrons and ions:

$$\frac{\partial n_e}{\partial t} + \nabla \cdot (n_e \mathbf{v}_e) = S_e, \quad (2.24)$$

$$\frac{\partial n_i}{\partial t} + \nabla \cdot (n_i \mathbf{v}_i) = S_i, \quad (2.25)$$

$$\mathbf{\Gamma}_e = n_e \mathbf{v}_e = -n_e \mu_e \mathbf{E} - \nabla(n_e D_e), \quad (2.26)$$

$$\mathbf{\Gamma}_i = n_i \mathbf{v}_i = n_i \mu_i \mathbf{E} - \nabla(n_i D_i), \quad (2.27)$$

$$\nabla^2 V = -\frac{e}{\epsilon_0}(n_i - n_e), \quad (2.28)$$

where n_e and n_i are the number of particles per volume, $\mathbf{\Gamma}_e$ and $\mathbf{\Gamma}_i$ fluxes, μ_e and μ_i mobility coefficients, D_e and D_i diffusion coefficients, S_e and S_i source terms for electrons and ions respectively. e is the unit charge and ϵ_0 is permittivity of free space [4]. At the cathode, $\mathbf{\Gamma}_e$ and $\mathbf{\Gamma}_i$ are related to each other by the secondary electron yield,

$$|\mathbf{\Gamma}_e| = \gamma |\mathbf{\Gamma}_i|, \quad (2.29)$$

where γ is the secondary electron yield coefficient. Secondary electron yield coefficient determines the emission rate of secondary particles at boundaries. Electric potential values at the

boundaries which are required to solve the Poisson's equations are in general Dirichlet type. Mobility, diffusion, and source terms are calculated according to the local values of the E/n , where n is the neutral gas particles per volume. E/n is, in general, given in terms of Td, where $1 \text{ Td} = 10^{-17} \text{ V cm}^2$ [4, 39].

Although fluid models are self-consistent, one should always be careful when modeling the glow discharges, because of two reasons:

1. The drift-diffusion approximation assumes local-thermodynamic equilibrium for each of the species, which may not be correct for non-local plasmas where mean free path (λ) of the particles may not be short enough compared to the plasma dimension
2. Using the local values of E/n when calculating the mobility, diffusion and source terms requires slowly changing or constant E at the position. The inequality below should be satisfied,

$$\lambda \frac{dE}{dx} \ll E. \quad (2.30)$$

According to Derzsi. et. al [23], for the selected set of parameters, fluid models are far from correctly modeling the low pressure low temperature gas discharge plasmas. Results of different simulation techniques and comparisons with the experimental density profiles obtained with a Langmuir probe measurement are given in the mentioned study, and solution with the pure fluid approach is far from accuracy.

2.7.1.3 Hybrid Approach

Ionization source in the fluid equations are calculated by Monte Carlo models of the fast electrons (which are able to create inelastic collisions). Rest of the particles, ions and slow electrons are treated as fluids. The method requires less system resources compared to the pure particle models, but benefits from their accuracy. In some advanced hybrid models, heavy ions and fast neutral particles are also tracked. More information about the approach can be found in the study of Donkó et. al. [4].

CHAPTER 3

PARTICLE IN CELL METHOD FOR LOW PRESSURE GLOW DISCHARGES: NUMERICAL METHOD, PARALLELIZATION AND SUBCYCLING

The main aim of this study is to correctly model and understand the low pressure glow discharge plasmas with parallel Particle in Cell/Monte Carlo Collision Method (PIC/MCC), so that the work can be extended and applied for the industrial applications.

3.1 PIC/MCC Model

Unlike continuum methods, PIC/MCC method deals with the charged super particles. Each super particle consist of predefined number of particles of the same type (i.e. electrons, Ar⁺, He⁺ ions etc.), and this number is called weighting (W) of the super particle. The algorithm of interest can be summarized as the following.

1. *Initialization:* At first step, charged particles are distributed between the boundaries according to selected density profile. Uniform random distribution is one of the choices. Velocity components of the particles are specified using a Maxwellian distribution in Cartesian coordinate system as

$$v_s = \sqrt{-\ln(R_1) \times 2k_B T/m} \times \sin(2\pi R_2), \quad (3.1)$$

where v_s is any of the three components (v_x , v_y , and v_z) [40]. Here k_B , T and m denote the Boltzmann constant, temperature and mass of the selected particle type respectively. Variables R_1 and R_2 refer to random numbers with uniform distribution between [0,1].

2. *Calculation of charged particle densities on grid points:* Now that positions of super particles are known, one can find the particle densities on the grid points by using appropriate weighting method. In this study first order weighting is used [11]. In one-dimensional system, densities n_{pk} and n_{pk+1} of particles of type p on the two neighbour grid nodes k and $k + 1$ are calculated using

$$n_{pk} = W_p \sum_{j=1}^N \frac{\Delta X_{j,k+1}}{\Delta x \Delta V}, \quad n_{pk+1} = W_p \sum_{j=1}^N \frac{\Delta X_{j,k}}{\Delta x \Delta V}, \quad (3.2)$$

where W_p is weighting of selected particle type, Δx is the size of the grid cell, $\Delta X_{j,k}$ and $\Delta X_{j,k+1}$ are the distances from the j th particle to the k and $k + 1$ nodes, N is the number of super particles of type p locating between these nodes, $\Delta V = \Delta x \Delta y \Delta z$ is the volume element, where Δy and Δz are equal to one unit of length in the one-dimensional system.

3. *Solution of Poisson's equation:* For a system with M types of charged plasma components, electric potential profile V for the electrostatic plasmas of interest can be calculated by solving the Poisson's equation

$$\nabla^2 V = -\frac{1}{\varepsilon_0} \sum_{p=1}^M n_p q_p, \quad (3.3)$$

where ε_0 is the permittivity of free space, q_p is the charge of the particle of type p .

4. *Electric field calculation:* After obtaining the electric potential profile, electric field value E on grid points is obtained using equation

$$\mathbf{E} = -\nabla V \quad (3.4)$$

with finite difference method. Fourth order central difference scheme for the inner nodes, forward and backward finite differences for the boundary nodes have been used in the simulations.

5. *Interpolation of electric field values to charged particles:* Electric field values on the grid points are interpolated to charged particles to obtain forces acting on them.
6. *Solution of Lorentz equation, and implementation of boundary conditions:* Equations

$$\frac{d\mathbf{r}_j}{dt} = \mathbf{v}_j \quad (3.5)$$

$$\frac{d\mathbf{v}_j}{dt} = \frac{q_j}{m_j} \mathbf{E}_j \quad (3.6)$$

are solved to determine positions and velocity components of the charged particles. Here q_j , m_j , \mathbf{r}_j , \mathbf{v}_j , and \mathbf{E}_j denote the charge, mass, position and velocity of the j th particle, and the electric field acting on it. We have used explicit velocity-verlet algorithm to advance the particles to new positions and update the velocity components. After manipulating the positions, the out of boundary particles are checked and deleted if they don't reflect. Secondary electrons are added to the system if the yield is included in the model. Reflection and secondary electron yield cases are decided using Monte Carlo algorithm by comparing random numbers to coefficients of interaction.

7. *Collisions:* In the low pressure plasmas of interest, charged particle densities are at least 3-4 orders of magnitude lower than the neutral background gas. Since in general neutral-charge particle collisions dominate the collision processes, only electron-neutral and ion-neutral collisions are taken into account for the problem of interests in

this study. Also metastables creation and interreactions are relatively low at low pressures of interest [41], hence we have not included stepwise ionizations and metastables in the low-pressure simulations. Ion-neutral collisions were modeled with hard-sphere approach by using isotropic and backward collision cross section data of the related gasses. Probability of collision of each super particle is:

$$P_j = 1 - \exp(-\nu_j \Delta t). \quad (3.7)$$

However doing calculation for all of the super particles can be time and task force consuming. Therefore, special algorithms such as null collision [16] can be applied to set which particle will collide. In this method, collision frequency for all the particles is set to be equal to maximum possible collision frequency. Some artificial collision frequency is added to all charged particles of interest,

$$\nu_{max} = \nu + \nu_{artificial}. \quad (3.8)$$

Here ν is the real collision frequency of the particle, $\nu_{artificial}$ artificial collision frequency, and ν_{max} maximum collision frequency. One could easily determine the possible number of collisions if all the charged particles had the maximum collision frequency,

$$N_{mc} = N \times P_{max} \quad (3.9)$$

$$= N \times (1 - e^{-\nu_{max} \Delta t}) \quad (3.10)$$

where N_{mc} , N and P_{max} are maximum number of possible collisions, number of particles and maximum possible collision probability. Then N_{mc} particles are randomly selected from the stack, and the real collision probability of each selected particles is found

$$P_{real} = 1 - e^{-\nu \Delta t}. \quad (3.11)$$

Then P_{real}/P_{max} value of each of the selection is compared with a random number to determine if there is collision or not for the selected particle. After the colliding particles are selected, types of collisions are identified by a Monte Carlo check according to illustrated algorithm in Figure 3.1. It should be underlined that collision cross sections for ion-neutral collisions are calculated by using centre of mass energy [42]. After collision types are determined for each of the charged particles, then new velocity components are assigned to collided ones. Whenever an electron does elastic collision with the neutral gas particle, it loses some portion of its kinetic energy.

$$\delta = 2(1 - \cos(\chi)) \frac{m_e}{M}, \quad (3.12)$$

Here, χ is the scattering angle (rad), m_e mass of electron, M mass of target atom. δ is the rate of the energy loss. Above equation can be deduced from conservation of total kinetic energy and momentum. For excitation, electron loses its predefined energy (dependent on the excitation level) and the new energy of the electron is calculated by

$$E_{scatter} = E_{incident} - E_{excitation}. \quad (3.13)$$

For ionization, electrons also loses energy (i.e. 15.8 eV for one step ionization of argon) and remaining energy is divided between the electrons,

$$E_{new} = E_{scatter} = (E_{incident} - E_{ionization})/2 \quad (3.14)$$

The energies and the speeds of the electrons are now known. It is now time to determine the new direction of the velocity vector. In general all electron collisions are taken to be isotropic. Two angles are required to determine the new velocity components, namely azimuth (η) and scattering (χ) angle. These angles are determined by using uniform random numbers between [0,1) (R_4 and R_5) again. Particle velocities are rotated according to Figure 3.2.

$$\eta = \arccos(1 - 2R_4), \quad (3.15)$$

$$\chi = 2\pi R_5. \quad (3.16)$$

Rotation in the lab frame can done with the help of matrix algebra,

$$\mathbf{v}' = \begin{bmatrix} \cos\theta & -\sin\theta & 0 \\ \sin\theta \cos\phi & \cos\theta \cos\phi & -\sin\phi \\ \sin\theta \sin\phi & \cos\theta \sin\phi & \cos\phi \end{bmatrix} \begin{bmatrix} \cos\chi \\ \sin\chi \cos\eta \\ \sin\chi \sin\eta \end{bmatrix}, \quad (3.17)$$

Where \mathbf{v}' is the new velocity vector after the collision. θ and ϕ are the pre-collision velocity angles, which can be determined from the equation,

$$\mathbf{v} = \begin{bmatrix} v_x \\ v_y \\ v_z \end{bmatrix} = \begin{bmatrix} \cos\theta \\ \sin\theta \cos\phi \\ \sin\theta \sin\phi \end{bmatrix}, \quad (3.18)$$

where \mathbf{v} is the pre-collision velocity vector. After these steps the algorithm returns back to step (ii) until convergence is obtained. The single processor (serial) PIC/MCC algorithm is summarized in Figure 3.3

3.1.1 Determination of Time Step Size (Δt), and Grid Size (Δx)

It is best to select grid size at the start. Grid size should be of the order of Debye length,

$$\lambda_D = \sqrt{\frac{\epsilon_0 k_B T_e}{n_e q_e^2}}, \quad (3.19)$$

where λ_D , T_e , n_e and q_e are Debye length, electron temperature, electron density and charge of the electron. During the simulation, since density values and electron temperature can change, assumptions for these two variables should be made. n_e can be taken as guessed

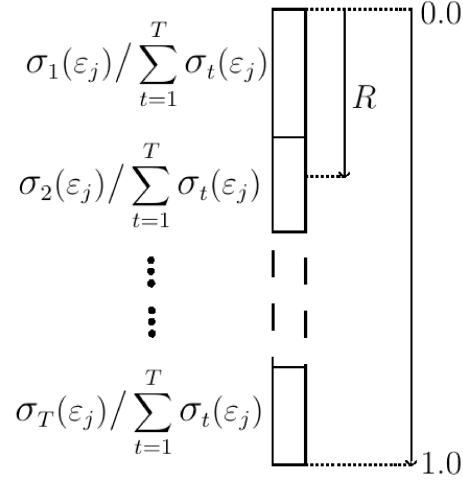


Figure 3.1: Selection of the collision type for a particle j , which can possibly do T types of collisions. Here $\sigma_t(\epsilon_j)$ is collision cross section of the particle for the specific collision type t . Energy of the particle j is denoted by ϵ_j .

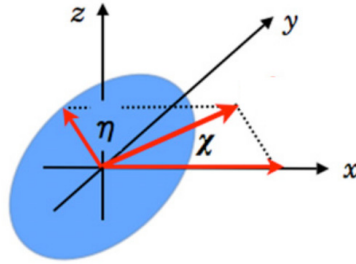


Figure 3.2: Azimuth and scatter angles in the collision frame. Note that azimuth angle is in yz plane [14].

maximum density value that can be obtained, and T_e can be taken as ambient temperature. Finally the guessed λ_D can be taken as Δx . In order to have a good statistics, there should be a reasonably high number of particles per Debye length, $N_D \gg 1$. Also, there are constraints while selecting space step Δx and time step Δt during the simulations: Δx must be of the order of the Debye length, and Δt should resolve oscillations of electrons, satisfy the Courant condition, and be sufficiently small to keep collision probability (3.7) reasonably small (for further details, see [14]). In general, for low pressure gas discharge simulations, the Courant condition

$$\Delta t < \Delta x / v_{\max} \quad (3.20)$$

is the most restrictive one. If it is not satisfied, particles may not move correctly and discontinuities in the total current profile may arise. To find the maximum possible speed v_{\max} , one can track the maximum velocity in the electron group in every time step, and set Δt ac-

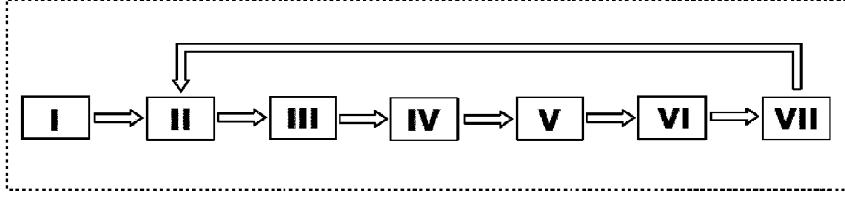


Figure 3.3: Single processor PIC/MCC algorithm. I) Initialization, II) Calculation of charged particle densities on grid points, III) Solution of Poisson’s equation, IV) Electric field calculation V) Interpolation of electric field values to charged particles, VI) Solution of Lorentz equations and implementation of boundary conditions, VII) Collisions.

cordingly. This is not an efficient approach, especially for the parallel codes. In our codes, maximum possible energy obtained by an electron during the simulations can be taken as absolute difference between the electrode potentials plus some arbitrary value (say 100 eV). The specified energy is converted to the maximum possible speed v_{\max} for the electrons, which can be used to calculate the time step size Δt . This algorithm is more efficient and much easier to implement.

3.2 The Parallel Algorithm

Imagine a big fast food restaurant, with plenty of workers efficiently working on food preparation. If there is only one pay desk, it is easy to say a long que is created in-front of it. This example is very appropriate for parallel programming. One may add many processors to a parallel system, but if there is a bottle neck situation on substantial portion of the code where program can not be parallelized, then the program may not run efficiently [43]. Imagine a cluster with n processors. Now, think about a program which can be finished by a single processor in 1 unit time. And this program can be parallelized in the ratio of p , then the non-parallelized ratio is $(1-p)$. In theory, this program can be complete by n processors in

$$(1 - p) + \frac{p}{n} \tag{3.21}$$

units of time. If one had unlimited computer resources, which means n goes to infinity, by taking the limit of req 3.21, we have

$$\lim_{n \rightarrow \infty} \left((1 - p) + \frac{p}{n} \right) = 1 - p, \tag{3.22}$$

which means the program can be finished in $1-p$ time. If there are non-parallelizable parts in a program, then the speed-up is limited. For example, for a program which is parallelizable by 80%, the speed up can be at most 5 times. If the user want to achive efficient and fast computation, the code should be parallelizable at least in the rate of 90%.

Figure 3.4 represents theoretical speed up of a program depending on how many processors are used and percent program parallelizable. Although the figure is theoretical, since communication and synchronization take time, it gives the idea of using more processors is not

always as efficient as it is expected. Algorithms and schemes used have special importance for the computational time. There are different parallelization schemes for PIC/MCC model. Now these approaches will be evaluated in terms of parallelization and coding efficiency.

For each processing unit or worker the number of calculations per second is limited. It is reasonable to reduce the work/process done by each of them by parallelization to progress faster in time steps and consequently to reduce simulation times. There are mainly two types of parallelization schemes for PIC/MCC method: (1) Each of the processors/workers/CPU's are responsible from certain regions of the discharge; (2) All the workers are responsible from all of the grid nodes between the electrodes, but not from all the particles. In the latter case, super particle population is equally shared among the workers as much as possible. The first scheme has some disadvantages compared to the second one. These are

- (i) The processors responsible from the border nodes are also assigned to manipulate the secondary electrons as well as to reflect the particles reaching the boundaries or remove them from the system. Therefore, there is a coding differentiation between the boundary and the inner workers, which makes coding more challenging.
- (ii) Super particles are not static, they move over time. Consequently they may not stay assigned to the same CPU or location. In every time step of the simulations, particles may move from one grid point to another, i.e. from one worker to another. This situation creates extra communication, and one worker must be assigned to deal with the arrangements of the charged super particles between the processors.
- (iii) If CPU's are responsible from equal number of grid points, then the CPU's responsible from quasi-neutral region of plasma deal with much more super particles than the ones accounted for the sheet regions. Hence the equal division of the work load may not be possible if this method is applied.

Our codes were developed according to the second scheme. With slight modifications, a standard single processor PIC/MCC code can be parallelized. Respectively, after the processors have calculated partial density profiles, these are sent to a predefined worker. (In our code processor #0 is assigned to this job, i.e. the master worker/processor). Master processor adds up all the density values coming from the other workers. Figure 3.5 illustrates the ion density profile contributed by one of the C workers and the overall ion density profile after the ion densities collected by the master worker. As the total density profile is computed by the master processor, the Poisson's equation can be solved,

$$\nabla^2 V = -\frac{1}{\epsilon_0} \sum_{c=0}^{C-1} \left(\sum_{p=1}^M n_p q_p \right)_c, \quad (3.23)$$

where C is the total number of processors. Master processor also calculates and broadcasts (CALL MPI_Bcast in MPI implementation of the fortran code) the electric field values. Processors only communicate at this part of the method. Summary of the parallel algorithm is shown in Figure 3.6.

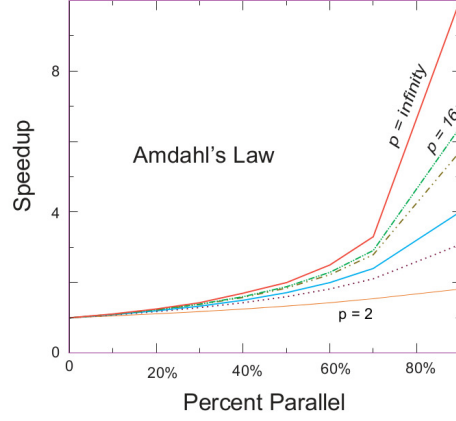


Figure 3.4: The theoretical speedup of a program as a function of the parallelized fraction of the program [43].

3.3 Subcycling

In addition to the parallelization, subcycling of ions and slow electrons can be used to speed up the simulations [22]. Using this approach, ions and low energetic (slow) electrons are moved and collided not in every, but in S_{se} 'th (slow electron subcycling coefficient) and S_i 'th (ion subcycling coefficient) time steps. Within this method, high gains can be obtained in terms of computational time.

Critical value of electron velocity, separating electrons into fast and slow subgroups, can be obtained from the Courant condition, $v_{e,crit} \leq \Delta x / (\Delta t S_{se})$. Additional restrictions imposed on the time step Δt

$$P_{se} = 1 - \exp(-v_{e,max} (S_{se}\Delta t)) \ll 1, \quad (3.24)$$

$$P_i = 1 - \exp(-v_{i,max} (S_i\Delta t)) \ll 1, \quad (3.25)$$

are required to keep collision probabilities of slow electrons and ions reasonably small [16]. Here $v_{e,max}$ and $v_{i,max}$ denote maximum values of total collision frequencies for electrons and ions respectively.

Slow electrons in sheet regions of discharge (including electrons emitted from the electrodes) may gain high velocities, thus violate the Courant condition before being transferred into the fast electron group. Therefore, in order to ensure reliable numerical results, all the sheet electrons are treated as fast ones and never subcycled.

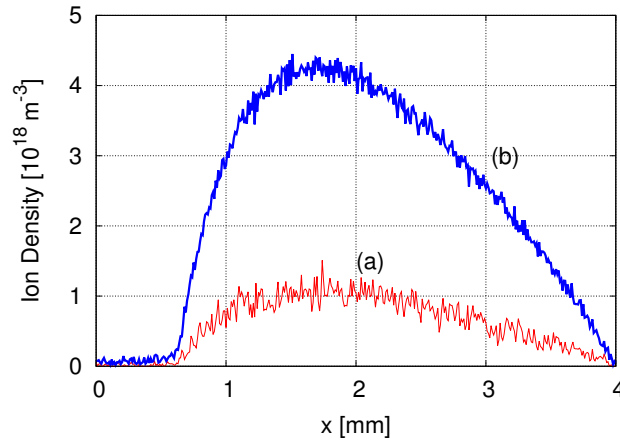


Figure 3.5: Example of parallel system with 4 processors: (a) ion densities [10^{18} m^{-3}] accounted by the processor #1 (b) global sum of the ion densities computed by the master worker.

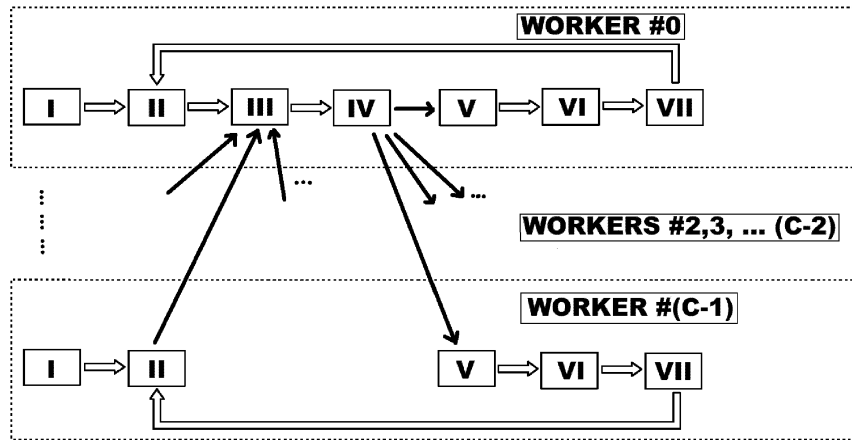


Figure 3.6: Parallel PIC/MCC algorithm for a system with C processors. Black arrows refer to a communication between the processors (MPI_Reduce & MPI_Bcast). Processor #0 is the master processor, responsible for density collection, electric potential and electric field calculation and delivering the results to remaining workers. I) Initialization, II) Calculation of charged particle densities on grid points, III) Solution of Poisson's equation, IV) Electric field calculation, V) Interpolation of electric field values to charged particles, VI) Solution of Lorentz equations and implementation of boundary conditions, VII) Collisions.

CHAPTER 4

VALIDATION OF THE PARALLEL PIC/MCC CODES

In this part of the thesis study, three different PIC/MCC examples were investigated and the results obtained were compared with the previously done studies. Schematic of the capacitively coupled gas discharge is given in Figure 4.1. The first two examples are for comparison or benchmarking only. In other words, only to display the reliability of the produced codes. A more detailed analysis for RF gas discharges is given in the third example.

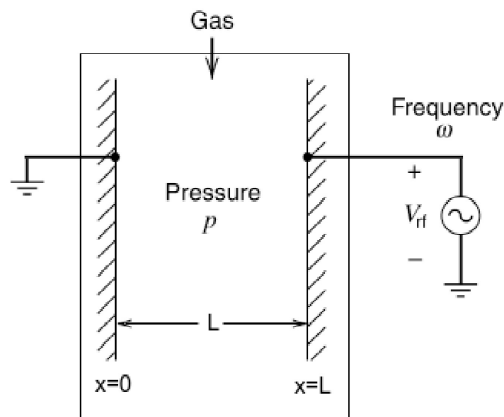


Figure 4.1: Schematic of the capacitively coupled RF gas discharge.

4.1 Helium RF Glow Discharge PIC/MCC Example

The conditions of the benchmark case II in Ref. [24] are employed to validate the performance of parallel 1d3v PIC/MCC code. Plasma of capacitive RF discharge in helium of density $32.1 \times 10^{20} \text{ m}^{-3}$ and temperature 300 K with parallel electrode configuration of amplitude 250 V and frequency 13.56 MHz is considered. Separation between the electrodes is 6.7 cm. (More details about the input and solution parameters can be found in the specified reference.) Code is implemented in Fortran 90 and carried out using a computer with Intel Core *i*7 CPU.

Comparison of the reference and the recent study results is given in Figure 4.3. Maximum relative error for the ion density profiles is found to be about 0.0165, which is quite satisfying for particle simulations.

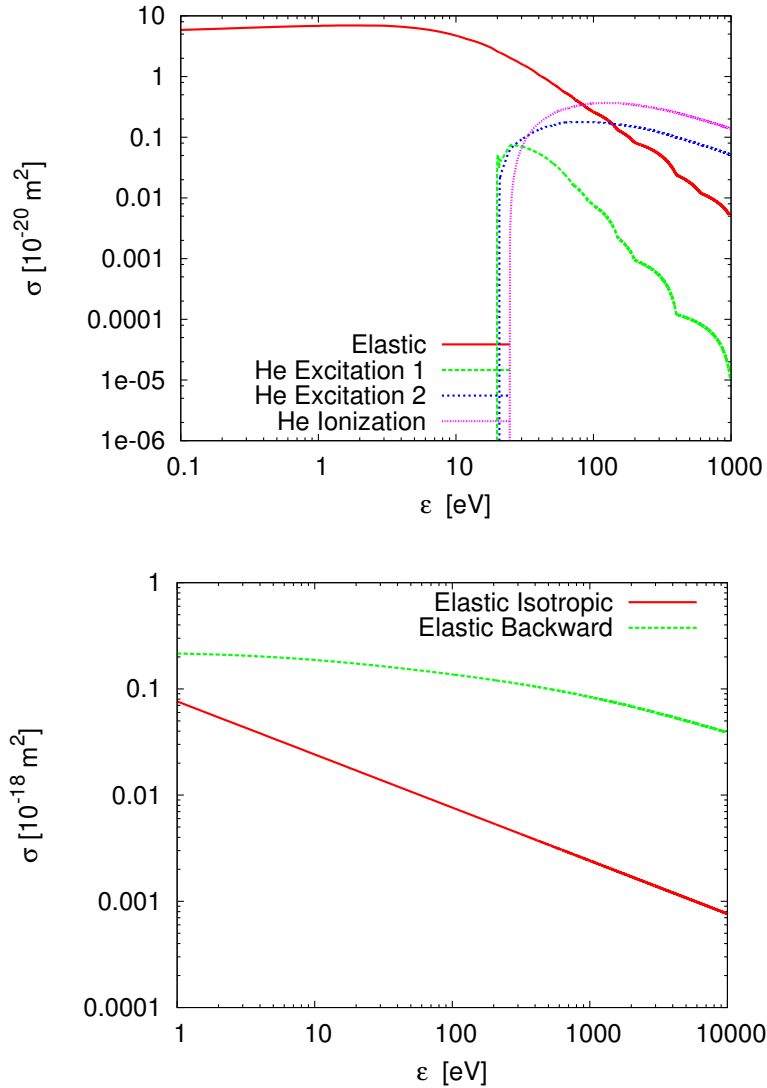


Figure 4.2: Collision cross sections used in the simulations for helium gas: (a) electron-neutral, (b) ion-neutral.

4.2 Argon RF Glow Discharge PIC/MCC Example

Glow discharges in terms of ionization source can be categorized into two, namely α and γ types. For α mode, ionization is mainly created in the sheath boundaries due to fluctuation of the electric field. On the other hand, for γ mode ionization is mainly created due to secondary

electrons emitted from the electrodes. Sheath voltage gradients are relatively high in the later type.

Test PIC/MCC simulation problem is taken from reference [44]. In this reference pure argon gas discharges for both α and γ modes were investigated. We have modeled discharges with the same input parameters, also selected the same collision cross sections as in the ref. [44] (Figure 2.2). But not enough information about the simulation parameters (such as number of grid points and number of super particles used) was given in the selected article. By selecting 601 grid points and using approximately 200,000 super particle, sufficiently close results were obtained (as guessed solution parameters). Although we are not able to compare spatio-temporal plots quantitatively, the results seem to be within 80-90% accuracy limit. As expected for both of the simulations, all the results are periodic with a period of $1/(13.56\text{ MHz}) = 73.7 \times 10^{-9}$ seconds.

4.2.1 α -Type Glow Discharge Analysis Results

In this section α type radio-frequency (RF) argon gas discharge problem considered in the reference [44] is investigated. Effect of the secondary electrons are neglected. Problem parameters selected as 80 Pa gas pressure and 350 K temperature, 100 V electrode potential difference, 1.5 cm electrode separation, $\gamma = 0$.

Spatio-temporal plots for electron density, electric field, and electron heating rates are given in Figure 4.4 and 4.5. In Figure 4.4-b electric field plot is given with different colormap to display more detailed information about the sheath regions of the discharge. Results from the reference is given in Figure 4.6.

4.2.2 γ -Type Glow Discharge Analysis Results

Problem parameters selected as 80 Pa gas pressure and 350 K temperature, 200 V electrode potential difference, 1.5 cm electrode separation, $\gamma = 0.2$. This problem has different electrode potential and secondary electron yield coefficient compared to the α type. Results of the current study are presented in Figures 4.7 and 4.8. The results of the reference [44] are seen in Figure 4.9.

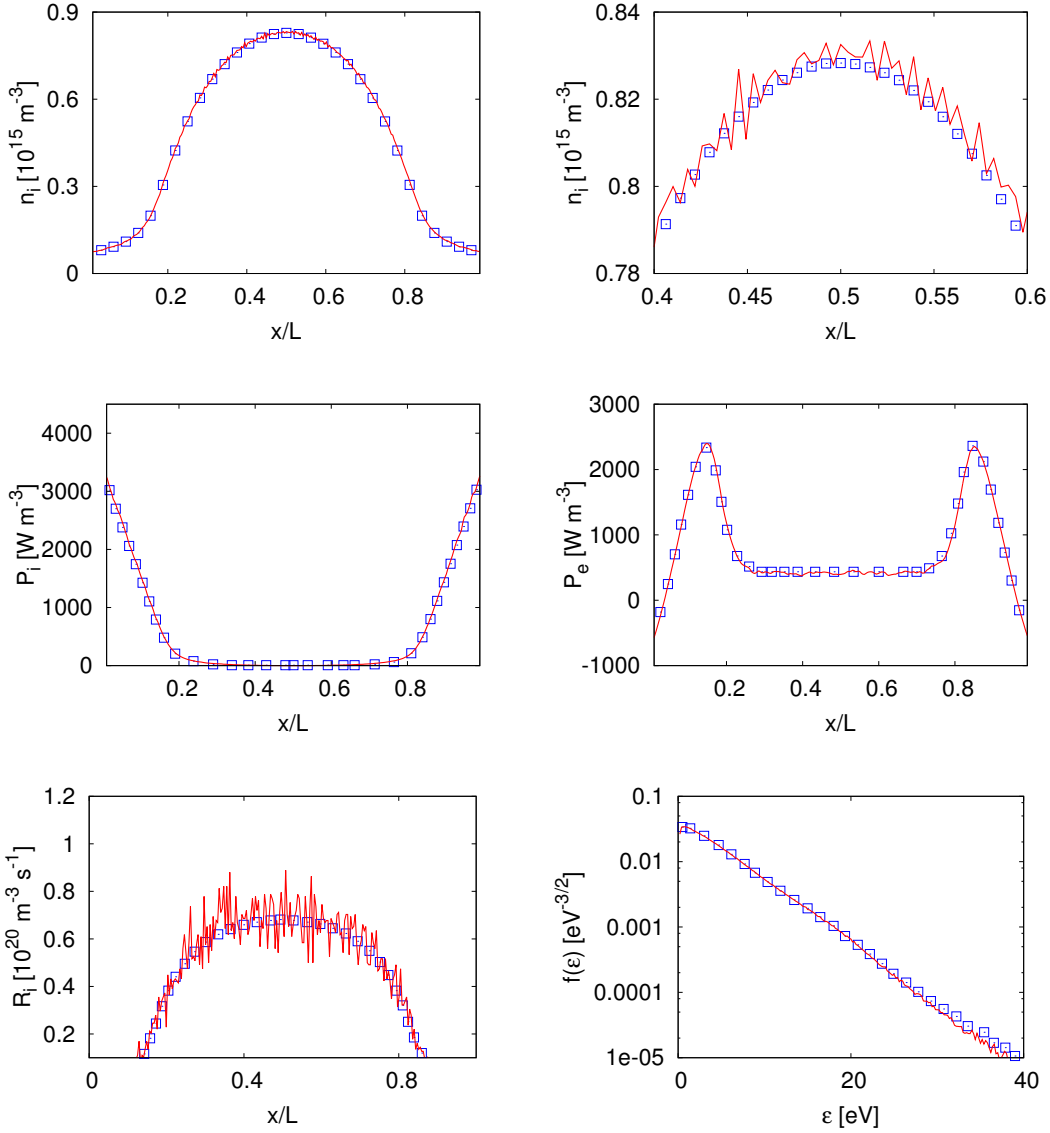
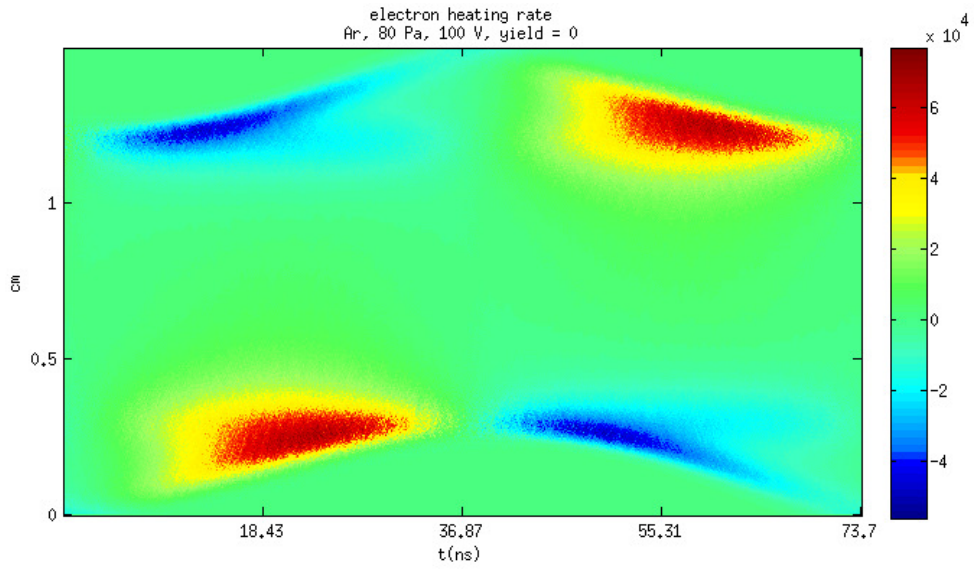
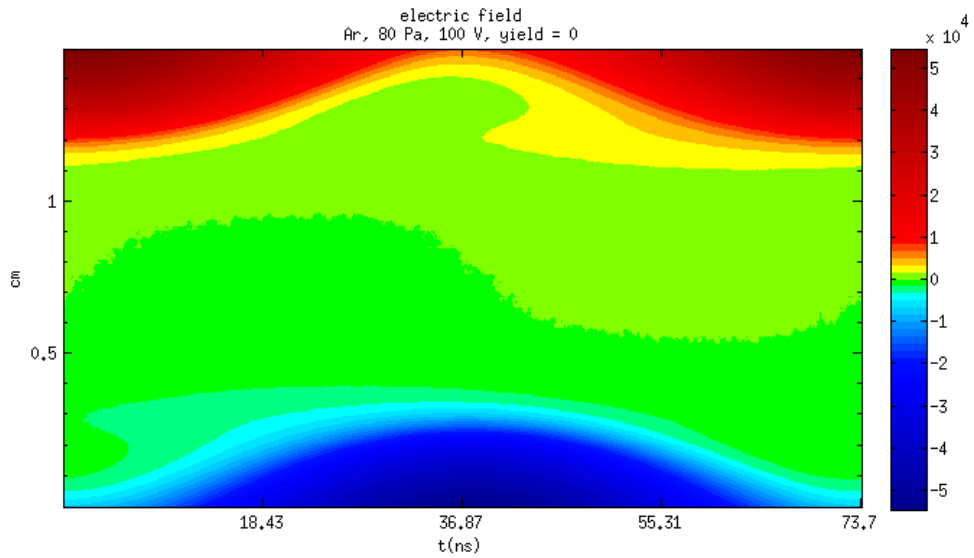


Figure 4.3: Comparison with the previously done PIC/MCC study [24]. The symbol \square refers to the case II in [24], and continuous linesto recent study. (a) Ion density profile, (b) ion density profile at the center of the discharge, (c) ion heating rate, (d) electron heating rate, (e) ionization source , (f) normalized electron energy distribution function $f(\varepsilon)$.

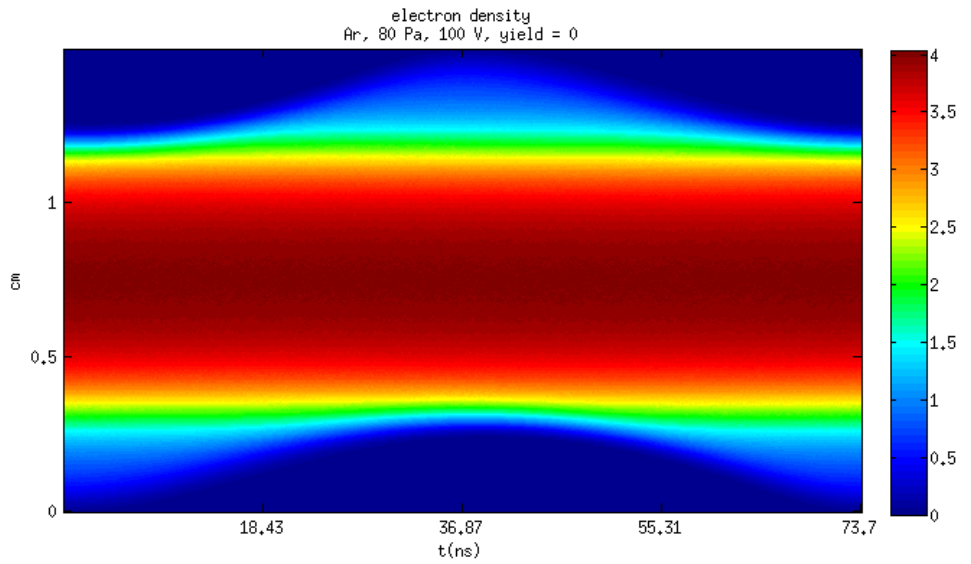


(a)

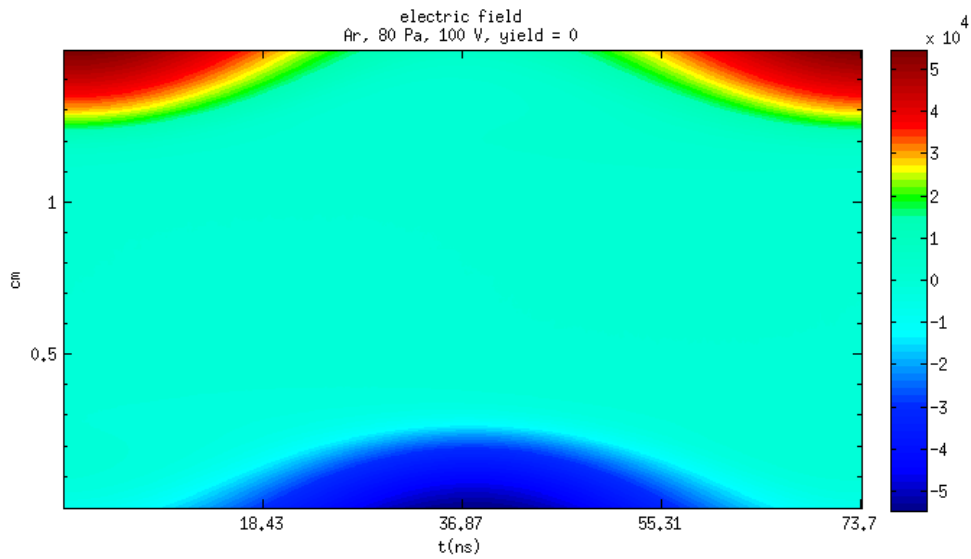


(b)

Figure 4.4: α -type discharge. Current study results. $p = 80$ Pa, $V = 100$ V, $L = 1.5$ cm, $f = 13.56$ MHz, $T = 350$ K, $\gamma = 0$. Spatio-temporal plots for (a) Electron heating rate [W], (b) Central region electric field detail [V/m].



(a)



(b)

Figure 4.5: α -type discharge. Current study results. $p = 80$ Pa, $V = 100$ V, $L = 1.5$ cm, $f = 13.56$ MHz, $T = 350$ K, $\gamma = 0$. Spatio-temporal plots for (a) Electron density [10^{15} m^{-3}], (b) Electric field [V/m].

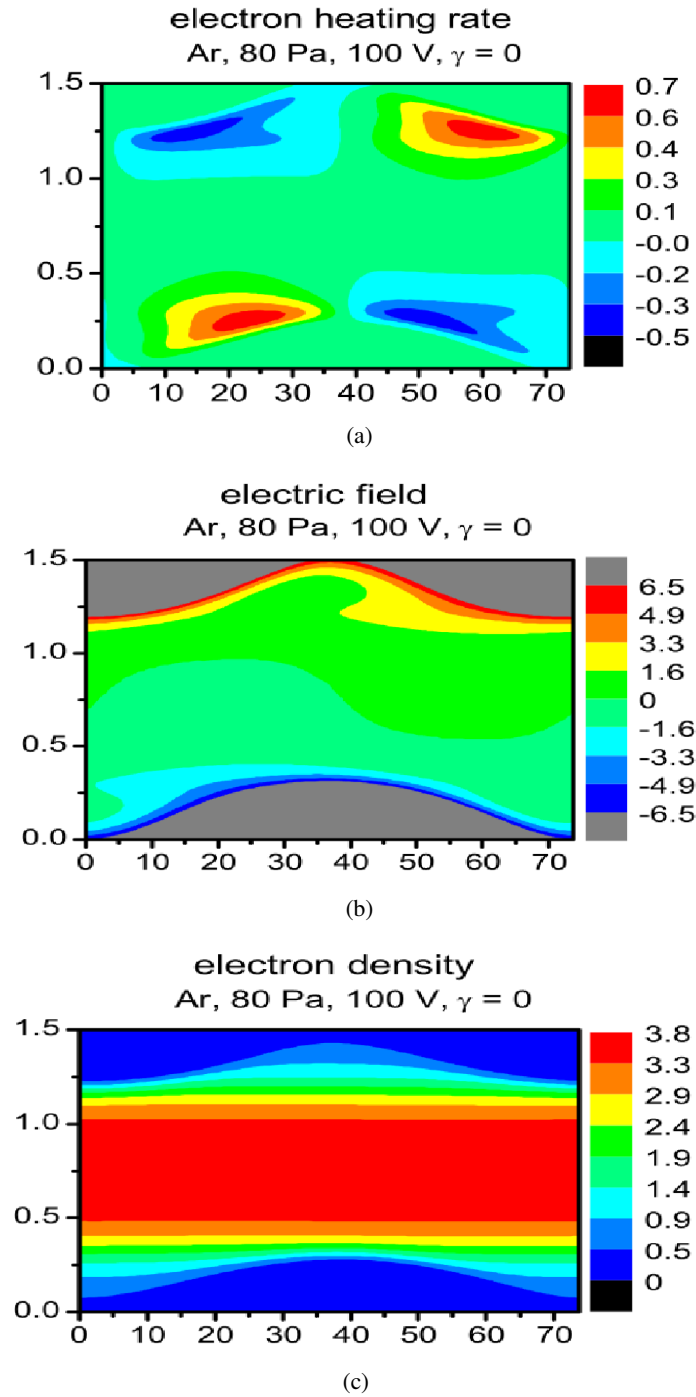
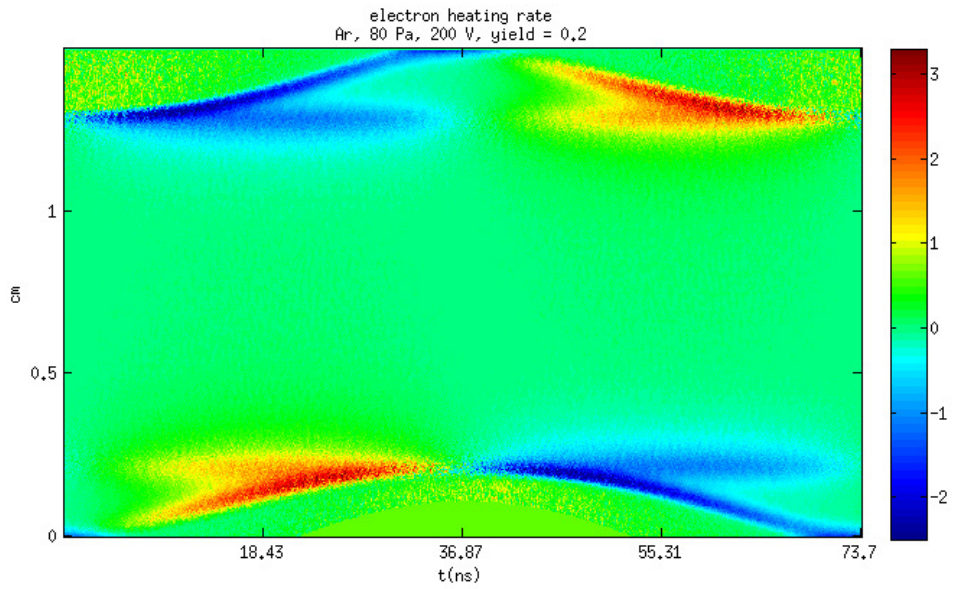
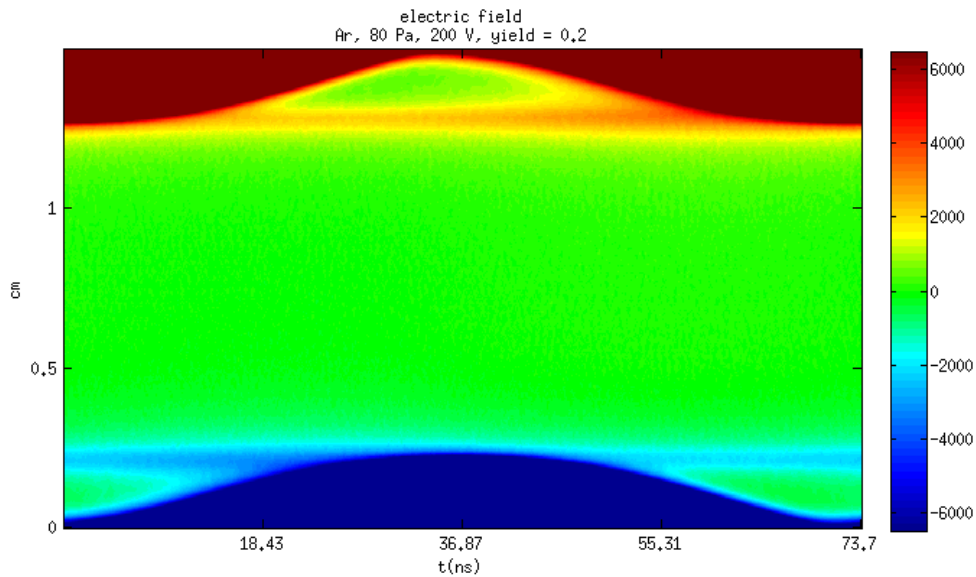


Figure 4.6: RF α type argon gas discharge. Results of reference [44]. $p = 80$ Pa, $V = 100$ V, $L = 1.5$ cm, $f = 13.56$ MHz, $T = 350$ K, $\gamma = 0$. Spatio-temporal plots for (a) Electron heating rate [10^5 W], (b) Central region electric field detail [10^3 V/m], (c) Electron density [10^{15} m $^{-3}$].

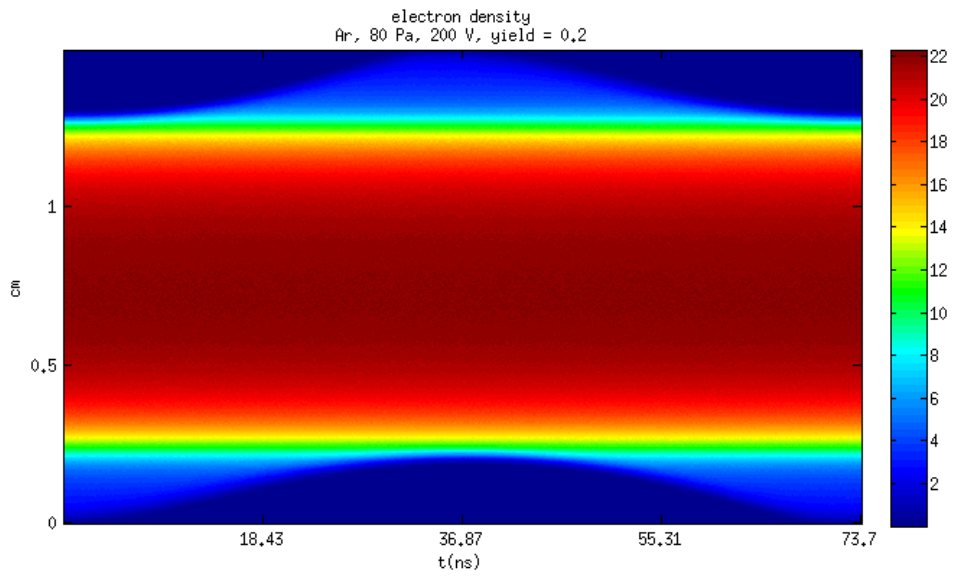


(a)

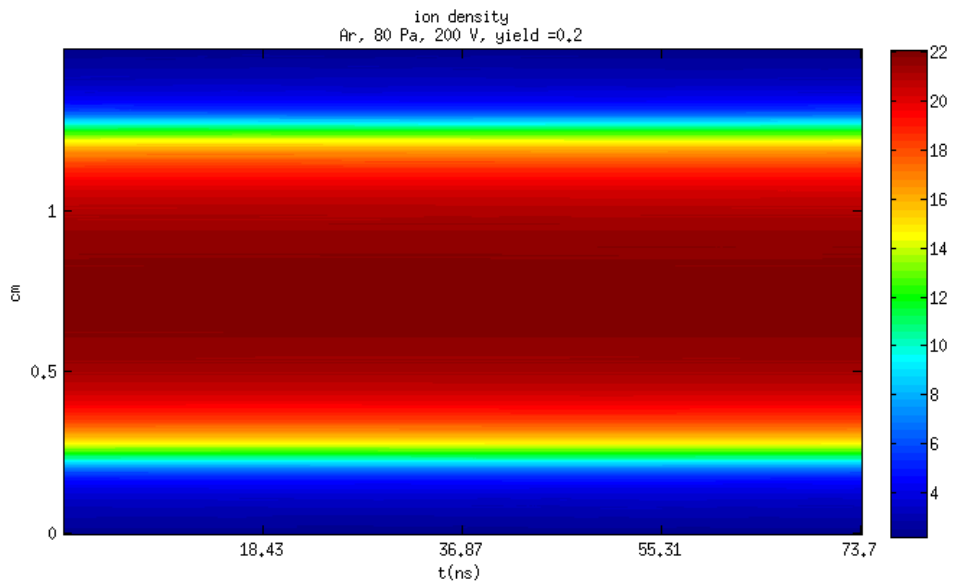


(b)

Figure 4.7: γ -type discharge. Current study results. $p = 80$ Pa, $V = 200$ V, $L = 1.5$ cm, $f = 13.56$ MHz, $T = 350$ K, $\gamma = 0.2$. Spatio-temporal plots for (a) Electron heating rate [10^5 W], (b) Central region electric field detail [V/m].



(a)



(b)

Figure 4.8: γ -type discharge. Current study results. $p = 80$ Pa, $V = 200$ V, $L = 1.5$ cm, $f = 13.56$ MHz, $T = 350$ K, $\gamma = 0.2$. Spatio-temporal plots for (a) Electron density [10^{15} m^{-3}], (b) Ion density [10^{15} m^{-3}].

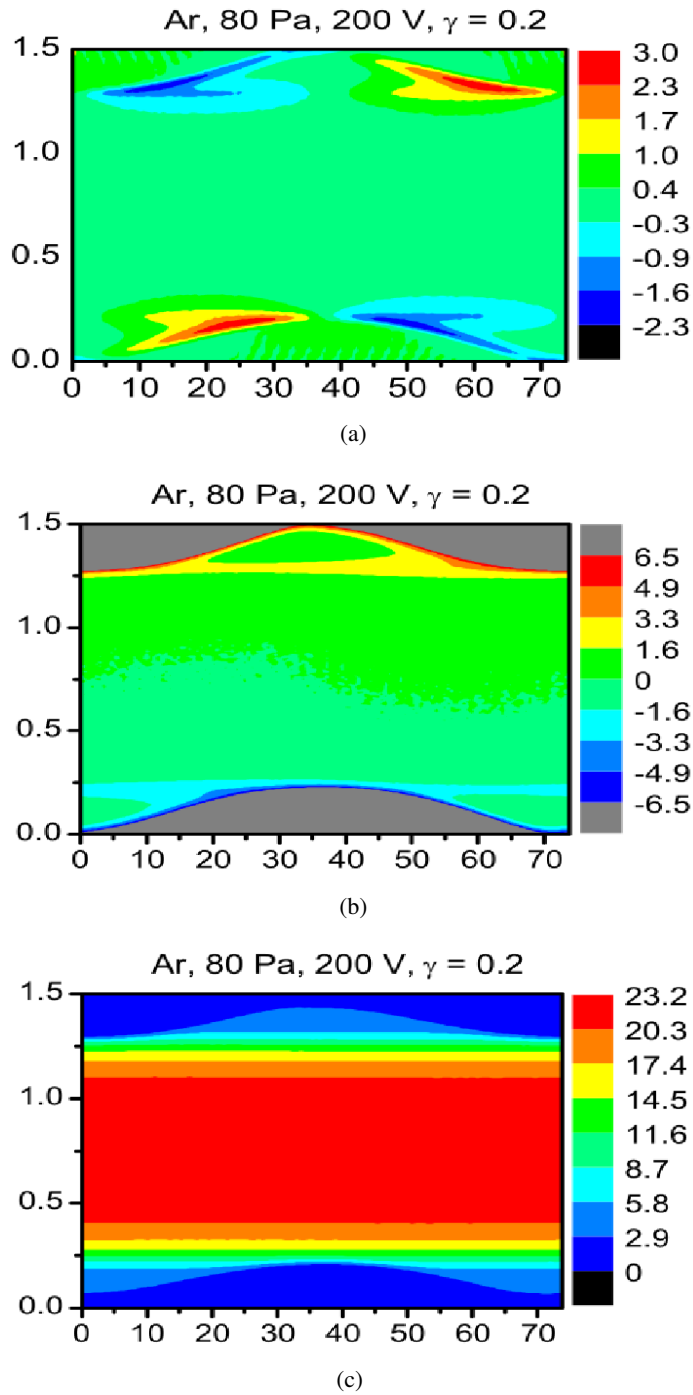


Figure 4.9: RF γ type argon gas discharge. Results of reference [44]. $p = 80$ Pa, $V = 200$ V, $L = 1.5$ cm, $f = 13.56$ MHz, $T = 350$ K, $\gamma = 0.2$. Spatio-temporal plots for (a) Electron heating rate [10^5 W], (b) Central region electric field detail [10^3 V/m], (c) Electron density [10^{15} m $^{-3}$].

4.3 Detailed RF Argon Glow Discharge PIC/MCC Test

Problem parameters taken from the reference [45] are given in table 4.1. Mean ion and electron densities averaged in 1 RF cycle and Ar^+ energies on the electrodes are displayed in Figure 4.10. When mean electron densities were compared with Donkó's results, maximum relative error (ϵ_{rel}) obtained is about 0.023.

$$\epsilon_{rel} = \frac{\max|n_{i_{ref}} - n_i|}{\max|n_{i_{ref}}|}. \quad (4.1)$$

Table4.1: 1D RF argon glow discharge. PIC/MCC model problem parameters.

Problem Parameter	Symbol	Value
Gas Type	Ar	Argon
Gas Pressure	p	10 [Pa]
Gas Temperature	T	350 [K]
Electrode Potential	V	250 [Volt]
RF Frequency	f	13.56 [MHz]
Electrode Distance	L	2.5 [cm]
Secondary Electron Yield Constant	γ	0.1
Reflection Constant	r	0.2
Number of Grid Points	ndx	600

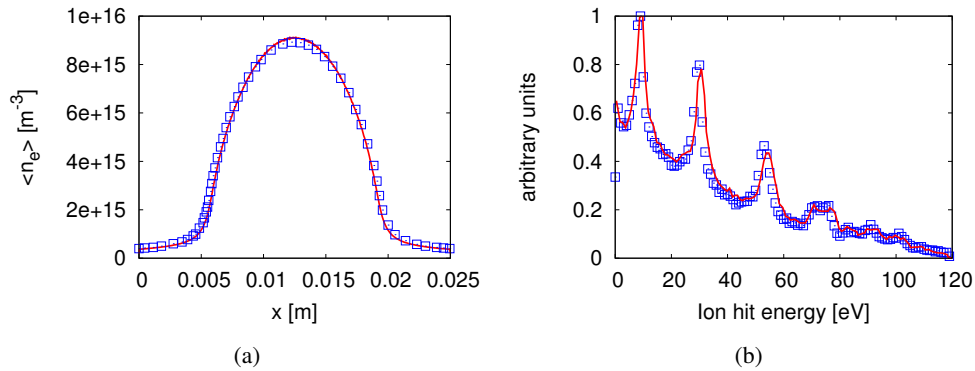


Figure 4.10: Comparison of the analysis results. Problem parameters are taken from [45]. $p = 10$ Pa, $V = 250$ V, $L = 2.5$ cm, $f = 13.56$ MHz, $T = 350$ K, $\gamma = 0.1$. The \square symbol indicates the results from [45] and continuous lines indicate the recent study results. (a) Mean electron density profile, (b) ion energy distribution on the electrodes.

4.3.1 Detailed Analysis of the Parallel Code

In this section, we give the results of the simulation with particle weightings (W_e, W_i) 1.5×10^8 . Left electrode potential ($V_{x=0}$) is taken as 0 and the right one ($V_{x=L}$) is dependent on time,

$$V_{x=L} = V \times \cos(2\pi ft). \quad (4.2)$$

48 processors were used to simulate 760,000 super ions and 730,000 super electrons over 20,000,000 time steps. To see the effect of particle weightings, we have done six different simulations with the same problem parameters but with different weightings. More information about the effect of charged particle weightings will be given in the next chapter.

4.3.1.1 Charge Densities

It is necessary to say that results are $1/f$ time periodic. Various results are indicated at the four distinct instants of an rf period: $\omega t/2\pi = 0$, $\omega t/2\pi = 0.25$, $\omega t/2\pi = 0.50$ and $\omega t/2\pi = 0.75$. Spatial ion and electron densities can be seen in Figures 4.11(b) and 4.11(a). The ion densities are almost independent of time. Electron densities are constant in the quasi-neutral region, but changing in the sheath regions. This situation for ions can be explained by the high mass of the ions compared to electrons. Besides, when comparing the two plots, it is obvious that there are always two sheath regions close to left and right electrodes. But depending on the electric potential configuration at that time, electron density, as well as the strength of the electric field on that sheath region changes. Another important point is that the densities when $\omega t/2\pi = 0$ and $\omega t/2\pi = 0.50$; $\omega t/2\pi = 0.25$ and $\omega t/2\pi = 0.75$ are symmetrical to each other. This symmetry is also valid for electric field (Figure 4.12(a)), spatial average ion and electron energies (Figure 4.14), and current density (Figure 4.13) plots. There is a symmetrical π rad phase shift in the results.

4.3.1.2 Electric Field

As expected, in Figure 4.12(a) electric field in the quasi-neutral region is close to zero, but varies on the sheath region. If the electric field is observed in detail (Figure 4.12(b)) an unexpected result is encountered. In two regions close to locations $x=0.005$ m and $x=0.020$ m electric field has local maximums, which means

$$\nabla \cdot \mathbf{E} = 0 \text{ or } \nabla^2 V = 0. \quad (4.3)$$

Surrendra [46] on PIC/MCC analysis and Sato et al. [47] experimentally faced with this phenomena before. This situation is explained by the following way:

1. If electrons are isothermal and have Maxwellian distributions, for regions where $\nabla^2(\log(n_e)) = 0$, then $\nabla^2 V = 0$ should be satisfied.

2. For current continuity, electric field adjusts itself on the regions where $\nabla \cdot \mathbf{E} = 0$.

4.3.1.3 Current Densities

There are four different types of currents in plasmas. Electron and ion currents depend on movement of the charged particles, displacement current depends on the time rate of change of the electric field. Electron J_{e_k} , ion J_{i_k} , and displacement J_{d_k} current densities at grid point k are determined from

$$J_{e_k} = n_e \langle v_{x_e} \rangle q_e, \quad (4.4)$$

$$J_{i_k} = n_i \langle v_{x_i} \rangle q_e, \quad (4.5)$$

$$J_{d_k} = \varepsilon_0 \frac{\partial E_k}{\partial t}, \quad (4.6)$$

where $\langle v_{x_e} \rangle$ and $\langle v_{x_i} \rangle$ are mean electron and ion velocities at the grid point k . Total current is obtained by summing up all these current values. Referring to Figure 4.13, current on the sheath regions is generated by the displacement, and in the quasi-neutral region by the electron current. Ion current is two orders smaller than electron and displacement currents. As seen from the total current plot, total current density is constant independent of the position but changes over time.

4.3.1.4 Average Particle Energies

In Figure 4.14 average particle energies can be observed. Electrons have increasing energy profile from electrodes to the quasi-neutral region, because the secondary electrons created from the electrodes gain higher velocities due to high electric field in the sheath regions. These electrons cause ionizations, hence they are one of the main reasons for plasma sustainability. In addition, the average energy of the ions increases from quasi-neutral regions to the electrodes. The reason for this will be explained later on. Ions and electrons have the lowest average energies in the quasi-neutral region. In this region, electrons have 1.3 eV and ions have about 0.03 eV average energies. 0.03 eV is approximately equal to 350 K, which is the neutral gas temperature, which means ions are at thermal equilibrium with the neutral gas. Average energies at the center of the discharge can be better observed from a log scale plot at $\omega t/2\pi = 0$ from Figure 4.15.

4.3.1.5 Energy Distribution Functions in the Quasi-neutral Region

We have analysed particle energy distribution functions from $x=0.010$ to $x=0.015$ in Figure 4.17. As expected, ions have Maxwellian energy distribution function, but the same cannot be said for electrons. Electrons have two energy groups and with high energy tail. Tail is caused by secondary electrons coming from the electrodes.

4.3.1.6 Single Ion Path

We have tracked the path (Figure 4.17(a)) and velocity (Figure 4.17(b)) of ion # 0 from 4,000,000th to 5,060,000th time steps. At the beginning, the particle is at node # 181, and at about 5,060,000th time step the ion hits the left boundary (grid # 0) and exits from the simulation. During this time period it experienced collisions and lost its speed. Even if the electric field is at the opposite direction to its movement, ion maintains its speed and continues to move to the left electrode all the time. If ion transit time is smaller than the plasma period, ions feel the electric field average, and they experience periodic speed-ups in the sheath regions [17]. This is the reason for increasing average energy of the ions near the electrodes as seen in Figure 4.14.

4.3.1.7 Ion Energies on the Electrodes

As stated previously, RF plasmas are used for surface modifications. One of the most important parameters of these applications is energy of the ions hitting the electrodes or the target material. Commented ion energies on the electrodes can be seen in Figure 4.18. Since this is a low pressure glow discharge, spiky non-Maxwellian distribution of ions is due to long mean free paths of the ions near electrodes [17].

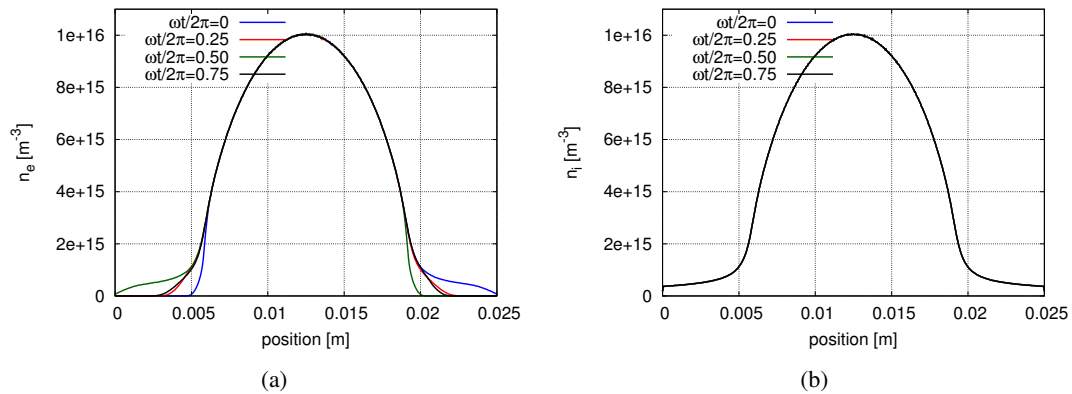


Figure 4.11: Problem parameters: $p = 10$ pa, $T = 350$ K, $V = 250$ V, $f = 13.56$ MHz, $L = 2.5$ cm, $\gamma = 0.1$, $W_e = W_i = 1.5 \times 10^8$. Results are displayed at $\omega t/2\pi = 0$, $\omega t/2\pi = 0.25$, $\omega t/2\pi = 0.50$ and $\omega t/2\pi = 0.75$. (a) Ion densities, (b) electron densities.

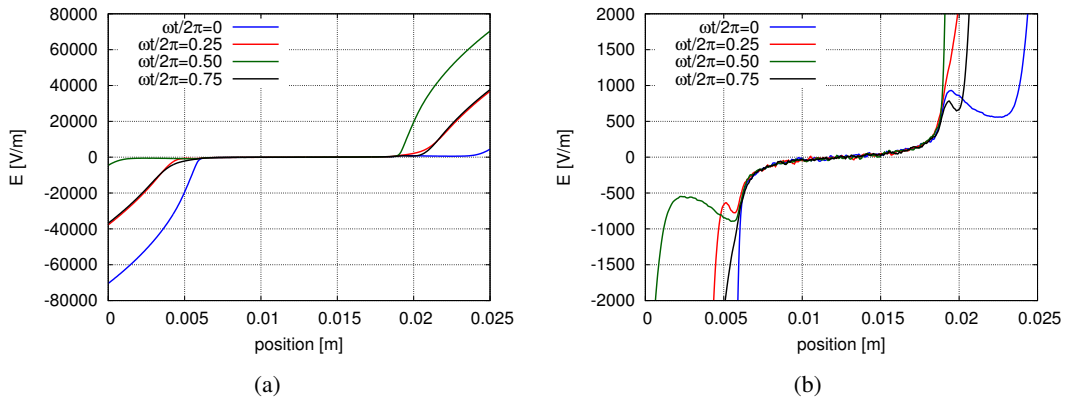


Figure 4.12: Problem parameters: $p = 10$ pa, $T = 350$ K, $V = 250$ V, $f = 13.56$ MHz, $L = 2.5$ cm, $\gamma = 0.1$, $W_e = W_i = 1.5 \times 10^8$. Results are displayed at $\omega t/2\pi = 0$, $\omega t/2\pi = 0.25$, $\omega t/2\pi = 0.50$ and $\omega t/2\pi = 0.75$. (a) Electric field, (b) electric field detail at the center of the discharge.

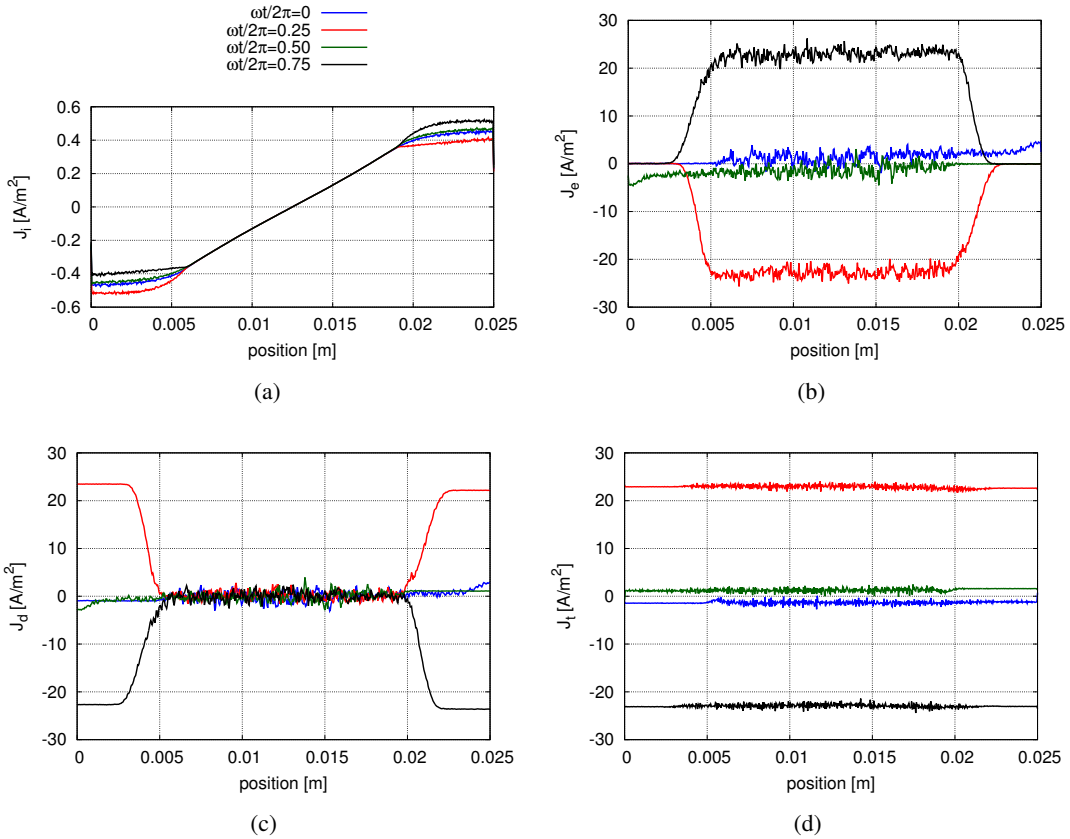


Figure 4.13: Problem parameters: $p = 10$ pa, $T = 350$ K, $V = 250$ V, $f = 13.56$ MHz, $L = 2.5$ cm, $\gamma = 0.1$, $W_e = W_i = 1.5 \times 10^8$. Results are displayed at $\omega t/2\pi = 0$, $\omega t/2\pi = 0.25$, $\omega t/2\pi = 0.50$ and $\omega t/2\pi = 0.75$. (a) Ion current density, (b) electron current density, (c) displacement current density, (d) total current density.

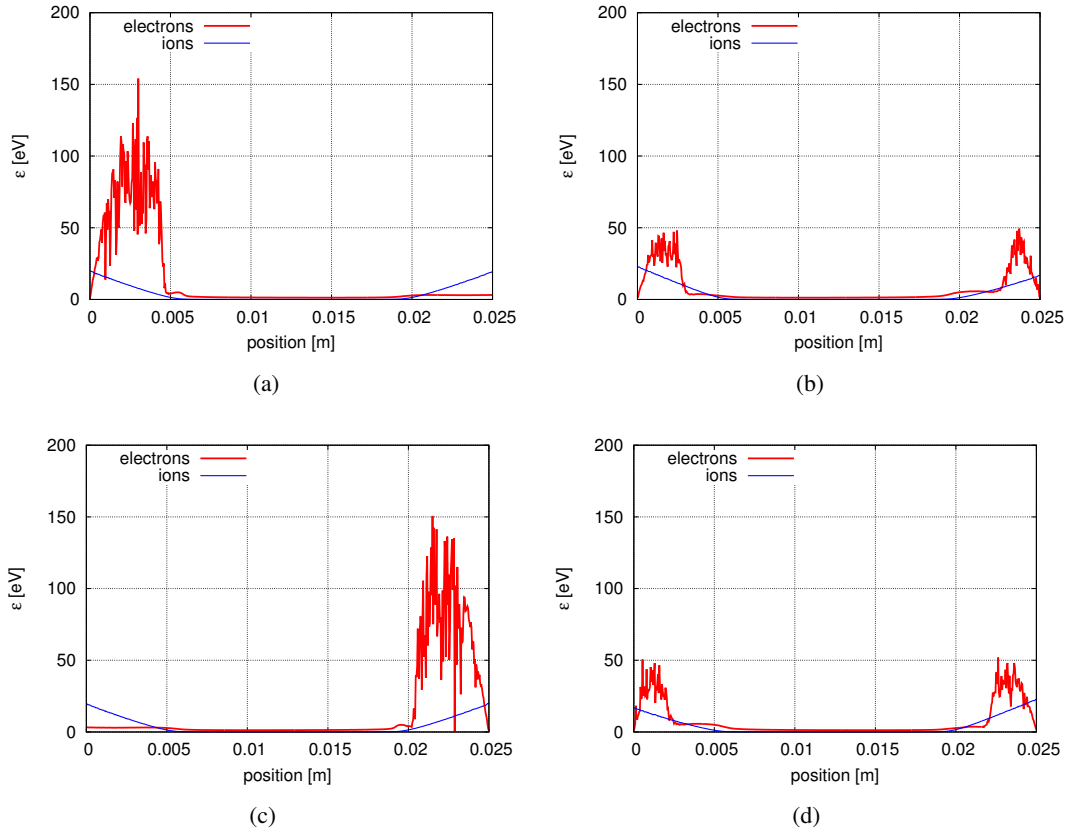


Figure 4.14: Problem parameters: $p = 10$ pa, $T = 350$ K, $V = 250$ V, $f = 13.56$ MHz, $L = 2.5$ cm, $\gamma = 0.1$, $W_e = W_i = 1.5 \times 10^8$. Average electron and ion energies at (a) $\omega t/2\pi = 0$, (b) $\omega t/2\pi = 0.25$, (c) $\omega t/2\pi = 0.50$, (d) $\omega t/2\pi = 0.75$.

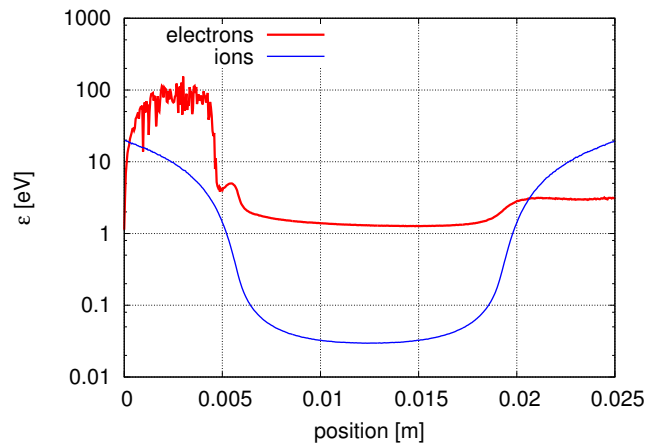


Figure 4.15: Problem parameters: $p = 10$ pa, $T = 350$ K, $V = 250$ V, $f = 13.56$ MHz, $L = 2.5$ cm, $\gamma = 0.1$, $W_e = W_i = 1.5 \times 10^8$. Average electron and ion energies at $\omega t/2\pi = 0$.

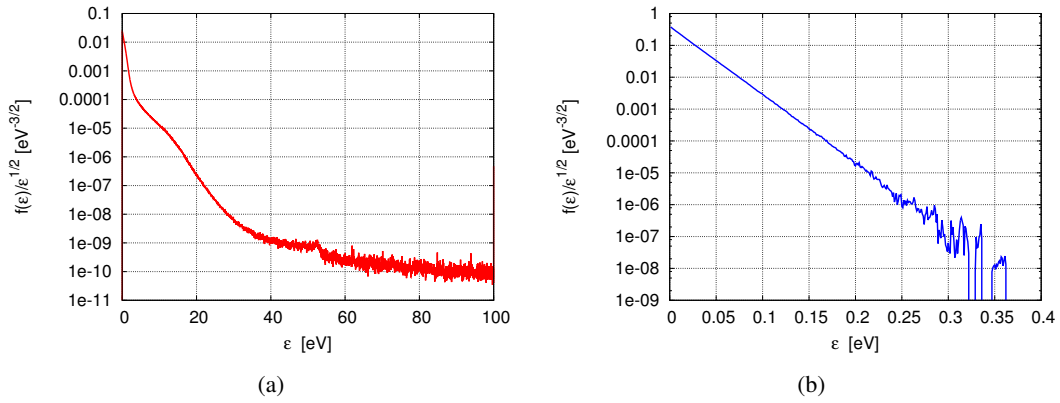


Figure 4.16: Problem parameters: $p = 10$ pa, $T = 350$ K, $V = 250$ V, $f = 13.56$ MHz, $L = 2.5$ cm, $\gamma = 0.1$, $W_e = W_i = 1.5 \times 10^8$. Average energy distribution functions at the center of discharge for (a) electrons, (b) ions.

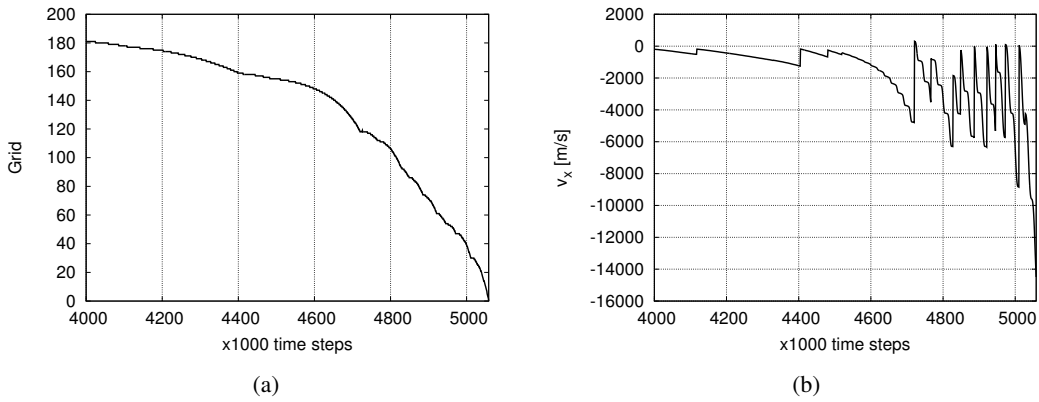


Figure 4.17: Problem parameters: $p = 10$ pa, $T = 350$ K, $V = 250$ V, $f = 13.56$ MHz, $L = 2.5$ cm, $\gamma = 0.1$, $W_e = W_i = 1.5 \times 10^8$. (a) Grid point position and (b) speed of the ion #0 as function of time.

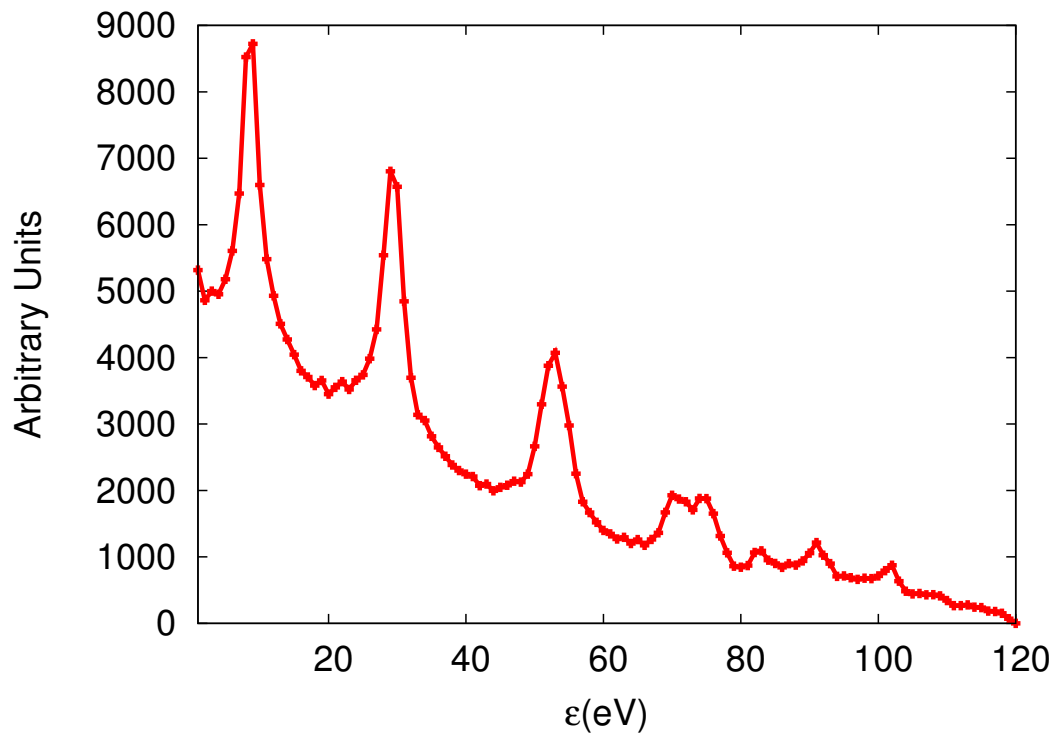


Figure 4.18: Problem parameters: $p = 10$ Pa, $T = 350$ K, $V = 250$ V, $f = 13.56$ MHz, $L = 2.5$ cm, $\gamma = 0.1$, $W_e = W_i = 1.5 \times 10^8$. Ion energy distributions at the electrodes.

CHAPTER 5

THE EFFECT OF NUMBER OF SUPER PARTICLES USED IN THE PIC/MCC SIMULATIONS

Kim et. al. [48] mentioned importance of the effect of super particle weighting in PIC/MCC simulations on particle densities and mean electron temperature in the bulk plasma. Donkó et. al. [4] investigated this effect in the case of DC (direct current) glow discharges. Turner [49] further extended these studies by also including Coulomb collisions into the models, at various pressures.

We consider a capacitively coupled RF discharge, driven by a sinusoidal voltage source, with $V = 250$ V, at frequency $f = 13.56$ MHz. Distance between the electrodes is $L = 2.5$ cm. The left electrode is grounded, $\varphi|_{x=0} = 0$, the right electrode voltage varies according to $\varphi|_{x=L} = V\cos(2\pi ft)$, where t is the simulation time. Background gas is pure argon at temperature 350 K and pressure 10 Pa. Secondary electron emission coefficient is 0.1. Using 600 grid points, we have done 6 different simulations by only changing the super particle weightings. Simulations are carried out using HPC resources [50]. The information about the simulations is given in Table 5.1.

Table5.1: Effect of particle weighting on the total number of super electrons, average number of super electrons per grid cell, Debye length, λ_D , and number of super electrons per Debye length, N_D , at the end of the simulations, $t \approx 7.37 \times 10^{-5}$ s. (λ_D and N_D are calculated at the midplane of the discharge.)

Simulation No	Weighting	Tot. num. of super electrons	Ave. num. of super electrons per grid cell	Debye length λ_D (m)	N_D
1	41.7×10^8	15746	26	1.74×10^{-4}	231
2	20.8×10^8	33822	56	1.56×10^{-4}	455
3	5.2×10^8	173054	288	1.11×10^{-4}	1713
4	3.0×10^8	339532	566	9.54×10^{-5}	2917
5	2.0×10^8	537500	896	8.79×10^{-5}	4272
6	1.5×10^8	737316	1229	8.42×10^{-5}	5635

Results presented in Figures 5.1–5.4 (as well as in Table 5.1) correspond to the simulation time $t \approx 7.37 \times 10^{-5}$ s (which covers 2×10^7 iterations and about 1100 simulation cycles),

achieving converged solutions. Charged particle densities increase with the increasing number of super particles (see Figure 5.1). As expected, numerical noise is reduced significantly. The increase in the density tends to saturate, and a converged profile is achieved, as seen in Figure 5.1d. Using about 1200 super electrons per grid cells, weighting independent results are achieved for the density profiles. The parameter N_D listed in Table 5.1 corresponds to maximum number of super particles per Debye length evaluated at the discharge midplane where the concentration of the particles is the highest.

Figure 5.2 shows profiles of total current density $J_t = J_e + J_i + J_d$ obtained from simulations #1 and #6 at three different times within the RF period ($\omega t/2\pi = 0.25, \omega t/2\pi = 0.50, \omega t/2\pi = 0.75$). Electron and ion current densities J_e and J_i and displacement current density J_d at grid point k are determined from

$$J_{e_k} = n_{e_k} \langle v_{e,x} \rangle q_e, \quad (5.1)$$

$$J_{i_k} = n_{i_k} \langle v_{i,x} \rangle q_i, \quad (5.2)$$

$$J_{d_k} = \varepsilon_0 \frac{\partial E_k}{\partial t}, \quad (5.3)$$

where $\langle v_{e,x} \rangle$ and $\langle v_{i,x} \rangle$ denote x components of mean electron and ion velocities at point k . Higher noise and noticeable total current discontinuity is remarkable for the simulations using less number of super particles. However, mean values of the corresponding total current densities are close to each other. Also, it should be noted that constant profile of total current density as a function of position supports the validity of the simulation (Fig. 5.2b).

Another marked difference is that the averaged electric field profiles tend to become less inclined and noisy at the center of the discharge with more particles involved in simulations (Figure 5.3 (a, b)).

Mean energy profiles of both ions and electrons in the quasi-neutral region (center of the discharge) are highly dependent on the particle weighting: more particles used, lesser the average energies (Figure 5.3 (c, d)).

Finally, as can be seen from Figure 5.4, ion energy distribution functions (EDF) retains the Maxwellian shape independent on the weighting used in the simulations. But for the electrons, if the particle weighting is not adequate, EDF becomes distorted, hence the simulations could not predict the distribution function correctly (Figure 5.4 (a)). Here the energy distribution functions are normalized according with

$$\int_0^\infty \sqrt{\varepsilon} f(\varepsilon) d\varepsilon = 1. \quad (5.4)$$

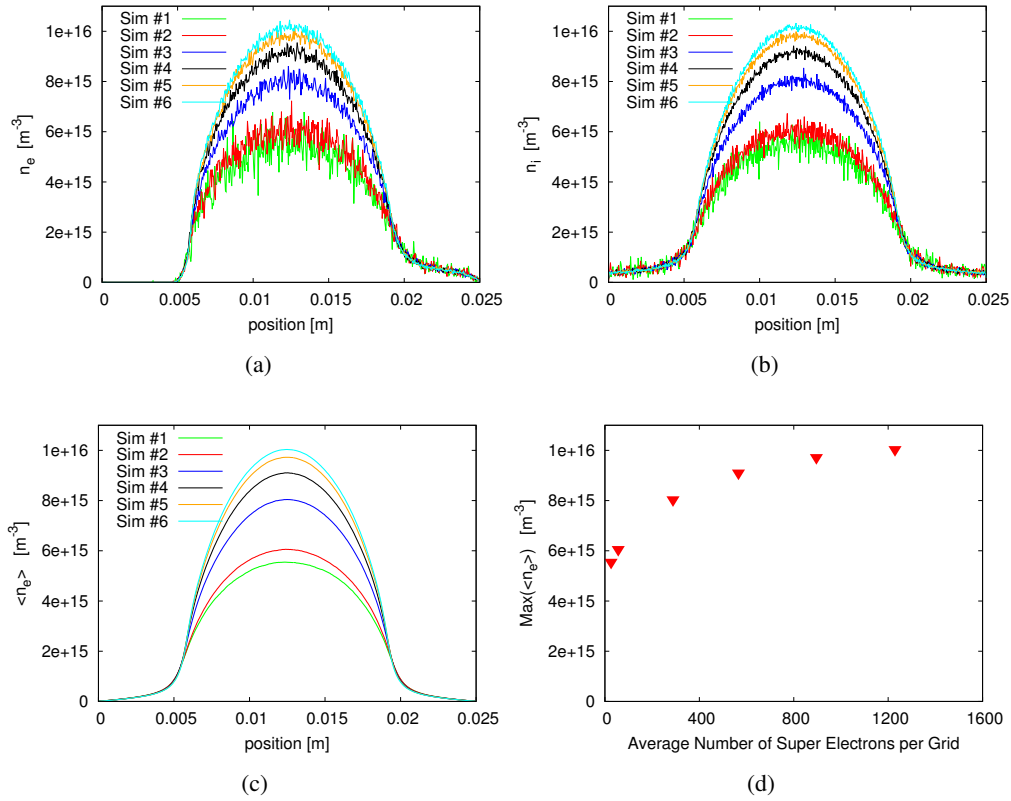


Figure 5.1: Effect of the super particle weightings on (a) the electron density profiles, (b) the ion density profiles, (c) the mean electron density profile over one RF cycle, (d) the maximum electron density vs average number of super electrons per grid, at simulation time $t \approx 7.37 \times 10^{-5}$ s.

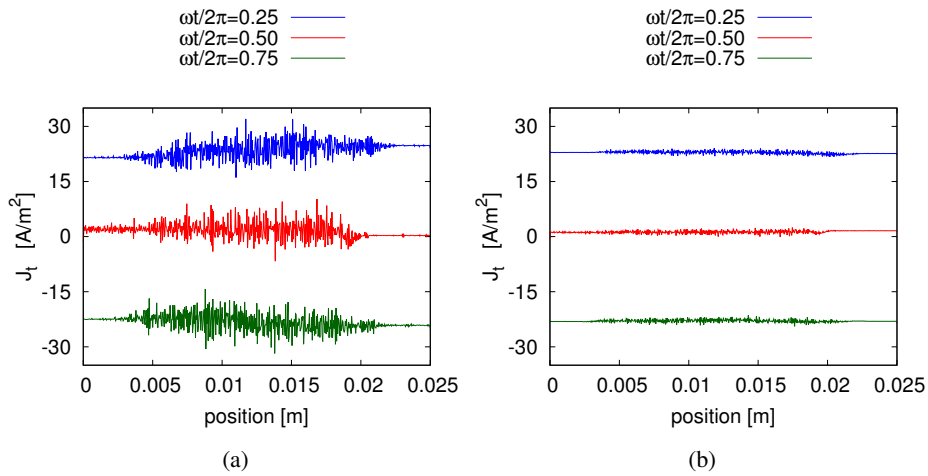


Figure 5.2: Effect of the super particle weightings on (a) Total current density profile for simulation #1, (b) Total current density profile for simulation #6 at time $\omega t/2\pi = 0.25$, $\omega t/2\pi = 0.50$, and $\omega t/2\pi = 0.75$.

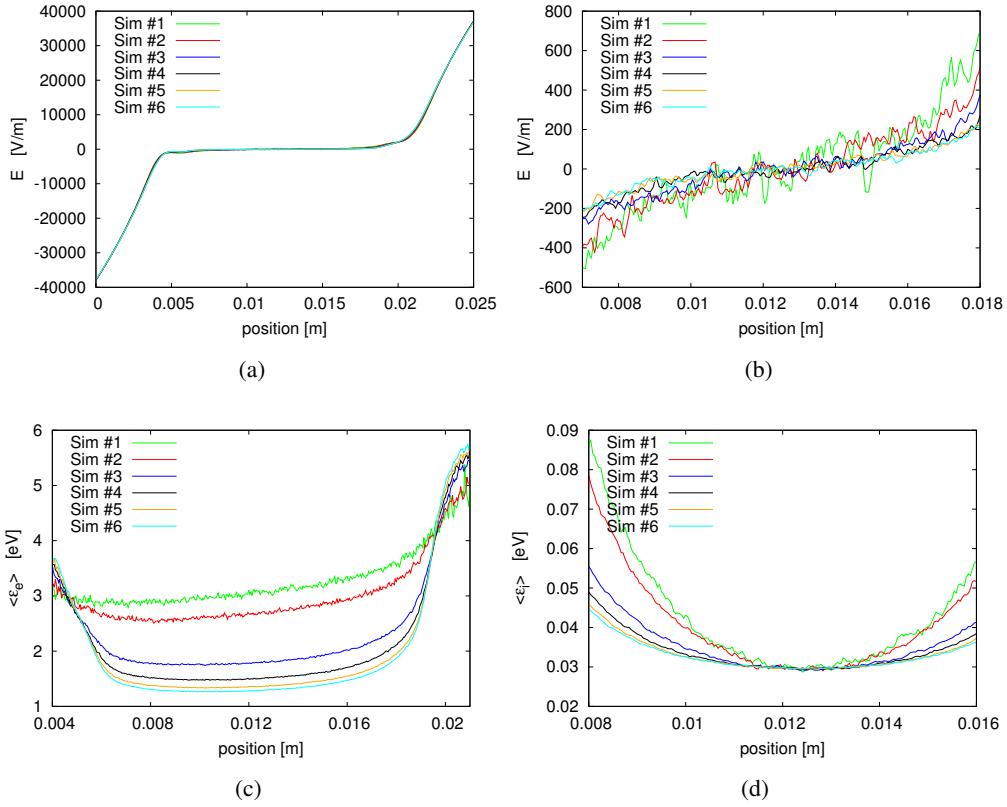


Figure 5.3: Effect of the super particle weighting on (a) electric field profiles, (b) electric field profile details at the center of the discharge, (c) mean electron energy profiles at the center of the discharge, (d) mean ion energy profiles at the center of the discharge. Time $\omega t/2\pi = 0.25$ of the RF period.

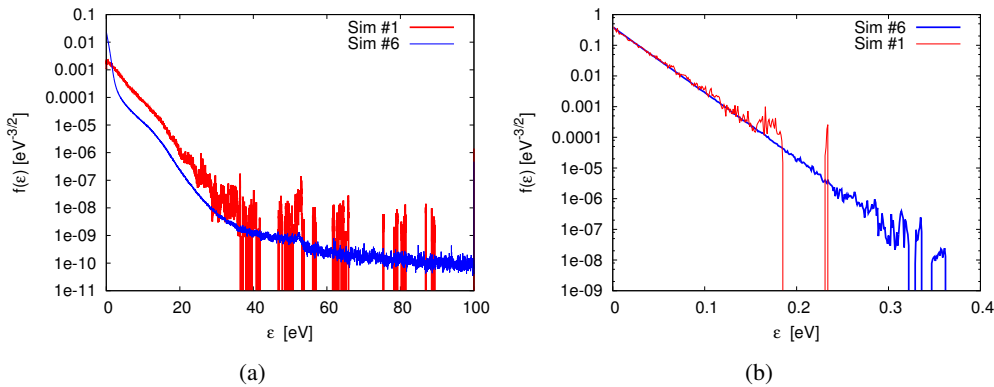


Figure 5.4: Effect of the super particle weighting on (a) electron energy distribution function at the center of the discharge, (b) ion energy distribution function at the center of the discharge. Time $\omega t/2\pi = 0.25$ of the RF period.

CHAPTER 6

3D3V MCC MODEL OF DC ARGON TOWNSEND DISCHARGE

Townsend discharge is a gas discharge type, where electrons accelerate by the electric field, and multiply in the form of avalanche. When the electrons get depleted from absorption on the boundaries, the process dies out. The process is known as "Townsend avalanche / Swarm". In general, process lasts in a very short period of time, and not enough charges are created to form quasi-neutral region at the center of the discharge. Hence, one may say that the electric field value between electrodes is constant throughout the process [14].

Townsend discharge simulations are important environments to understand the motion of the charged particles in detail. Also, it is possible to obtain transport coefficients (mobility, diffusion, Townsend ionization coefficient) from the swarm experiments. A 3D3v (three dimensional in both space and velocity) Townsend discharge simulation were previously done by Z. Donkó [14]. These are also studied in this thesis study. Problem parameters are given in Table 6.1. Right electrode is the anode ($V_R=150$ V), and the left is cathode ($V_L=0$ V). Collision reactions (elastic, excitation, ionization), and cross sections for electrons are taken from the reference [12]. At the start 500,000 electrons with 1 eV energy are injected from the cathode, and their motion is tracked until all the electrons absorbed by the boundaries.

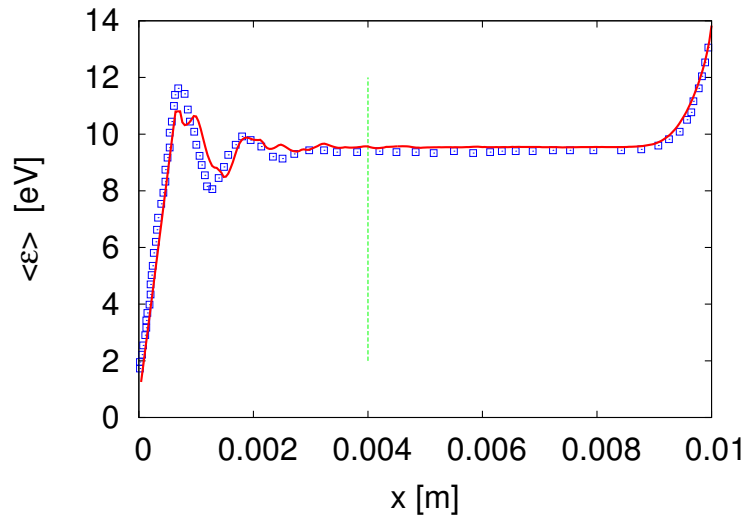
Mean energy ($\langle \varepsilon \rangle$), drift velocity (v_{dr} , mean velocity of the electrons), Townsend ionization coefficient (α) parameters were calculated from the swarm simulation. Results were compared with the study of Donkó [14]. α was calculated from the electron flux

$$\alpha = \frac{d\Gamma(x)}{\Gamma(x) dx} \quad (6.1)$$

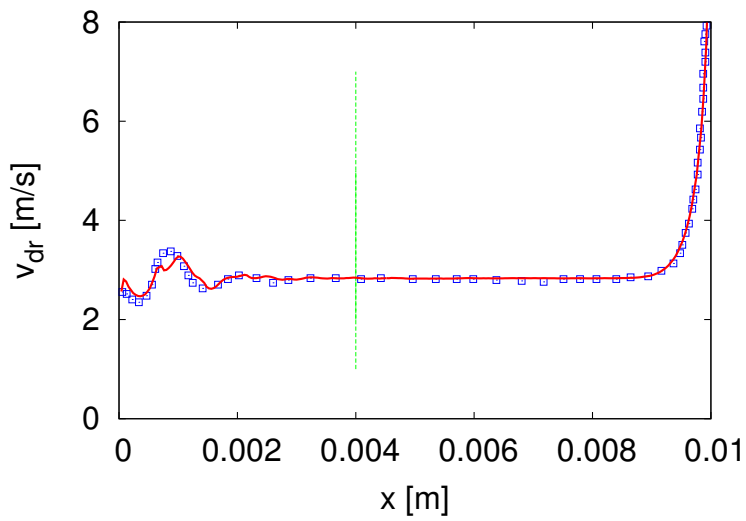
displayed in Figure 6.1 and 6.2, where $\Gamma(x)$ is the flux of the electrons. In each of the figures three different regions are obvious. In the first region, close to the cathode, electron energies are below the ionization threshold. Swarm is not in equilibrium. As moving into the center of the discharge, the electron energies increase, and transport parameters reach their equilibrium values (vertical lines). In the location close to the anode, as slow electron groups are neutralized in the electrode, transport parameters change abruptly. Electrons require some interval to reach equilibrium in the discharges. The requirement of the equation, [4]

$$\lambda \frac{dE}{dx} \ll E, \quad (6.2)$$

for the continuum approach has been confirmed once again, where λ mean free path of the particles.

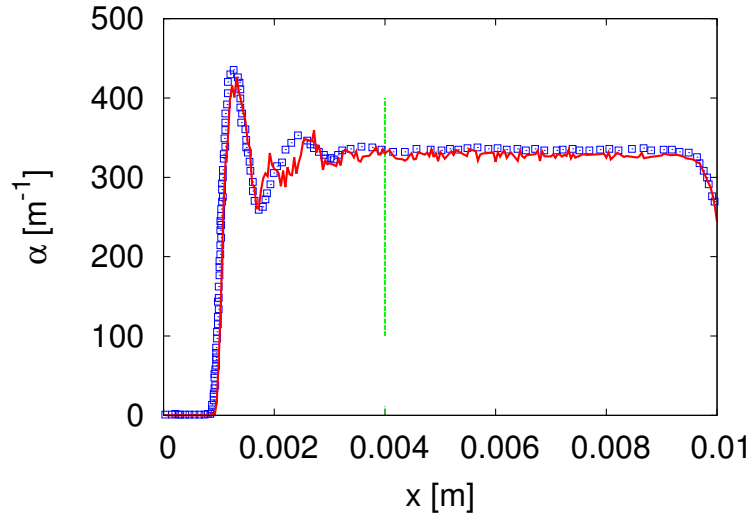


(a)



(b)

Figure 6.1: $L=1$ cm, $E/n= 500$ Td. Transport parameters of an electron swarm in argon gas: (a) mean energy, (b) drift velocity. The symbol \square refers to results from Donkó et. al. [14], and continuous lines show recent study results.



(a)

Figure 6.2: $L=1$ cm, $E/n=500$ Td. Transport parameters of an electron swarm in argon gas: Townsend ionization coefficient. The symbol \square refers to results from Donkó et. al. [14], and continuous lines show recent study results.

Table6.1: Townsend swarm 3D3v MCC simulation problem parameters.

Problem Parameter	Symbol	Value
Gas Type	Ar	Argon
Gas Pressure	p	1 [Torr]
Gas Temperature	T	300 [K]
Electrode Potential	V	160.94 [Volt]
Electrode Distance	L	1 [cm]
Reduced Electric Field	E/n	500 [Td]
Secondary Electron Yield Constant	γ	0
Reflection Constant	r	0

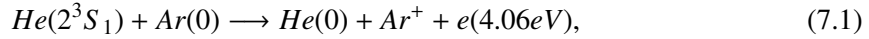
CHAPTER 7

DC COLLISIONAL ELECTRON SPECTROSCOPY: NUMERICAL MODEL AND INVESTIGATION OF THE RESULTS

7.1 Modeling of DC Collisional Electron Spectroscopy (CES) of Helium-Argon Gas Mixture Discharge by Using PIC/MCC Method

7.1.1 Problem and Parameters

As previously stated in chapter 2.4.2, a peak on the electron energy distribution at about 4.06 eV has been experimentally obtained for the mixture containing 0.4% argon impurity at 26 Torr helium gas (figure 2.11) [29]. According to this information,



is the dominant reaction for the discharge. By adding this reaction into the code, argon-helium mixture gas discharge model was analysed by using PIC/MCC algorithm. The initial aim of this chapter is to obtain similar peaks in the EEDF as in references [28, 29]. Problem parameters are given in Table 7.2. Some assumptions were made in the current PIC/MCC model:

- Electrons are only able to do collisions with the neutral helium gas (elastic, excitation, ionization). Ions are able to do isotropic and backward scattering collisions. Electron-helium gas collision cross section data is taken from Miles et. al. [24]. 2^1S_1 excitation collision was not included in the model. Only 2^3S_1 excitation was modeled. Since 2^1S_1 is neglected, electron-neutral excitation cross section data (2^3S_1) was multiplied by two.
- Metastables (2^3S_1) were modeled as fluid by using drift diffusion approximation. Diffusion coefficient for metastables (D_m) was calculated according to [51],

$$D_m [\text{cm}^2 \text{ s}^{-1}] = (420/p[\text{Torr}]) \times (T_g[\text{eV}]/0.025)^{1.5},$$

Table7.1: 1D DC Helium-Argon Mixture Problem Parameters.

Problem Parameter	Symbol	Value
Gas Type	He-Ar	Helium(%99)-Argon(%1)
Gas Pressure	p	2261 [Pa]
Gas Temperature	T	400 [K]
Electrode Potential	V	400 [Volt]
Electrode Distance	L	4 [mm]
Secondary Electron Yield Coefficient	γ	0.15
Electron Reflection Coefficient	r	0.2

Table7.2: 1D DC Helium-Argon Gas Mixture Solution Parameters.

Solution Parameter	Symbol	Value
Number of Grid Points	ndx	401
Number of Super Particles	NSP	21,874 e^- and 23,430 He^+
Initial Densities	n_i and n_e	$10^{15} [m^{-3}]$
Ion Subcycling Parameter	isc	6
Slow Electron Subcycling Parameter	esc	3
Super Particle Weightings	$W_i = W_e$	3.4133×10^{11}

where p [Torr] and T_g [eV] are pressure and gas temperature. Metastable flux at the boundaries (Γ_m) is calculated by using

$$\Gamma_m = \frac{1}{4} n_m v_{th}^m,$$

where n_m and v_{th}^m are metastable density and thermal velocity respectively.

- The reaction 7.1 (the significant process) was modeled by taking the collision cross section from Howard et. al. [52]. The data is energy independent.
- Slow electrons were also subcycled, since it takes too long for DC glow discharge simulations to converge compared to RF types.

The rest of the parameters are also shown in Table 7.2.

7.1.2 Results of CES PIC/MCC Model

In Figure 7.1 results of the simulation at time step 91,000,000 ($t = 7.6714 \times 10^{-5}$ [s]) is shown. About 22,000 super electrons and 23,000 super ions were used to obtain the results. Although relatively high charged particle densities obtained (in the order of $\approx 10^{18} m^{-3}$) and the Penning ionization source is sufficiently high (in the order of $\approx 10^{24} m^{-3} s^{-1}$ and comparable

with the direct ionization source), we weren't able to detect a peak in the electron energy distribution function. Since there is enough Penning electron creation, the loss of the energies of the Penning electrons is obvious. In the next subsection, the reasons which may cause this problem will be discussed.

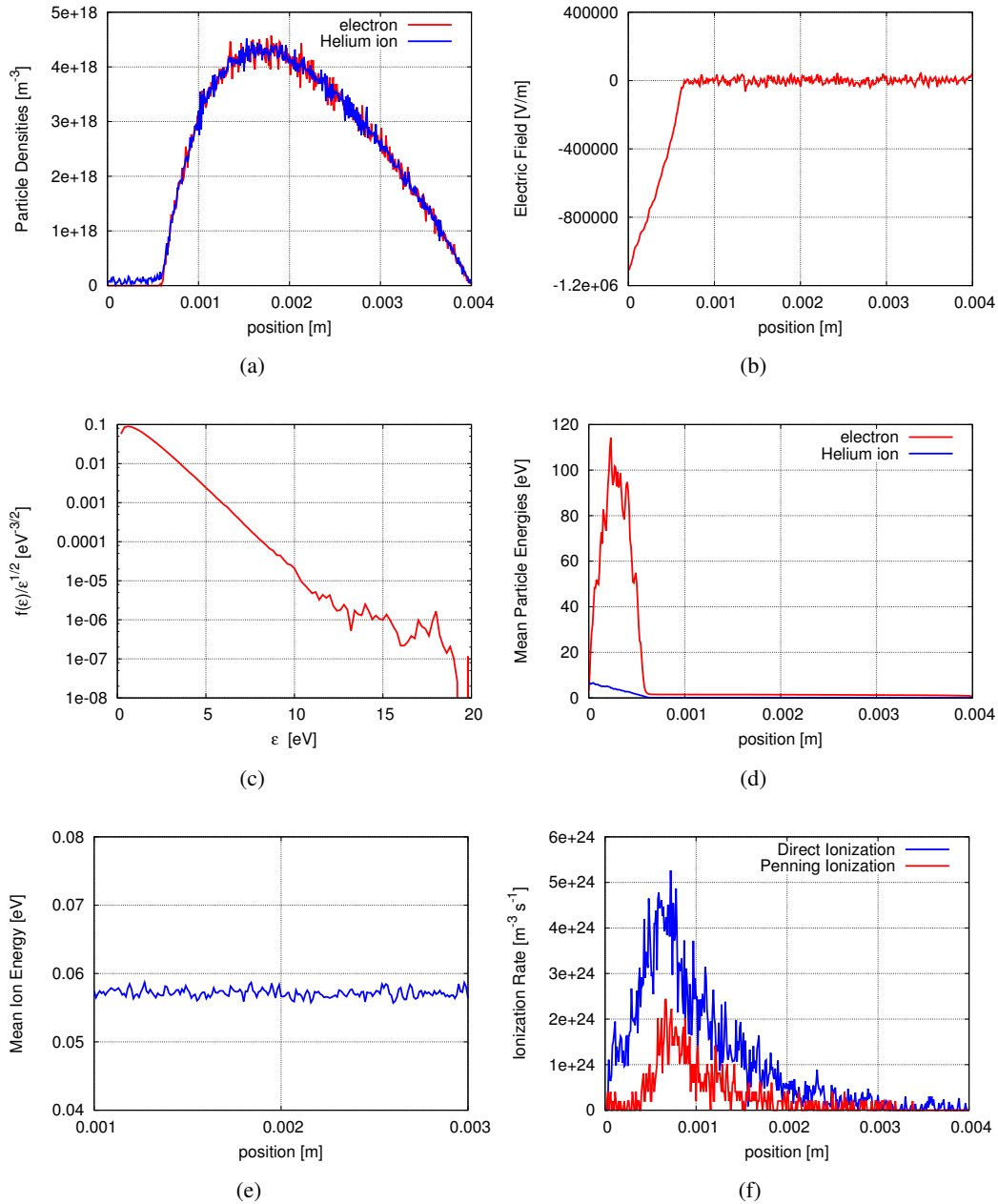


Figure 7.1: Results of the PIC/MCC analysis for DC CES example.

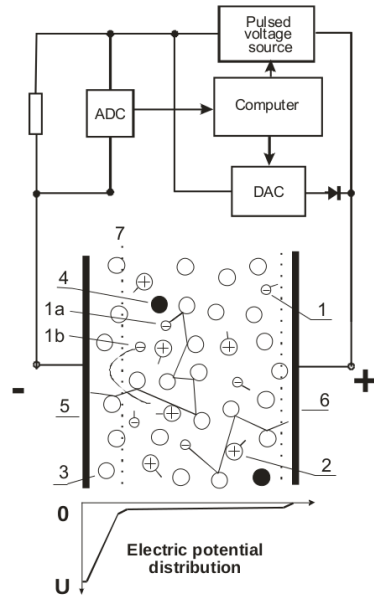


Figure 7.2: Example CES configuration, setup and electric potential [27].

7.2 The Effect of Electric Field Configuration at the Center of the Discharge

In figure 7.2 an example CES gas discharge setup and electric potential configuration is observed. According to the figure, the DC CES discharge consist of helium neutral atoms (3) and impurity atoms such as argon (4). In the quasineutral region, where electric field value is relatively low compared with sheath regions, Penning electrons are created by the Penning ionization (number 1a, 1b, 1c). Some of these electrons do elastic collisions with the surrounding atoms and stay inside the quasineutral region (1a). Some of the electrons pass to cathode sheath region, but return back to quasineutral region with the same kinetic energy. Some of the electrons are directed to the anode (1c). According with the theory, only total energy loss for electrons is due to collisions [27].

The electric potential configuration in the example above was the ideal case. The question is how Penning electrons behave and how their energy changes in noisy electric field configurations (as in the previous CES PIC/MCC simulation). To answer the question, three small MCC analysis for Penning electrons were done for three different electric field configurations. Input electric field configurations are given in figure 7.3. In these three MCC analysis, Penning electrons with energy 4.06 eV were inserted to the center of the discharge, and their positions and energies were tracked during 16.9×10^{-6} s (80,000 time steps). $p=16.96$ Torr, $L=0.4$ cm, $T=400$ K, $\Delta t=10^{-12}$ s are the simulation parameters.

For Test 1, the one with the ideal electric field configuration, electron energy and position of one of the Penning electrons with time are shown in figure 7.4. If electron enters the

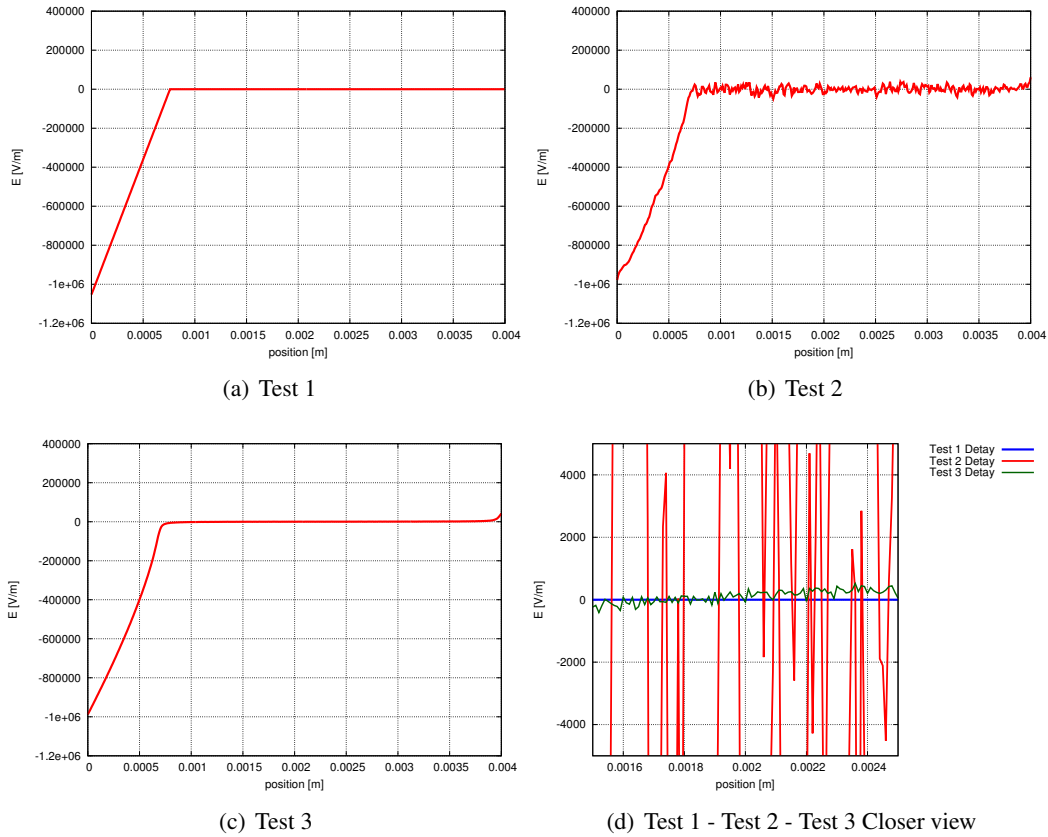


Figure 7.3: Input electric field configurations for test MCC simulations. (a) Ideal case - Test 1, (b) Input electric field from the analysis in 7.1.2 - Test 2, (c) Averaged electric field profile with reduced noise from the analysis in 7.1.2 - Test 3, (d) Closer view of the electric field configurations of Test 1 - Test 2- Test 3.

sheath region, its kinetic energy suddenly drops, but recovers after returning to quasineutral region. Also there is continuous drop in the electron energy due to elastic collisions (referring to equation 3.12). Electron energy varies between 4.06-0.2 eV.

For Test 2, in which the input electric field data is taken from the actual PIC/MCC CES simulation (from section 7.1.2), Penning electron MCC simulation results are shown in Figure 7.5. For this kind of variable electron energy, it is impossible to track Penning electrons from EEDF. The effect of the noisy electric field data on the electron energies is obviously distorting. As time passes, the expectation was reduction of the electron energy due to collisions, but on the contrary, the electron gained energy higher than its initial energy. The reason is clearly the numeric heating due to noisy electric field arised from insufficient number of particles.

For Test 3, in which the electric field (less-noisy compared to test 2) obtained from the PIC/MCC CES simulation (taken from section 7.1.2) is the averaged. The energy variance of the electron is reasonable, it is possible to track the Penning electrons from the EEDF for this configuration.

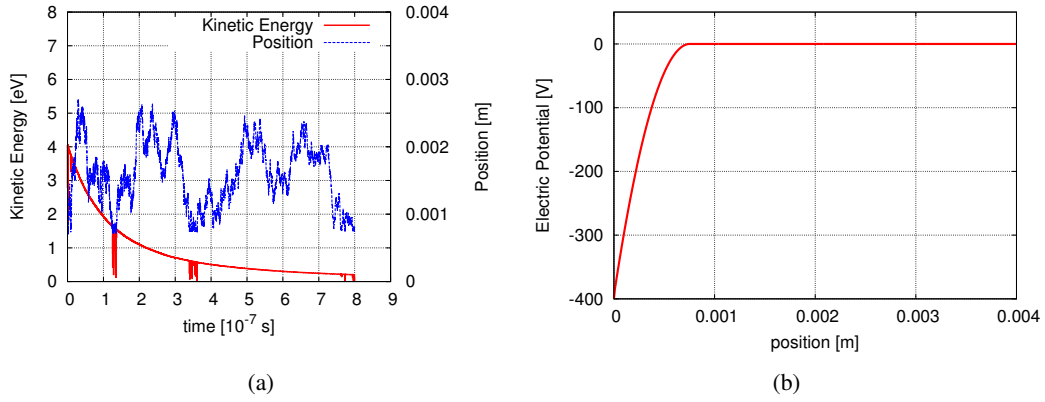


Figure 7.4: Results of Test 1. (a) Kinetic energy and position of a random Penning electron versus time (b) Electric potential configuration.

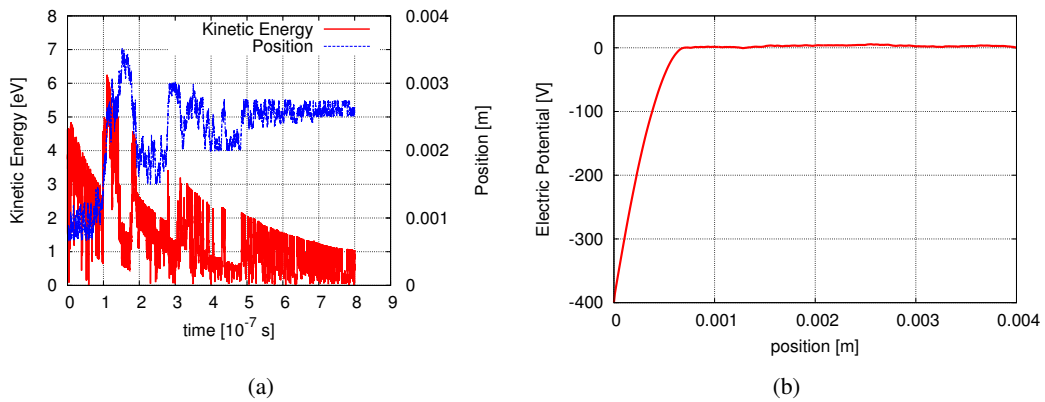


Figure 7.5: Results of Test 2. (a) Kinetic energy and position of a random Penning electron versus time (b) Electric potential configuration.

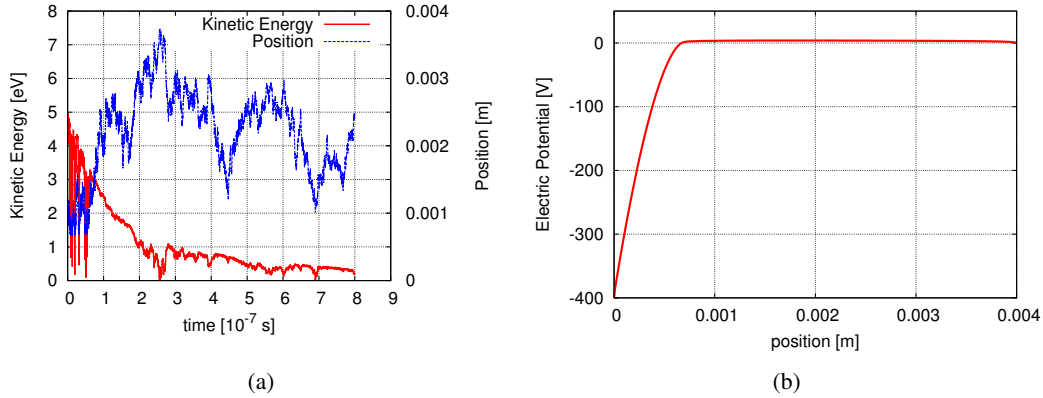


Figure 7.6: Results of Test 3. (a) Kinetic energy and position of a random Penning electron versus time (b) Electric potential configuration.

7.2.1 Conclusions concerning the Penning Electron MCC Analysis

Disturbing effects of the noisy electric field is obvious on the electron energies. To able to see the peaks in the EEDF, one has to use averaged/filtered electric field data. Reduction of the noise can be achieved as follows,

- As stated in Chapter 5, by using enough number of super particles in the simulations, both noise of the electric field values and the average electron energy reduce.
- Developing special algorithms to filter or average the electric field at the center of the discharge. In addition, to observe the Penning electron energy peak easier, cesium-helium mixture can be modeled [53]. Work is still underway.

CHAPTER 8

CONCLUSION

In this thesis study, PIC/MCC codes for glow discharge simulations were developed. The method is based on the simultaneous solution of Lorentz equations of motion of superparticles, coupled with the Poisson's equation for the electric field. Collisions between the particles are modelled by Monte Carlo method. PIC/MCC codes for helium and argon gas discharges was validated. The issue which is often ignored but crucial for developing efficient particle simulation algorithms, namely, the effect of particle weighting on the PIC simulations was studied. For the case of capacitive RF discharge in argon gas, we demonstrated effect of weighting on the main characteristics of the discharge such as charged particle densities, electric field, current densities, average energies of charged particles and energy distribution functions. Results show that the discharge characteristics are highly dependent on the number of particles used in simulations. It was shown that the adequate number of super particle per grid cell, sufficient to obtain weighting independent results, is about 1200, in the studied parameter regime.

DC Townsend discharges were simulated by 3d3v MCC model for different E/n values. Transport parameters (diffusion, mobility and Townsend ionization coefficients) for argon plasma were calculated and for the selected set of simulation parameters results were validated.

Also collisional electron spectroscopy (CES) method for DC gas discharges was studied. Although the preliminary results are not in perfect agreement with the ones obtained in the experiments, the reasons were investigated. Reducing the noise levels in the quasineutral region of the plasma may help obtain satisfactory results for the CES studies. Ongoing research will mainly be focusing on noise reduction and filtering.

REFERENCES

- [1] A. Bogaerts, E. Neyts, R. Gijbels, and J. Mullen, "Gas discharge plasmas and their applications," *Plasma Sources Sci. Technol.*, vol. B57, p. 609, 2002.
- [2] F. F. Chen, "Industrial applications of low-temperature plasma physics," *Phys. Plasmas*, vol. 2, 1995.
- [3] F. F. Chen and J. P. Chang, *Lecture notes of principles of plasma processing, 1st edition*. Kluwer Academic / Plenum Publishers, 2003.
- [4] Z. Donkó, "On the reliability of low-pressure dc glow discharge modelling," *Plasma Sources Sci. Technol.*, vol. 15, 2006.
- [5] J. M. Dawson, "One-dimensional plasma model," *Phys. Fluids*, vol. 5, 1962.
- [6] J. M. Dawson, "Thermal relaxation in a one-species, one-dimensional plasma," *Phys. Fluids*, vol. 7, 1964.
- [7] H. R. Skullerud, "The stochastic computer simulation of ion motion in a gas subjected to a constant electric field," *J. Phys. D: Appl. Phys.*, vol. 1, 1968.
- [8] N. A. Tran, E. Marode, and P. C. Johnson, "Monte carlo simulation of electrons within the cathode fall of a glow discharge in helium," *J. Phys. D: Appl. Phys.*, vol. 10, 1977.
- [9] C. K. Birdsall and A. B. Langdon, *Plasma Physics via Computer Simulation*. New York: McGraw Hill, 1985.
- [10] R. Boswell and I. J. Morey, "Self-consistent simulation of a parallel-plate rf discharge," *Appl. Phys. Lett.*, vol. 52, 1988.
- [11] C. K. Birdsall, "Particle-in-Cell charged-particle simulations, plus Monte Carlo collisions with neutral atoms, PIC-MCC," *IEEE Trans. Plasma Sci.*, vol. 19, 1991.
- [12] A. V. Phelps and Z. L. Petrovic, "Cold-cathode discharges and breakdown in argon: surface and gas phase production of secondary electrons," *Plasma Sources Sci. Technol.*, vol. 8, 1999.
- [13] A. V. Phelps, "The application of scattering cross sections to ion flux models in discharge sheaths," *Journal of Applied Physics*, vol. 76, 1994.
- [14] Z. Donkó, "Particle simulation methods for studies of low-pressure plasma sources," *Plasma Sources Sci. Technol.*, vol. 20, 2011.
- [15] V. Vahedi, G. DiPeso, C. K. Birdsall, M. A. Lieberman, and T. Rognlien, "Capacitive rf discharges modelled by particle-in-cell Monte Carlo simulation. i. analysis of numerical techniques," *Plasma Sources Sci. Technol.*, vol. 2, 1993.

- [16] J. P. Verboncoeur, "Particle simulation of plasmas: review and advances," *Plasma Phys. Control. Fusion*, vol. 47, p. A231, 2005.
- [17] Z. Donkó, "Particle simulation methods for studies of low-pressure plasma sources ii." Bochum University Presentation, 2010.
- [18] N. Sato and H. Tagashira, "A hybrid monte carlo/fluid model of rf plasmas in a sih_4/h_2 mixture," *IEEE Trans. Plasma Sci.*, vol. 19, 1991.
- [19] R. K. Porteous and D. B. Graves, "Modeling and simulation of magnetically confined low-pressure plasmas in two dimensions," *IEEE Trans. Plasma Sci.*, vol. 19, 1991.
- [20] V. P. Gopinath, J. P. Verboncoeur, and C. K. Birdsall, "Multipactor electron discharge physics using an improved secondary emission model," *Phys. Plasmas*, vol. 5, 1998.
- [21] W. N. G. Hitchon, *Plasma Processes for Semiconductor Fabrication*. Cambridge University Press, 1991.
- [22] E. Kawamura, C. K. Birdsall, and V. Vahedi, "Physical and numerical methods of speeding up particle codes and paralleling as applied to RF discharges," *Plasma Sources Sci. Technol.*, vol. 9, p. 413, 2000.
- [23] Derzsi, P. Hartmann, I. Korolov, J. Karacsony, G. Bano, and Z. Donkó, "On the accuracy and limitations of fluid models of the cathode region of dc glow discharges," *J. Phys. D: Appl. Phys.*, vol. 42, 2009.
- [24] M. M. Turner, A. Derzsi, Z. Donkó, D. Eremin, and S. J. Kelly, "Simulation benchmarks for low-pressure plasmas: Capacitive discharges," *Phys. Plasmas*, vol. 20, p. 013507, 2013.
- [25] A. Kudryavtsev, "A new method of gas analysis using penning-electron energy spectra, in book of abstracts international workshop / results of fundamental research for investments," *Russian Technologies for Industrial Applications, St.Petersburg Russia*, 1999.
- [26] E. A. Bogdanov, A. S. Chirtsov, K. D. Kapustin, A. Kudryavtsev, and A. B. Tsyganov, "The basic characteristics of the pulse helium microplasma source for analysis of gases by the method of collision electron spectroscopy CES," *36th EPS Conference on Plasma Phys. Paper, Sofia, Bulgaria*, 2009.
- [27] A. Chirtsov, A. Kudryavtsev, A. Mustafaev, and A. Tsyganov, "Micro-plasma detector based on collisional electron spectroscopy (ces) method for gas mixtures diagnostics," *30th ICPIG, Belfast, Northern Ireland, UK*, vol. 7, 2011.
- [28] V. I. Demidov, S. F. Adams, J. Blessington, M. E. Koepke, and J. M. Williamson, "Short dc discharge with wall probe as a gas analytical detector," *Contrib. Plasma Phys.*, vol. 50, 2010.
- [29] A. Kudryavtsev, "Registration of gas impurities in nonlocal plasma of helium microdischarge by an additional electrode - sensor," *Journal of Instrumentation*, vol. 7, 2012.
- [30] F. F. Chen, *Introduction to Plasma Physics and Controlled Fusion: Volume 1: Plasma Physics, 2nd edition*. Springer, 2006.
- [31] M. A. Lieberman and A. J. Lichtenberg, *Principles of plasma discharges and materials processing*. John Wiley & Sons Inc Publication, 2nd edition, 2005.

- [32] Y. P. Raizer, *Gas discharge physics, 1st edition*. Springer Verlag, 1991.
- [33] G. G. Lister, "Low-pressure gas discharge modeling," *J. Phys. D: Appl. Phys.*, vol. 25, 1992.
- [34] L. D. Tsendin, "Nonlocal electron kinetics in gas-discharge plasma," *Phys. Usp.*, vol. 53, p. 133, 2010.
- [35] I. W. Rangelow, "Dry etching-based silicon micro-machining for MEMS," *Vacuum*, vol. 62, 2001.
- [36] H. gas energy levels. http://raptor.physics.wisc.edu/talk/helium_e.gifx. Retrieved August 15, 2013.
- [37] I. energies of atoms. http://commons.wikimedia.org/wiki/File:Ionization_energies.svg. Retrieved August 15, 2013.
- [38] A. Piel, *Plasma Physics: An Introduction to Laboratory, Space, and Fusion Plasmas*. Springer, 2010.
- [39] I. Rafatov, R. Akbar, and S. Bilikmen, "Modelling of non uniform dc driven glow discharge in argon gas," *Phys. Lett. A*, vol. 367, 2007.
- [40] S. Ross, *A First Course in Probability*. New Jersey: Pearson, 2010.
- [41] H. Wang, W. Jiang, and Y. Wang, "Implicit and electrostatic particle-in-cell/monte carlo model in two-dimensional and axisymmetric geometry: I. analysis of numerical techniques," *J. Plasma Sources Sci. Technol.*, vol. 19, 2011.
- [42] V. Vahedi and M. Surendra, "A monte carlo collision model for the particle-in-cell method: applications to argon and oxygen discharges," *Comp. Phys. Comm.*, vol. 87, p. 179, 1995.
- [43] R. H. Landan, "A beginner's guide to high-performance computing." <http://www.shodor.org/petascale/materials/UPModules/beginnersGuideHPC/>. Retrieved December 02, 2012.
- [44] J. Schulze, U. Czarnetzki, A. Derzsi, P. Hartmann, I. Korolov, and E. Schungel, "Fundamental investigations of capacitive radio frequency plasmas: simulations and experiments," *Plasma Phys. Control. Fusion*, vol. 54, 2012.
- [45] Z. Donkó, "Private communication." Private mail communication between E Erden & Z Donkó, 2012.
- [46] M. Surendra, "Ph D. dissertation, University of California Berkeley." ProQuest Dissertations and Theses; 1991; ProQuest Dissertations & Theses(PQDT), 1991.
- [47] A. H. Sato and M. A. Lieberman, "Electron-beam probe measurements of electric fields in rf discharges," *J. Appl. Phys.*, vol. 68, 1990.
- [48] H. C. Kim, F. Iza, S. S. Yang, M. Radmilović-Radjenović, and J. Lee, "Particle and fluid simulations of low-temperature plasma discharges: benchmarks and kinetic effects," *J. Phys. D: Appl. Phys.*, vol. 38, 2005.
- [49] M. M. Turner, "Kinetic properties of particle-in-cell simulations compromised by monte carlo collisions," *Phys. Plasmas*, vol. 13, p. 033506, 2006.

- [50] H. F. of the Department of Computer Engineering at METU. <http://www.ceng.metu.edu.tr/hpc/index>.
- [51] Q. Wang, "Simulation of direct current microplasma discharge in helium atmospheric pressure," *Journal of Applied Physics*, vol. 100, 2006.
- [52] J. S. Howard, J. P. Riola, R. D. Rundel, and R. F. Stebbings, "Chemi-ionization in collisions between helium metastable atoms and argon," *Phys. Rev. Lett.*, vol. 29, 1972.
- [53] A. Kudryavtsev, "Private communication." Private communication between E Erden & A Kudryavtsev, 2013.

APPENDIX A

INFORMATION ABOUT THE PARALLEL PIC/MCC FORTRAN CODES

Matlab, C and Fortran programming languages were used during the thesis study. The most recent and the improved codes were developed with Fortran and MPI implementation. In this section, information about the code developed for helium gas discharge (in section 4.1) will be given. Parallel fortran code mainly consists of three separate f90 files. Namely initializer (PFPIC1D_Init_He_v10.f90), main part (PFPIC1D_Main_He_v10.f90), subroutines pack (PFPIC1D_subroutines_He_v10.f90).

- **Initializer:** Initializer code is compiled,

```
mpif90 -o INIT_PIC PFPIC1D_Init_He_v10.f90  
PFPIC1D_subroutines_He_v10.f90 -O3
```

and run,

```
mpirun -np X INIT_PIC
```

with linux terminal commands, where **X** is the number of processors that will be used in the simulations. After the run, initial charged particle arrays and information about the simulation is saved into the "saved_arrays" folder (the folder has to be created inside the same folder where the program files reside). The main program reads the information from the specified directory to start up the analysis, and it may also save the progress into this folder. In short the initializer program has to be used when first starting the iterations.

Input parameters are declared at the initializer. Some of the input parameters, types and their units are given table A.1. If the user wants to simulate a DC gas discharge with the code, he/she has to enter 0 for the *RF_mode* variable, and input the values of the left and right electrode potential parameters (*V_l_DC* and *V_r_DC*) in the appropriate rows. Similar approach can be used for single and dual frequency RF gas discharge simulations. It should be noted that for single frequency, only parameters of 1st frequency is used, 2nd frequency or DC parameter entries are redundant.

In this f90 file, solution parameters are also entered into the program. List of these parameters is given in Table A.2. Distance between the electrodes is divided into equal ndx distances, where number of grid points can be calculated by adding one to this value. One RF cycle period ($1/f$) is also divided into $tspc$ equal parts, hence time step size (Δt) can be derived. Position and velocity of the charged particles (position, x-y and z velocity components, energy) are stored in equal sized arrays for each of the processors. The variables $array_size_e$ and $array_size_i$ are the parameters defining the sizes of these arrays for electrons and ions respectively. Initial global densities at the start of the simulation for electrons and ions are $start_n_e$ and $start_n_i$. The super particles are distributed as equal as possible into the domain at the start. The variable $fill_rate$ identifies the initial fill rate of these arrays, and the number of charged particles used at the start of the simulation. It also directly effects the weighting of the charged particles. As an example, weighting of the super electrons (W_e) can be derived from

$$W_e = \frac{start_n_e \times L}{fill_rate \times array_size_e \times n_p}, \quad (\text{A.1})$$

where n_p is the number of parallel processors used in the simulation. The final solution parameter, isc , is for the ion subcycling. If subcycling will not be used, then the value has to be set to 1. If $display_parameter$ is set to value 1, then the results show up on the screen during the run of the program. This selection can be quite handy when running the codes in desktop or laptop computers, to detect the possible problems and the status of the simulation. Section of the initializer, where input and solution parameters are entered into the program can be seen in Figure A.1.

- **Main Program:** This part of the code reads (loads) the information from the *.txt files inside the saved_arrays folder, and helps to run the simulations. To compile this part,

```
mpif90 -o PIC PFPIC1D_Main_He_v10.f90 inverse.f90
PFPIC1D_subroutines_He_v10.f90
```

and to run,

```
mpirun -np X PIC
```

commands are entered into the terminal.

When running the code, $array_size_i$, $array_size_e$, ndx and $tspc$ parameters with the loaded text files and the parameters inside the main program are compared for consistency check. If there are any discrepancies, the program gives detailed error message and program halts. cos_or_sin parameter is responsible from wave type of the electrode potentials. The parameter $poisson_solver$ defines the order of the Poisson's equation solver, and the $tnts$ parameter is the total number of iterations to be done. The program also checks, if $tnts$ is greater than the iteration number at the start of the program, else warns the user for an appropriate input.

TableA.1: Information about the input parameters in the parallel helium PIC/MCC initializer (PFPIC1D_Init_He_v10.f90). REAL(8) format refers to double precision (64 bit) floating point number.

Input Parameter	Parameter Type	Unit	Extra Information
Ambient Pressure - p	REAL(8)	[Pa]	
Ambient Temperature - T	REAL(8)	[K]	
Electrode Distance - L	REAL(8)	[m]	
Discharge Type - RF_mode	INTEGER	-	0 for DC, 1 for RF, 2 for Dual-RF
Reflection - $reflect$	REAL(8)	-	
Secondary Electron Yield - $yield$	REAL(8)	-	
Max. Yield Elec. En. - max_sey_en	REAL(8)	[eV]	

TableA.2: Information about the solution parameters in the parallel helium PIC/MCC initializer (PFPIC1D_Init_He_v10.f90). REAL(8) format refers to double precision (64 bit) floating point number.

Solution Parameter	Parameter Type	Unit
Number of Grid Distances - ndx	INTEGER	-
Time Step per RF Cycle - $tspc$	INTEGER	-
Size of the Electron Arrays - $array_size_e$	INTEGER	-
Initial Electron Density - $start_n_e$	REAL(8)	[m ⁻³]
Size of the Ion Arrays - $array_size_i$	INTEGER	-
Initial Ion Density - $start_n_i$	REAL(8)	[m ⁻³]
Ion Subcycling Parameter - isc	INTEGER	-
Initial Array Fill Rates - $fill_rate$	REAL(8)	-

Display and save parameters are also defined in the main program. If the display parameter (*display_parameter*) is set to 1, the results show up on the screen at every *time_step_dp*. For RF and dual-RF simulations *cycles_to_be_saved* defines how many RF cycles will be used for final simulation results. It is a parameter for averaging the results or noise reduction. On the other hand, *ts_to_be_saved* is the save parameter for the DC simulations since the results are not periodic as in the RF cases. Energy distribution function parameters define the resolution and range of the electron and ion energy distribution functions. Section of the main program, where solution and display parameters are entered into the program can be seen in Figure A.2.

The output files of the simulation is stored inside "outputs" folder. With the help of an appropriate plotting program, such as gnuplot, results can be displayed as plots. Illustration of the root program folder can be seen in Figure A.3.

- **Subroutines:** This file is compilation of the required subroutines and functions to run the codes.

```

!*****INITIALIZER*****!

PROGRAM main

! Purpose:
! Particle in Cell / Monte Carlo, Parallel 1D Fortran INITIALIZER (DC/RF/dual-RF)
! For Helium Gas

! Record of revisions:
! Date                Programmer                Description of change
! =====
! 03.06.2013          Emrah Erden                Transformed Argon to Helium Code (First version)

! REVISIONS ARE WRITTEN IN MAIN

! Type to terminal:
! mpi90 -o INIT_PIC PFPIC1D_Init_He_v10.f90 PFPIC1D_subroutines_He_v10.f90 -O3      ! Compiles the initialization code
! mpirun -np 4 INIT_PIC                                                            ! Runs the initialization code as parallel with mpi

IMPLICIT NONE

! MPI library variables - DO NOT CHANGE HERE
Include 'mpi.fh'
INTEGER worker_number
INTEGER number_of_workers
INTEGER ierr

! Data dictionary: Declare problem parameters
! ATTENTION - YOU MAY CHANGE PARAMETERS BELOW*****
REAL(8), PARAMETER :: p = 4.00D0          ! Ambient pressure [pa]
REAL(8), PARAMETER :: T = 300.D0         ! Ambient temperature [K]
REAL(8), PARAMETER :: L = 0.067D0        ! Distance between the electrodes [m]

INTEGER, PARAMETER :: RF_mode = 1        ! 0 for DC, 1 for RF electrode (1st frequency and components selected)
                                           ! 2 for Dual_RF voltage configuration

! DC case variables
REAL(8), PARAMETER :: V_l_DC = 0.D0      ! DC : Left electrode potential [V] - constant
REAL(8), PARAMETER :: V_r_DC = 0.D0      ! DC : Right electrode potential [V] - constant

! RF and Dual-RF case variables
REAL(8), PARAMETER :: V_l_amp_1 = 0.D0    ! RF: Left electrode potential - amplitude [V] 1st frequency
REAL(8), PARAMETER :: V_r_amp_1 = 450.D0 ! RF: Right electrode potential - amplitude [V] 1st frequency
REAL(8), PARAMETER :: V_l_amp_2 = 0.D0    ! RF: Left electrode potential - amplitude [V] 2nd frequency
REAL(8), PARAMETER :: V_r_amp_2 = 0.D0    ! RF: Right electrode potential - amplitude [V] 2nd frequency
REAL(8), PARAMETER :: rf_1 = 13.56D6      ! RF: Electrode frequency [Hz] 1st frequency
REAL(8), PARAMETER :: rf_2 = 0.0D0        ! RF: Electrode frequency [Hz] 2nd frequency

REAL(8), PARAMETER :: reflect = 0.0D0     ! Reflection rate for electrons
REAL(8), PARAMETER :: yield = 0.0D0       ! Secondary electron yield rate for ions. Energy independent
REAL(8), PARAMETER :: max_sey_en = 1.D0    ! Maximum secondary electron energy for the specified gas [eV]

! Data dictionary: Declare solution parameters
INTEGER, PARAMETER :: ndx = 128           ! Number of grid distances. Number of grid points is +1 added to this value
INTEGER :: tstep = 400                   ! Number of time steps per cycle for single & dual RF glow discharges
INTEGER, PARAMETER :: array_size_e = 41000 ! Electron array size for each worker/processor
REAL(8), PARAMETER :: start_n_e = 2.56D14 ! Electron density at the start
INTEGER, PARAMETER :: array_size_i = 41000 ! Ion array size for each worker/processor
REAL(8), PARAMETER :: start_n_i = 2.56D14 ! Ion density at the start
INTEGER, PARAMETER :: isc = 1            ! Ion subcycling
REAL(8), PARAMETER :: fill_rate = 0.4D0  ! Electron and Ion arrays, initial fill rate. Should be less than 0.5!!!

! Display parameters
INTEGER, PARAMETER :: display_parameter = 1 ! If this parameter is equal to "1", then the results show up on the screen

! Data dictionary: Declare universal parameters
REAL(8), PARAMETER :: excitation_1_en = 19.82D0 ! 1st Excitation energy for helium gas
REAL(8), PARAMETER :: excitation_2_en = 20.61D0 ! 2nd Excitation energy for helium gas
REAL(8), PARAMETER :: ionization_en = 24.59D0  ! Ionization energy for helium gas

REAL(8), PARAMETER :: pi = 3.141592653589793D0 ! Pi number
REAL(8), PARAMETER :: k = 1.3806488D-23        ! Boltzmann constant
REAL(8), PARAMETER :: e0 = 8.85418782D-12      ! Permittivity of free space
REAL(8), PARAMETER :: me = 9.109D-31          ! Mass of an electron [kg]
REAL(8), PARAMETER :: mi = 6.67D-27           ! Mass of an helium atom [kg]
REAL(8), PARAMETER :: q = 1.602176565D-19     ! Unit charge [C]
REAL(8), PARAMETER :: cV = 1.602176565D-19    ! [eV] to [J] conversion

!WARNING*****
! DO NOT CHANGE ANYTHING, AFTER THIS PART!!!
! DO NOT CHANGE ANYTHING, AFTER THIS PART!!!
! DO NOT CHANGE ANYTHING, AFTER THIS PART!!!
!WARNING*****

! Parameters and variables, derived from constant parameters
INTEGER :: exist_e = INT(DFLOAT(array_size_e)*fill_rate) ! Number of existing electrons for each worker, and initializing
INTEGER :: exist_i = INT(DFLOAT(array_size_e)*fill_rate) ! Number of ions for each worker, and initializing
INTEGER :: l_exist_e = 0 ! Total number of existing electrons, for all the workers (global sum of all exist_e)
INTEGER :: l_exist_i = 0 ! Total number of existing electrons, for all the workers (global sum of all exist_i)

```

Figure A.1: Section of the initializing program, PFPIC1D_Init_He_v10.f90, where input and solution parameters are entered into the program.

```

! Type to terminal:
! mpiF90 -o PIC PFPIC1D_Main_He_v10.f90 inverse.f90 PFPIC1D_subroutines_He_v10.f90 ! Compiles the initialization code
! mpirun -np X PIC ! Runs the initialization code as parallel with mpi

! Add -fbounds-check for overflow checking
! As mpiF90 -o PIC PFPIC1D_Main_He_v10.f90 -fbounds-check PFPIC1D_subroutines_He_v10.f90

! For Profiling:
! mpiF90 -g -pg -o profiling_PIC PFPIC1D_Main_He_v10.f90 inverse.f90 PFPIC1D_subroutines_He_v10.f90
! mpirun -np X profiling_PIC
! gprof --line profiling_PIC gmon.out
! gprof --line profiling_PIC gmon.out | tee profiler_output.txt (To see all the profiling output in the text file)

! http://gcc.gnu.org/onlinedocs/gfortran/Error-and-Warning-Options.html
! SOME IMPORTANT ERROR FLAGS
! -Wconversion-extra : Warn about implicit conversions between different types and kinds.
! -Wimplicit-procedure : Warn if a procedure is called that has neither an explicit interface nor has been declared as EXTERNAL.

IMPLICIT NONE

! MPI library variables - DO NOT CHANGE HERE
Include 'mpif.h'
INTEGER worker_number
INTEGER number_of_workers
INTEGER ierr

!*****
! YOU MAY CHANGE THE PARAMETERS BELOW, UP TO WARNING
!*****
!!!!!!!!!!!!!!!!!!!!!!!!!!!!!!!!!!!!!!!!!!!!!!!!!!!!!!!!!!!!!!!!!!!!!!!!!!!!!!!!!!!!!!!!!!!!!!!!!!!!!!!!!!!!!!!!!!!!!!!!
! Program variables are taken from the txt files of the "saved_arrays" folder. But these 3 variables should match with the
! ones in "saved_arrays/SaveVariables.txt". Also the number of workers/processors/cores used in the program will be checked for consistency
INTEGER, PARAMETER :: array_size_i = 41000 ! Ion array size, this has to be "set" same with value in "saved_arrays/SaveVariables.txt"
INTEGER, PARAMETER :: array_size_c = 41000 ! Ion array size, this has to be "set" same with value in "saved_arrays/SaveVariables.txt"
INTEGER, PARAMETER :: ndx = 128 ! L=ndx*dx, this has to be "set" same with value in "saved_arrays/SaveVariables.txt"
INTEGER, PARAMETER :: tstep = 400 ! Time steps per RF cycle
INTEGER, PARAMETER :: cos_or_sin = 2 ! 1 for cosine, 2 for sine
INTEGER, PARAMETER :: poisson_solver = 0 ! 0 for 2nd order accuracy (default), 1 for 4th order which is much slower
INTEGER, PARAMETER :: nts = 612000 ! Total number of time steps, or iterations
!!!!!!!!!!!!!!!!!!!!!!!!!!!!!!!!!!!!!!!!!!!!!!!!!!!!!!!!!!!!!!!!!!!!!!!!!!!!!!!!!!!!!!!!!!!!!!!!!!!!!!!!!!!!!!!!!!!!!!!!

! DISPLAY AND SAVE PARAMETERS
! DISPLAY PARAMETER*****
INTEGER, PARAMETER :: display_parameter = 1 ! If this parameter is equal to "1", then the results show up on the screen
INTEGER, PARAMETER :: time_step_dp = 10000 ! At every time_step_dp, results show up on the screen
!*****

! SAVE PARAMETERS*****
! For all the conditions save to text files will be done, it is not optional as the display on the screen
INTEGER, PARAMETER :: ts_to_be_saved = 10000 ! How many time steps will be saved for the "DC" glow discharge (for final saves)
INTEGER, PARAMETER :: cycles_to_be_saved = 32 ! How many cycles will be saved for the single and dual
! RF glow discharge (for final saves)
INTEGER, PARAMETER :: updating_save_freq = 10000 ! How often parameters will be saved to *.txt files,
! to update the user. Such as: t_n_e.txt, E.txt, V.txt, Update.txt etc.
!*****

! ENERGY DISTRIBUTION FUNCTION PARAMETERS*****
REAL(8), PARAMETER :: W_Sheet_frac = 0.1D0 ! Width of left sheet regions / L
REAL(8), PARAMETER :: W_Quasineutral_frac = 0.1D0 ! Width of quasi-neutral region / L
INTEGER, PARAMETER :: edf_array_size = 1000 ! Energy distribution functions, array sizes
INTEGER, PARAMETER :: eedf_range = 200 ! Electron energy distribution function upper range [eV]
INTEGER, PARAMETER :: iedf_range = 5 ! Ion energy distribution function upper range [eV]
INTEGER, PARAMETER :: ion0_path_array_size = 20000 ! Array save size of the ion #0 at the processor # 0
! Path will be saved
!*****

!WARNING*****
! DO NOT CHANGE ANYTHING, AFTER THIS PART!!!
! DO NOT CHANGE ANYTHING, AFTER THIS PART!!!
! DO NOT CHANGE ANYTHING, AFTER THIS PART!!!
!WARNING*****

! Variables READ from TXT FILES
INTEGER :: RF_mode ! 0 for DC, 1 for RF, 2 for dual-RF
REAL(8) :: p ! Pressure [Pa]
REAL(8) :: T ! Temperature [K]
REAL(8) :: L ! Electrode Distance [m]
REAL(8) :: reflect ! Energy Independent Electron Reflection Coefficient
REAL(8) :: yield ! Energy Independent Secondary Electron Yield Coefficient for Ions
REAL(8) :: excitation_en_1 ! 1st excitation energy for the gas
REAL(8) :: excitation_en_2 ! 2nd excitation energy for the gas
REAL(8) :: ionization_en ! Ionization energy for the gas
REAL(8) :: max_scy_en ! Maximum secondary electron yield energy for electrons
REAL(8) :: start_n_e ! Initial electron density
REAL(8) :: start_n_i ! Initial ion density
INTEGER :: isc ! Ion sub-cycling parameter
REAL(8) :: pi ! Pi
REAL(8) :: k ! Boltzmann constant
REAL(8) :: e0 ! Permittivity of free space
REAL(8) :: me ! Mass of electron
REAL(8) :: mi ! Mass of ion

```

Figure A.2: Section of the main program, PFPIC1D_Main_He_v10.f90, where solution and display parameters are entered into the program.

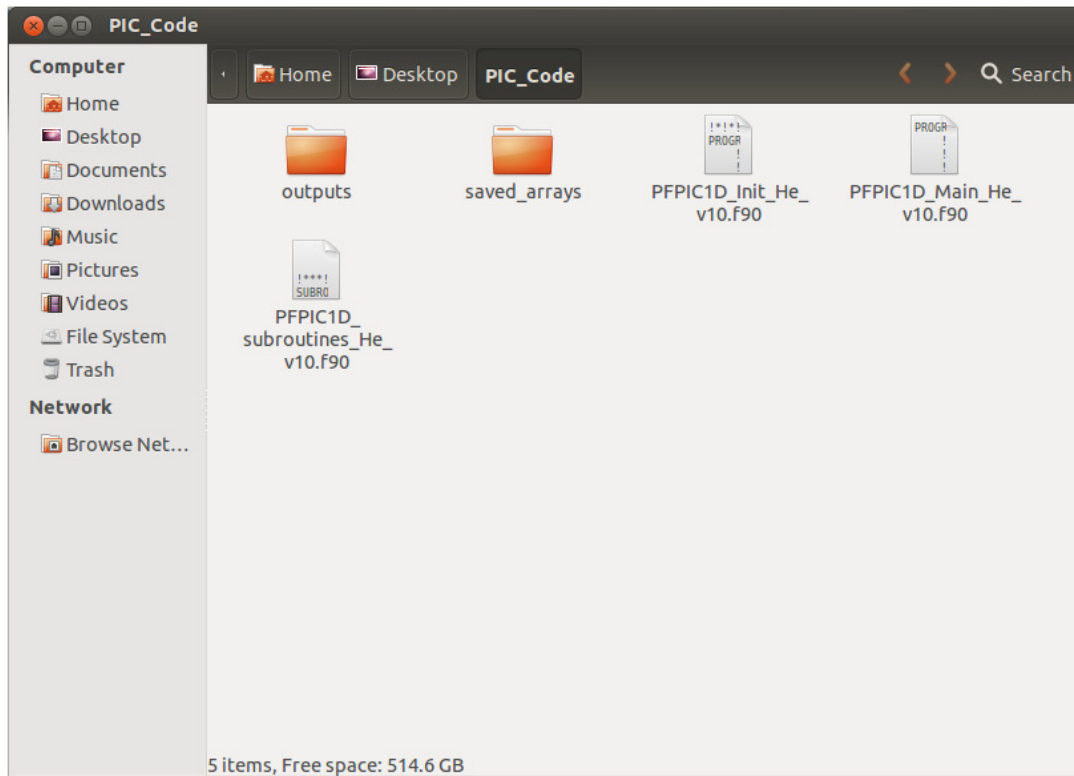


Figure A.3: Illustration of the root program folder.